Université de Montréal

Three-dimensional flow structure, turbulence and bank erosion in a 180° meander loop

Par
Mike Tilston

Département de Géographie
Faculté d'Arts et Sciences

Mémoire présenté à la Faculté des études supérieures
en vue de l'obtention du grade de M.Sc.
en Géographie

Avril, 2006

Université de Montréal
Faculté des études supérieures

Cet mémoire intitulé:

Three-dimensional flow structure, turbulence and bank erosion in a 180° meander loop

Présenté par:

Mike Tilston

A été évalué par un jury composé des personnes suivantes:

André G. Roy
Pascale M. Biron
Thomas Buffin-Bélanger

Sommaire

Les boucles de méandre sont des composantes très dynamiques des systèmes fluviaux, et elles peuvent potentiellement éroder les terres agricoles et aussi détruire certaines infrastructures durant leur migration. C'est pourquoi plusieurs techniques de stabilisation des berges ont été développées, de l'utilisation de grosses pierres ("rip rap") à des mesures plus naturelles se servant de la végétation. Les objectifs de cette étude sont 1) d'investiguer la structure tri-dimensionnnelle de l'écoulement et les caractéristiques turbulentes d'une boucle de méandre de 180 degrés ; 2) d'examiner les liens entre la turbulence, la contrainte de cisaillement et le décrochement des berges ; et 3) d'évaluer le succès de mesures de protection des berges utilisées le long d'une boucle de méandre. Des mesures tri-dimensionnelles de vitesse ont été recueillies à neuf reprises, six d'entre elles à l'aide d'un courantomètre acoustic Doppler (ADV), et trois grâce à un profileur acoustic Doppler (PC-ADP). Puisque le PC-ADP est un appareil relativement récent, un test de comparaison avec l'ADV a été effectué. Les résultats indiquent que les données moyennes de vitesse d'écoulement étaient semblables, mais que les statistiques turbulentes des deux appareils sont assez différentes en raison du plus grand volume d'échantilllonnage et de la plus faible fréquence d'enregistrement des données du PC-ADP. L'écoulement est caractérisé par des structures turbulentes à grande échelle dans la composante longitudinale de vitesse, qui semblent produire des mouvements cohérents semblables dans les plans latéral et vertical. La zone de vitesse plus élevée à l'amont du méandre décélère en prenant une expansion latérale, et engendre une cellule de recirculation principale ainsi qu'une faible cellule secondaire de rotation opposée près de la berge externe entre l'entrée et la sortie du méandre. La

localisation des zones d'intensité turbulente maximales varie en fonction du débit, avec des valeurs maximales à l'entrée et à la sortie du méandre pour des débits faibles et élevés, respectivement. Différentes méthodes d'estimé des contraintes de cisaillement ont été comparées et, en se basant sur les observations visuelles de transport de sédiments, il a été établi que la méthode d'énergie cinétique turbulente (basée sur les trois composantes de l'écoulement) était la plus adéquate. Des zones d'érosion des berges ont été détectées à l'entrée et à la sortie du méandre, ce qui correspond aux zones de plus fortes contraintes de cisaillement. Durant cette étude, la berge externe de la rivière a été stabilisée en réduisant sa pente et en utilisant de la végétation pour retenir le sol. L'année suivant ces travaux, l'ajustement du cours d'eau s'est effectué par un dépôt massif de sédiments le long de la berge interne. L'entrée et la sortie du méandre ont encore subi des événements de décrochement depuis que les mesures de stabilisation ont été mises en place, mais un suivi à plus long terme est requis pour réellement évaluer le succès de ces mesures.

Mots-clés : méandre, structure de l'écoulement, contrainte de cisaillement, érosion des berges, stabilisation des berges.

Abstract

Meander loops are one of the more dynamic feature in fluvial systems, and have the potential to erode cropland and destroy infrastructure through their migration. As such, various techniques have been developed to stabilize river banks, ranging from rip-rap to vegetative based approaches. The objectives of this study are to: 1) investigate the three-dimensional flow structure and turbulence characteristics of a 180 degree meander loop, 2) examine the link between turbulence, shear stress and bank failure, and 3) gauge the success of bank protection measures taken along the study bend. In stream three-dimensional velocity measurements were taken on nine separate surveying dates, six of which were performed using an acoustic Doppler velocimeter (ADV) and three with a pulse coherence acoustic Doppler profiler (PC-ADP). Since the PC-ADP is a relatively new sampling device, a test was conducted to evaluate its performance against the ADV. Results indicate that while they produce similar mean flow measurements, their turbulence statistics are quite different, which is the result of the PC-ADP's larger sampling volume and lower sampling frequency. Flow is characterized by large-scale coherent flow structures in the downstream plane which appear to produce similar coherent motions in the lateral and vertical planes. The flow's high velocity core upstream from the bend decelerates as it expands laterally, develops a main circulation cell and a weaker counter-rotating cell adjacent to the outer bank between the bend entrance and exit. Locations of highest turbulence intensities are stage-dependent, with maximum values at the bend entrance and bend exit for low and high discharges, respectively. Different bed shear stress estimation methods were compared, and based on field observations of sediment transport, it was determined that the most accurate

estimates were obtained using the three-dimensional turbulent kinetic energy technique. Bank erosion itself was localized at the entrance and exit of the bend, which match the locations of maximum shear stress. During the course of this study, the outer bank of the channel was stabilized by lowering the bank slope and using vegetation to anchor the soil. Over the following year, the channel reacted to these measures through a massive sediment deposition event along the inner bank. While it appears that the bend entrance and exit have experienced bank failure events since stabilization measures were implemented, further monitoring is required to fully gauge its success.

Keywords: Meander loop, flow structure, turbulence, bed shear stress, bank erosion, bank stabilization

Acknowledgements

I would like to take this opportunity to thank Dr. P. M. Biron, not only for the chance to study this topic, but also all the guidance she has given me while collecting and analyzing the data, and for her patience with me and her help in the writing of this thesis. I would also like to thank the government of Quebec, specifically FCAR, for providing me with the funding to perform this research. I deeply appreciate the help of Tim Haltigin, Lara H., Ivan Dolinsek, Bruno Vallée, Tracy LeBlanc, Lisa LeBlanc and anyone else who I may have omitted for aiding in the long process of data collection. Finally, I would like to thank Claire Lemieux of Nature-Action for her help in finding an appropriate site to perform this thesis. Thank-you all so very much.

Table of Contents

List of Figures

List of Tables

1. Introduction

1.1. Background and Objectives

River bends are inherently highly dynamic systems that continuously erode sediments from one bank and deposit them along the other. It is necessary to study meanders since reaches are rarely straight for more that a few times the rivers width. There are many research questions left unanswered due to a lack of consensus as to their dominant flow structure (Rhoads and Welford, 1991), turbulence patterns (Shiono and Muto, 1998; Blanckaert and Graf, 2001), scour distributions (Whiting and Dietrich, 1993a) and hence their evolution.

Although bank retreat in meandering rivers is a natural process, it has become a serious problem throughout North America. It has been estimated that of the 3.5 million miles of rivers within the United States, roughly 575,000 miles of their banks are retreating (Biedenharn *et al.*, 1997). Since it results in the loss of vast amounts of private and public land, a reduction in water quality and sedimentation of rivers, which can impede the transportation of goods through waterways and degrade wildlife habitat, bank erosion has severe economical and environmental impacts (Piegay *et al.*, 1997).

In order to effectively deal with this environmental problem, a variety of studies have been performed to identify the factors involved in assessing bank instability (Darby and Thorne, 1996; Allen *et al.*, 1999; Simon and Collison, 2001). Yet, these studies tended to focus on the mechanics of bank failure itself rather than on the interaction of flow dynamics and bank erosion. A number of empirical models have been developed and applied to numerical simulators, which have been validated through the use of historical datasets (Jia and Wang, 1999; Wu *et al.*, 2000). However, these simulations

have been applied to watershed scale situations rather than individual bends. Those which have been applied to reach scale projects have not been validated (Mosselman *et al.*, 2000) or have greatly oversimplified the process, leading to some questionable results (Darby and Delbono, 2002; Darby *et al.*, 2002). This should come as no surprise since the majority of field studies have centered on monitoring erosion rates through the use of erosion pins (Couper *et al.*, 2002) or historical datasets of aerial photographs (Gilvear *et al.*, 2000; Simon *et al.*, 2002) rather than focusing of the hydraulic forces acting on the channel boundaries.

While the aforementioned field techniques are appropriate for watershed scale studies, they are not suitable for studies involving a single meander loop where bank characteristics are relatively homogeneous. Moreover, there has been a proliferation in various types of Doppler based technologies in recent years for sampling three-dimensional flow structures, yet there is no consensus amongst the scientific community as to which instruments are appropriate for sampling the mean properties, versus the turbulence characteristics of a flow. Therefore, the objectives of this study are to: 1) Asses the performance of a pulse-coherent acoustic Doppler profiler (PC-ADP) against an acoustic Doppler velocimeter (ADV); 2) Investigate the three-dimensional flow dynamics of a meander loop; 3) Examine the link between turbulence, shear stress and bank failure. This will be accomplished through analyzing a series of in-stream three-dimensional velocity datasets and comparing shear stress values with topographic surveys of the river bed and banks.

1.2. Thesis Structure

This thesis has been organized in the following manner: ***Chapter 2*** is an overview of previous studies relating to the three-dimensional flow structure and bank erosion in river bends. The section begins by identifying the mechanics of failure and reviewing different methods of stabilizing river banks. This is followed by an appraisal of the various steady flow and turbulence based approaches of estimating bed shear stress. ***Chapter 3*** outlines the manner in which the data were collected, treated and analysed for this project. It begins by describing the study site and the sampling technique used to collect sediment samples, topography measurements of the channel bed and river banks and three-dimensional velocity. The procedure for evaluating the estimates of bed shear stress obtained by the different calculation techniques is also described. ***Chapter 4*** presents the results of the study, which are subsequently discussed in ***Chapter 5***. Finally, ***Chapter 6*** presents the conclusions of the study.

Due to the negative economical and environmental impacts of bank erosion associated with the lateral migration of meandering rivers, and to the ubiquity of these rivers throughout the world, large amounts of money have been invested into preventing their migration, particularly in North America. Historically, this has been accomplished by dredging the river to create a linear canal (Figure 1). Yet, it is well accepted that

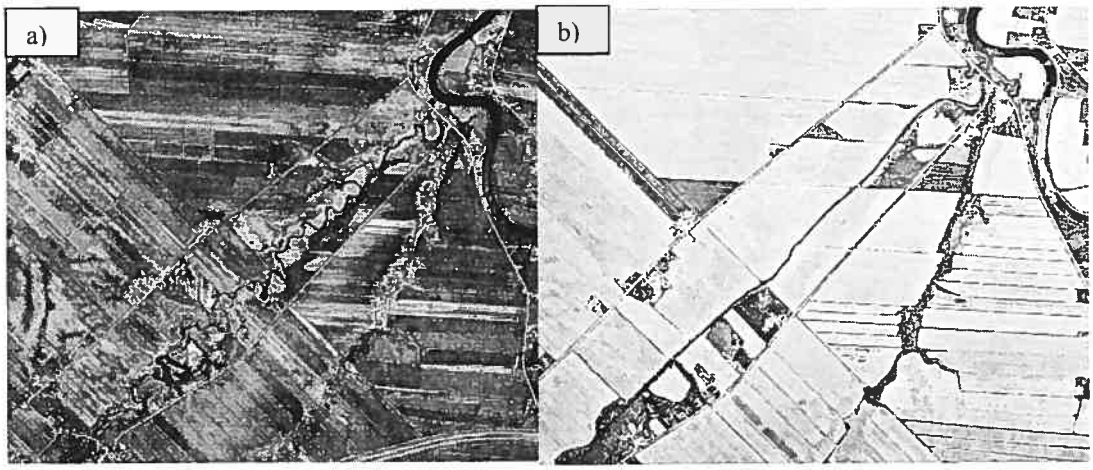

Figure 1: Plan geometry prior to (a) and following (b) a river straightening project of the Sud-Ouest river (neat St. Césaire).

these straightening projects are expensive, result in the degradation of riverine ecosystems, and require a significant degree of maintenance to prevent the canal from re-meandering (Rhoads and Welford, 1991). As such, engineers currently use less intrusive approaches that are applied locally to prevent channel migration. In general, these techniques serve to do one of two things: 1) divert the flow away from the banks, or 2) reinforce the channel boundaries.

As the name implies, the aim of diversion approaches is to redirect the high velocity core of the flow away from the banks, thereby displacing the zone of maximum bed scour from the bank toe towards the center of the channel. Traditionally, this is

accomplished by installing hydraulic structures such as dykes and retards along the near-bank region of the bed. By contrast, reinforcement approaches serve to reduce erosion rates by armouring the channel boundaries rather than modifying their flow fields. While a variety of materials can be used to create an armour layer, this is normally achieved by placing graded stones, more commonly known as rip-rap, on the bed and banks of the river (Figure 2). Here, larger boulders serve to resist the shear forces of the flow, and are anchored in place by filling their interstitial spaces with smaller cobbles.

Figure 2: Hard-engineering stabilization technique (rip-rap) used in the Petite Barbue River downstream of the study reach.

Yet, much like the case of river straightening projects, the hydrologic, ecologic and aesthetic impacts of these stabilization techniques have caused another fundamental shift towards more environmentally friendly solutions (Rinaldi and Johnson, 1997).

Currently, pilot projects are underway in Quebec to determine if the more environmentally friendly approaches of preventing bank erosion do indeed provide a

viable alternative to the more traditional stabilization techniques. Contrary to the aforementioned "hard-engineering" methods, "soft-engineering" solutions rely on the root systems of water tolerant woody vegetation for reinforcement after the bank slope is reduced rather than rip-rap (Figure 3). This is occasionally accompanied by inserting

Figure 3: Soft-engineering stabilization technique (using vegetation) implemented in June 2003 in the study reach.

thick branches into the banks below the water line to slow flow velocity, thereby reducing the shear forces acting at the toe of the bank.

Evidently, long-term monitoring projects are required to evaluate the effectiveness of "soft-engineering" techniques against their "hard-engineering" counterparts. However, previous research indicates that vegetative approaches are indeed effective at reducing the frequency of bank erosion events. As noted by Abernethy and Rutherfurd (1998), previous studies indicate bank sediments that are reinforced with roots are up to 20,000 times more resistant to erosion.

While still in its infancy relative to hard-engineering approaches, vegetative stabilization methods are becoming increasingly favoured for a variety of reasons (Lee *et al.*, 1997). Aside from being more aesthetically pleasing, they are far less harmful to the ecology of the stream and they have a minimal influence on ground water flow patterns in the surrounding regions, which is especially important for the case of agricultural areas. Moreover, the cost of this method has been greatly reduced over the past few years from $\$100/m^2$ to $\$10/m^2$. In Québec, the government covers 75% of the cost. Despite these improvements, stabilization projects are still expensive. Because the migration rate of an unstable reach will vary between bends and even within a single meander, the elevated costs can be partially mitigated through stabilizing only the most dynamic sections of the river.

Although river bank failure has recently become the focus of intense modelling research with varying degrees of success (Mosselman *et al.*, 2000; Nagata *et al.*,2000; Duan *et al.*, 2001; Darby and Delbono, 2002; Darby *et al.*, 2002; Lancaster and Bras, 2002; Richardson, 2002, Olsen, 2003), *in situ* studies dealing with this process are sparse. Those which focused on determining bank retreat have done so by reconstructing the history of the river through aerial photography (Gilvear *et al.*, 2000; Simon *et al.*, 2002), examining a single cross-section over various bends within a reach, or have used an array of pins to measure retreat directly (Couper *et al.*, 2002). Using these field techniques, predictions of bank stability can be made by extrapolating the historical trends of channel migration. Yet, historic sets of aerial photographs are often incomplete or non-existent for rural areas, and they are rarely at a scale which can be used for this purpose. Additionally, the time constraints of engineering projects prevent

monitoring the river over a period of years. As such, practical stabilization schemes require that predictions of bank erosion patterns are improved by the use of a Newtonian framework that quantifies the forces exerted on the banks by a three-dimensional flow field.

2.1. Bank Erosion – Causes, Types and Mechanics of Failure

It is well known that unregulated Canadian rivers are characterized by high flow stages in the spring, moderate levels in the fall and low discharges during the summer and winter months. As such, regime theory dictates that they are constantly evolving in order to strike a balance between channel geometry and bed sediments with flow conditions (Chang, 2002). Although this is typically achieved through bed scour in rivers with cohesive bank sediments, this situation is slightly different for the case of regulated rivers. Here, upstream dams prevent the influx of coarse bed sediments, and therefore bank erosion is the primary mechanism by which they react to excessive hydraulic forces. At the reach scale, the increase in sinuosity associated with bank failure reduces the channel slope, which decreases the speed and hence the hydraulic forces of the flow. At the bend scale, failure events increase the cross-sectional area of the channel, and the principle of continuity dictates that water velocity, and therefore the shear stress exerted by the flow, must decrease.

In their study of the Latrobe River in south-east river Australia, Abernethy and Rutherfurd (1998) observed that bank erosion is characterized by four types of sporadic, large scale failure events: shallow slides, toppling slabs, deep-seated rotational and deep-seated translational failures (Figure 4). Shallow slides were most common on steep

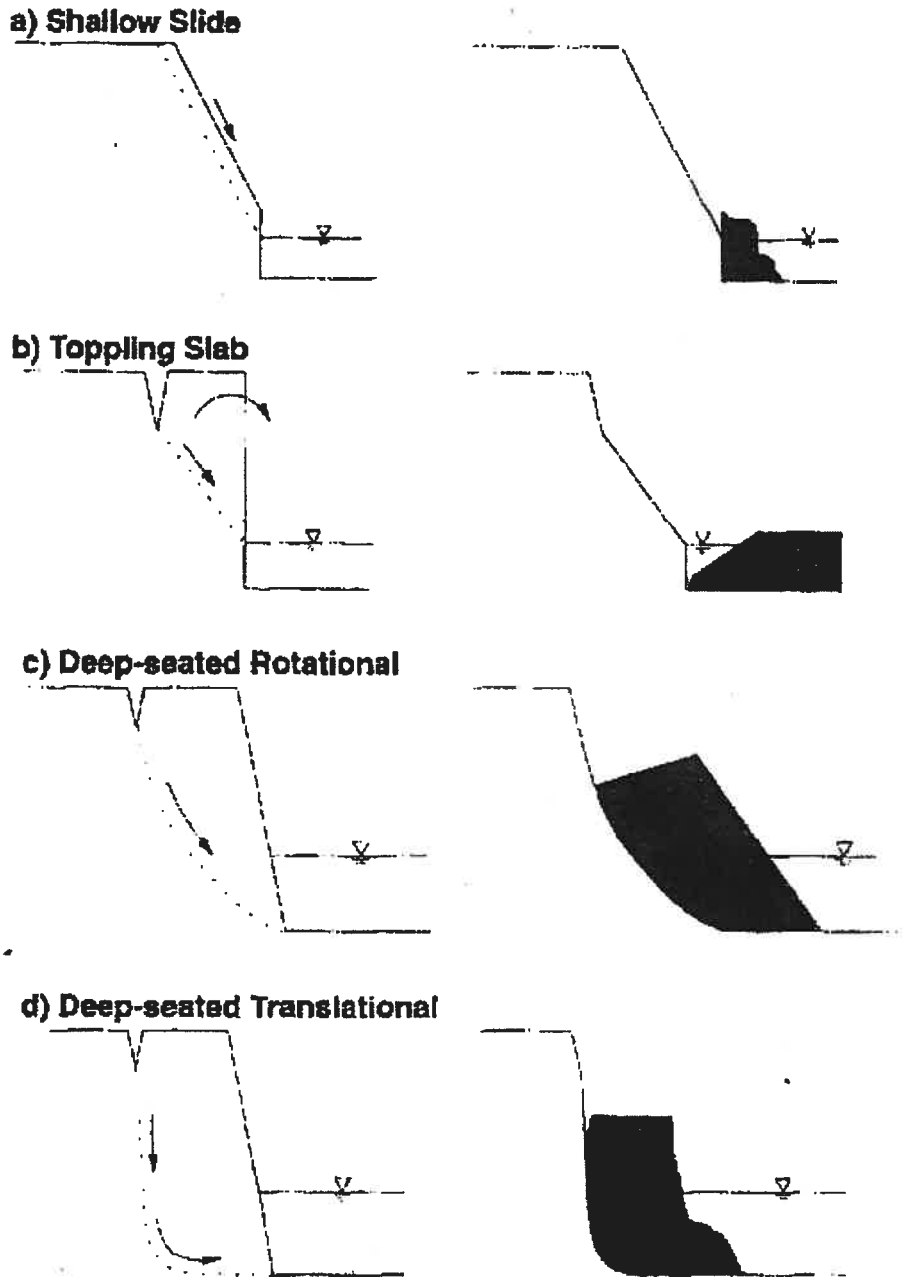

Figure 4: Different modes of bank failure (Abernethy and Rutherfurd, 1998).

bank faces (>40°) where the vegetation's root system did not penetrate deeply into the soil. Although they were less common than shallow slides, deep-seated rotational and

translation failures were also common with these bank characteristics, whereas toppling slabs was the dominant mode of failure on low bank sections with steep faces.

However, bank erosion is a complicated process where the frequency of failure events is governed by the planform geometry (Hodskinson and Ferguson, 1998), flow conditions and sediments of the stream (Petit, 1990), as well as local climatic conditions (Simon *et al.*, 2002). Moreover, bank properties also affect the frequency of failure events since stability is related to the response angle, vegetative coverage and pore water pressure of the bank, as well as the cohesiveness of their sediments and the presence of tension cracks (Darby and Thorne, 1996; Duan *et al.*, 2001; Simon and Collison., 2001). Yet agricultural sites tend to display uniform moisture levels and sediment properties along the banks, thereby greatly reducing the number of bank variables involved in the failure process. As such, bank angle is the primary variable affecting stability, which is controlled by the hydraulic forces of the flow.

The lateral migration rate of river bends is controlled primarily by the extent of scour at the bank toe (Darby and Delbono, 2002) (Figure 5), which is governed by the balance between bed shear stress and the critical threshold required for sediment entrainment (Petit, 1990). While modelling this phenomenon, Nagata *et al.* (2000) were

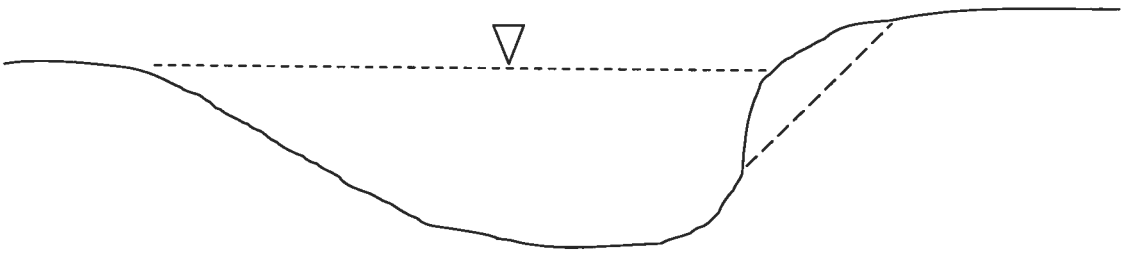

Figure 5: Causes and effects of bank failure (modified from Darby and Thorne, 1996).

able to identify four key steps in the bank erosion process. First, high shear stresses progressively scour the bed at the toe of the outer bank, which increases the bank angle; then the instability that occurs once a critical bank angle is surpassed causes failure. The collapsed bank material is then deposited at the front of the bank and transported away from the site of failure. Similar descriptive models have been successfully applied in many other numerical simulators (Darby and Delbono, 2002; Darby *et al.*, 2002). Therefore, the shear stress distribution along the bed of a meander loop must be determined as well as the bank angles to predict the pattern of channel migration.

2.2. Dynamics of Meanders

2.2.1. Bed Shear Stress Patterns in River Bends

A fundamental aspect of applied fluvial geomorphology is to predict channel evolution by analyzing the spatial distribution of the resistive and erosive forces within the reach. Although the flow structure and resistive forces along natural rivers can vary greatly over the course of a year, a decommissioned upstream dam will not only maintain a relatively constant base-flow level, but it will also regulate the size of the channel bed sediments. As such, tractive forces and critical shear stresses tend to remain fairly stable under these circumstances, thereby simplifying the process driving channel evolution. Yet even relatively benign variations in discharge can alter the flow dynamics of a reach (Chang, 2002). Given that boundary shear stress provides a means of lnking flow dynamics with sediment transport rates, quantifying this variable and examining its distribution along river bends has been the subject of intense research (Dietrich and Smith, 1984; Dietrich and Whiting, 1989; Petit, 1990).

2.2.1.1. Mean Shear Stress

As can be seen in Figure 6, shear stress distributions vary both laterally and longitudinally along a river bend. Meanders are characterized by a cross-stream stress gradient where the highest stress values are found at the toe of the outer bank and

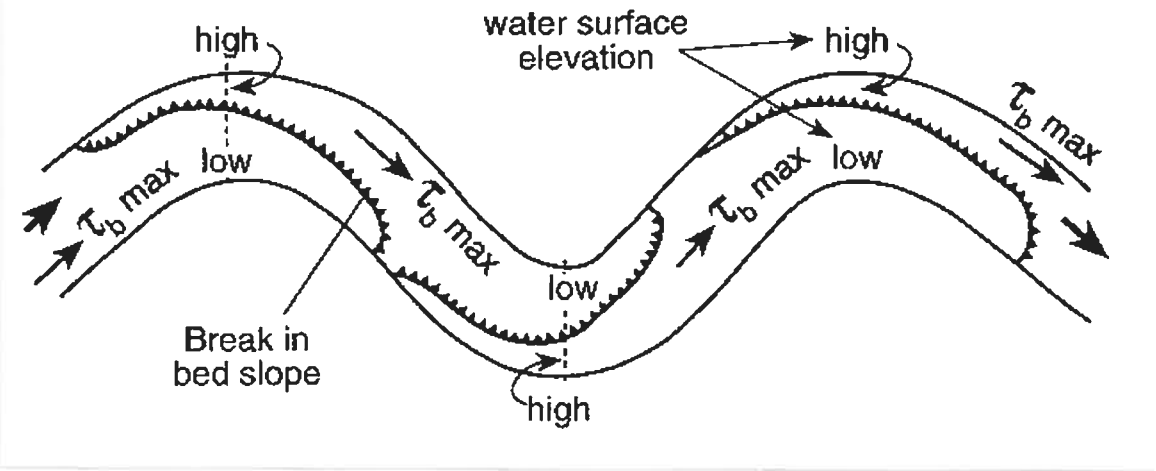

Figure 6: Boundary shear stress distribution through a meandering river (Knighton, 1998).

steadily decrease towards the inner half of the channel. Furthermore, the values of shear stress in the outer half of the channel begin to increase upon entering the meander loop and continue to rise until reaching their maximum value downstream of the bend apex. From their study of a sand bedded meander loop, Dietrich and Smith (1984) associated the shift in zones of maximum shear stress to the deflection of the high flow velocity core towards the outer bank. Bedload transport also shifted following the same trajectory as bed shear stress.

The obvious implication of the aforementioned longitudinal pattern of bed shear stress is that river bends must migrate downstream rather than expanding laterally along its axis. While regular trends of migration have been reported in numerical simulations of meander evolution (Jia and Wang, 1999; Nagata *et al.*, 2000; Olsen, 2003), natural

rivers are unlikely to display such trends due to non-uniform bank stability and irregular stress patterns.

In contrast to flume studies and numerical simulation of meander development, the critical failure angle of natural riverbanks will vary throughout a reach since their spatially non-uniform sediment composition will affect their stability. Furthermore, previous research has acknowledged that shear stress distributions can deviate from those of conceptual models even under simple conditions (Whiting and Dietrich, 1993a; Ferguson *et al.*, 2003).

While analyzing bed development of meanders in a laboratory setting, Whiting and Dietrich (1993a) found that multiple pools tend to develop along the outer banks of large amplitude river bends. Surprisingly, the deepest of these pools was the first one to develop at the entrance of the bend. Running against the work of Leeder and Bridge (1975) who found that maximum velocity and bank erosion rates occurred in the distal half of a bend, indicating that this is the site of maximum shear stress, these results suggest that the highest shear stress values are located at the bend entrance. While authors postulated that the centrifugal forces created by their bend were not strong enough to completely dampen the sinuous high flow velocity core as seen in straight reaches (Whiting and Dietrich, 1993b), similar trends of maximum velocity and bank erosion occurring upstream of the apex have been observed in tight bends (Ferguson *et al.*, 2003) and in the upstream loop of a compound meander (Frothingham and Rhoads, 2003). Moreover, multiple pools have been observed in similar flume experiments with tighter bends (Blanckaert and Graf, 2001).

The situation in natural rivers is complicated further by the effects of variable discharge levels on the flow pattern in a channel. Previous studies have clearly demonstrated that part of the reason why the core of high velocity is deflected towards the outer bank of river bends can be attributed to topographic steering effects caused by the point bar (Whiting and Dietrich, 1991). It has also been established that the degree to which bedforms distort flow structure is directly proportional to their height with respect to water depth (Buffin-Bélanger *et al.*, 2000a), and similar findings have been noted in studies on the impact of relative step height in river confluences (De Serres *et al.*, 1999). Therefore, flow deflection by point bars should be stronger at low discharge levels, thereby shifting the zone of maximum shear stress towards the bend entrance. Following this logic, accurate shear stress measurements must be obtained over a range of flow conditions in order to implement localized bank protection measures along river bends.

Although many approaches have been developed to calculate bed shear stress, some of these may give unrealistic estimates in complex flow fields. As such, identifying a suitable technique to quantify hydraulic forces in river bends is of great importance.

2.2.1.2. Turbulent Shear Stress

It is now well accepted that turbulence production is an organized and intermittent process that is inherent to all flows, even in the absence of bed forms and sediments (ex: Kline *et al.*, 1967). While point values of turbulence intensity scale directly with flow speed and sediment size (Grass, 1971), frequency, intensity and spatial distributions of strong events do not necessarily follow the same trend. Although

several studies have verified the existence of organized and intermittent processes in fluids, there is a large degree of scatter in their results on various turbulent properties, such as burst period (Luchik and Tiederman, 1987; Lapointe, 1992). Nonetheless, results from laboratory experiments suggest that this process plays a critical role in a range of fluvial processes, especially in terms of bedform development and sediment transport (Jackson, 1976; Williams *et al.*, 1989; Lapointe, 1992; Best, 1993; Nelson *et al.*, 1995) (Figure 7).

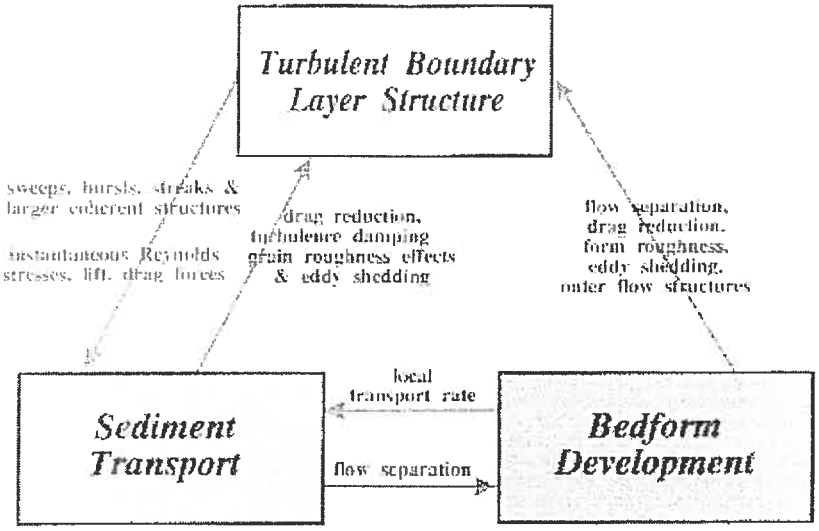

Figure 7: Feedbacks between the turbulent boundary layer, bedform development and sediment transport (Best, 1993).

While the mean flow techniques of estimating shear stress may be appropriate in designing stable channels, the aforementioned studies suggest that their ability to assess sediment transport in natural river bends is questionable, especially while under near-equilibrium conditions. In their visualization study along a straight reach, Drake *et al.* (1988) noted that sediment transport occurred in patches that were randomly distributed in space and time, despite the shear stress values obtained using mean flow techniques

being just below the critical threshold. Given the intermittent nature of sediment transport, Drake *et al.* (1988) concluded that it was being driven by turbulent structures. Considering that decommissioned dams serve to limit variations in flow stage and sediment characteristics, reaches whose dynamics are controlled by upstream dams are, inherently, under near-equilibrium conditions for the majority of the year. Therefore, even slight increases in flow speeds can cause a significant amount of sediment transport; hence it is reasonable to assume that turbulent velocity fluctuations must play a fundamental role in their evolution.

Conceptually, the instantaneous velocity fluctuations that characterize turbulent flow signals affect sediment mobility since they cause temporal variations in stress levels (Figure 8). Moreover, research on turbulence over the past forty years has

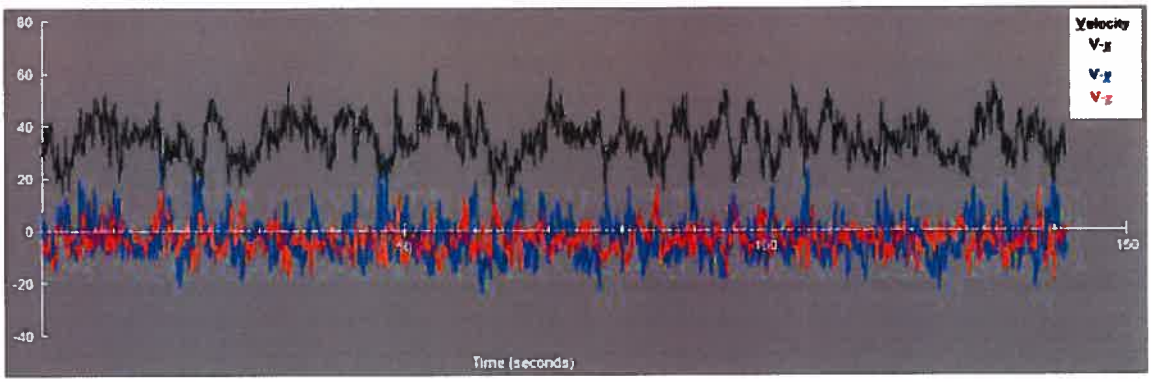

Figure 8: Velocity signal of a turbulent flow where Vx = downstream, Vy = lateral and Vz = vertical flow velocities.

clearly demonstrated that it is not a chaotic process; rather, it is an organized phenomenon consisting of coherent structures operating on different spatial and temporal scales (Robinson, 1991). Through a combination of flow visualization techniques and instantaneous velocity measurements in a flume study, Falco (1977) demonstrated that turbulent structures can be envisioned as operating on two distinct

scales: large scale motion of either high or low speed velocity and smaller "typical" eddies superimposed within them. More recently, the presence of these large coherent structures has been confirmed in natural rivers (Buffin-Bélanger *et al.*, 2000b; Roy *et al.*, 2004). The characterization of these eddies was of particular importance to the current understanding of turbulent flows as they make large contributions to the Reynolds stress through the bursting cycle (Kline *et al.*, 1967; Kim *et al.*, 1970; Falco, 1977).

As described by previous researchers (e.g.: Kline *et al.*, 1967; Kim *et al*,1970) bursting is initiated in regions containing a steep velocity gradient. This imposes a shear force on a volume of fluid, which generates a Kelvin-Helmholtz instability, thereby forming an eddy (Yalin, 1992). As the eddy grows, it is ejected towards the overlying high speed fluid and convected downstream at a rate slower than the mean velocity (Figure 9). As this slow moving eddy travels towards the water surface and decays into progressively smaller vorticities, a high speed sweep of fluid travelling towards the bed enters the region which the ejected fluid once occupied, which completes the cycle.

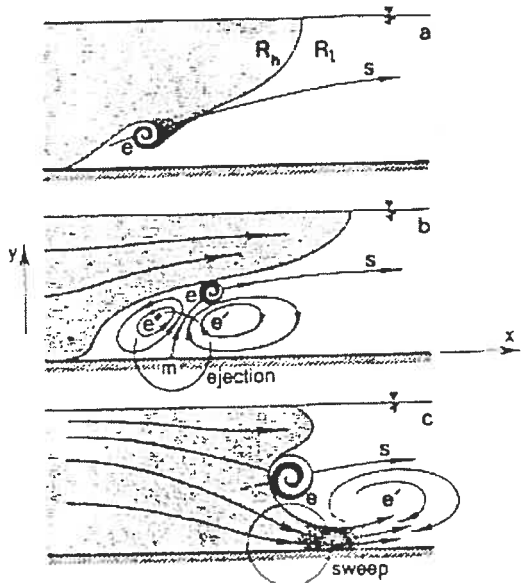

Figure 9: Burst cycle (Yalin, 1992).

Moreover, it has been proposed that bedforms can intensify these large turbulent structures; this was perhaps first proposed by Matthes (1947) after observations on relationship between dunes and boils, which are believed to be the surface manifestation of intense bursting events. As water travels over a dune, it is accelerated up the dune face and the flow becomes separated at the crest and then reattaches downstream of the dune (Bridge and Best, 1988). This pattern is characterized by an intense shear layer separating the overlying high-speed fluid and the underlying separated recirculation cell (Bennett and Best, 1995) (Figure 10(1)), thereby providing the steep velocity gradient required to initiate bursting. As such, this typical flow pattern produces a characteristic turbulence distribution. Bennett and Best (1995) found maximum downstream turbulence intensities at and just beyond the point of flow reattachment, and to a lesser extent within the flow separation cell; by contrast, maximum vertical velocity fluctuations are located in and above the shear layer, and in the region that advects and diffuses downstream (Figure 10(2)). The Reynolds stress was also maximised in the shear layer, which is dominated by intense shedding activity, whereas the point of flow re-attachment and the dune crest contained strong and frequent high speed, bed oriented structures. Similar flow structure and turbulence Reynolds stress distributions have also been noted over dunes by other researchers (Bridge and Best, 1988; Best, 1993), as well as in a flume study over a backwards step (Nelson *et al.*, 1995), indicating that such trends are not unique to dunes, but rather tend to occur in regions with rapid changes in downstream bed topography that induce flow separation.

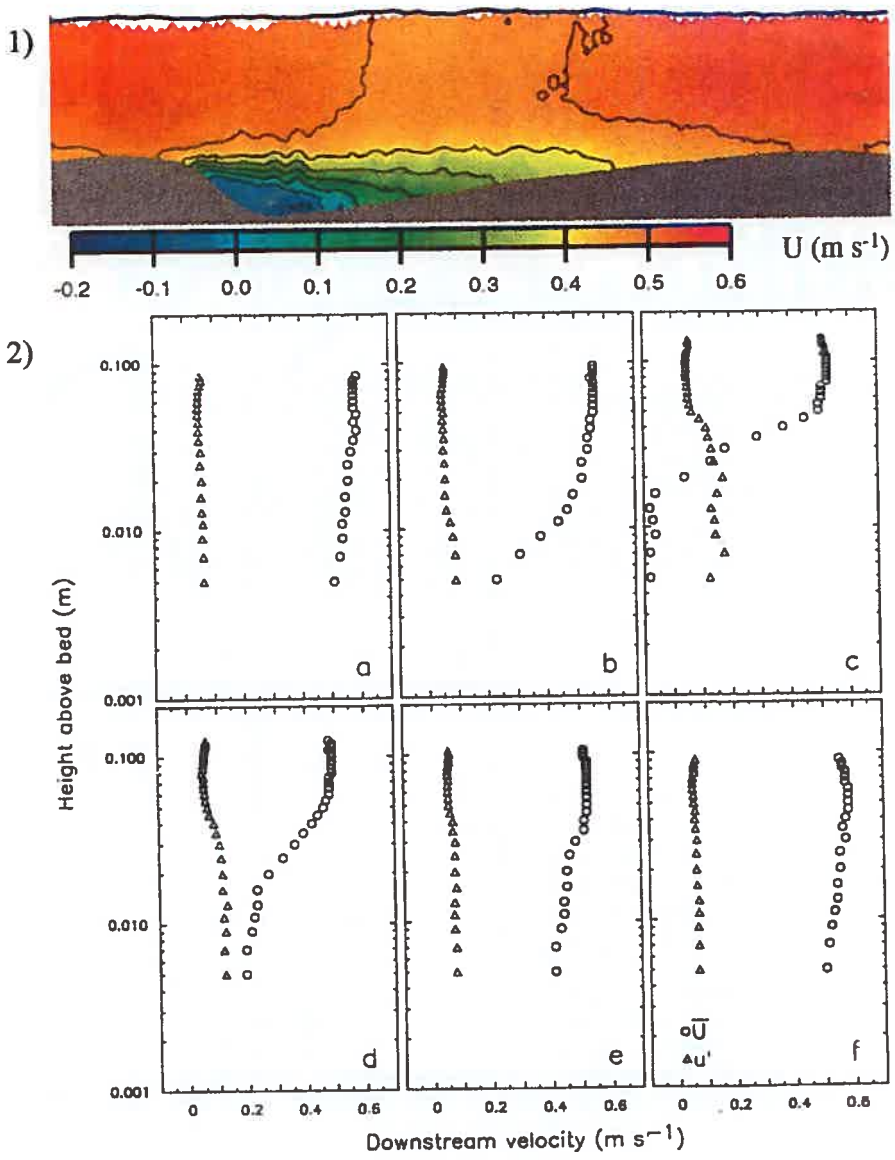

Figure 10: (1) Evidence of recirculation (negative velocity) zone in dune trough (Bennett and Best, 1995). (2) Velocity profiles (circles) over a fixed dune (a) upstream of crest, (b) just downstream of crest line, (c) within center of flow separation, (d) just downstream of reattachment point, (e) mid-face of subsequent dune and (f) just upstream of subsequent dune crest line (Bennett and Best, 1995).

While the structure of topographically induced turbulence is controlled by the formation, magnitude and downstream extent of the flow separation zone (Bennett and Best, 1995), it has been postulated that the shear layer displays a flapping motion (Lapointe, 1992), indicating that the spatial distribution of flow separation changes over

time. A possible explanation for this trend is that natural flows display oscillations in their velocity about their mean value (e.g.: Lapointe, 1992; Best, 1993). Research using an array of electro-magnetic current meters in a gravel bedded river has provided valuable insight into the macro-turbulent structure of natural flows (Kirkbride and Fergusen, 1995; Buffin-Bélanger *et al.,* 2000b; Roy *et al.*, 2004). They confirmed the presence of distinct, alternating zones of high and low speed fluid that was observed by Falco's (1977) flow visualization study (Figure 11); these macro-turbulent structures are coherent throughout the entire flow depth, and could explain the presence of a flapping shear layer over dunes; similar structures have been observed in gravel bed rivers (Buffin-Bélanger *et al.,* 2000b; Roy *et al.*, 2004). From these

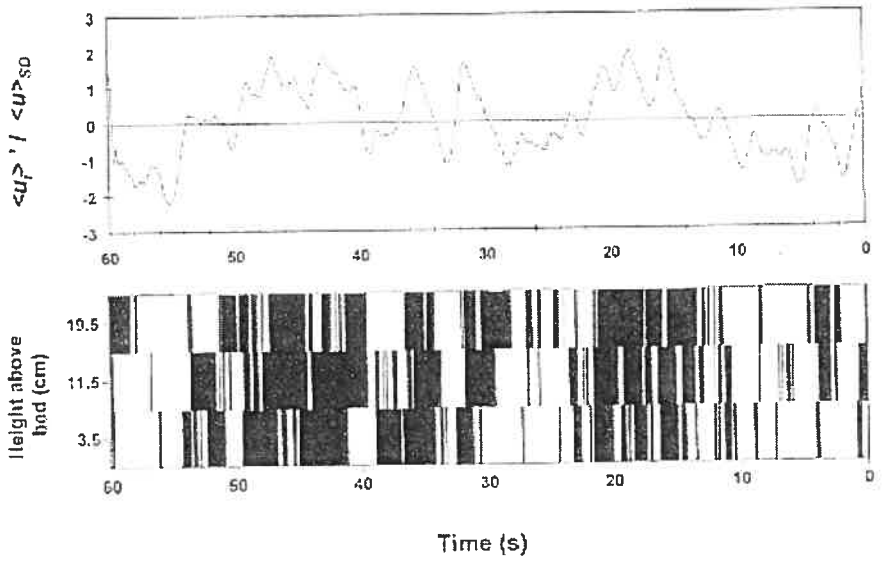

Figure 11: Alternating region of high and low speed fluid (Buffin-Bélanger et al., 2000b).

observations, Buffin-Bélanger *et al.* (2000b) postulated that "typical" eddies, which make the largest contributions to the Reynolds stress, were generated at the interface of these zones of high and low speed fluid where velocity gradients are the highest, thereby

initiating the bursting cycle. Yet the angle of this interface was variable, which raises the question on the effects of vertical velocity gradients on turbulence distributions.

It appears as though vertical velocity distributions play a fundamental role in turbulence generation. In their study of turbulence in a straight flume with a smooth bed and walls, Song and Chiew (2001) found that turbulence intensities were highest in the downstream direction, followed by the transverse and vertical components. The Root Mean Square (RMS) of the downstream and vertical components of velocity, as well as the Reynolds shear stress, will decrease from their maximum value at the bed where velocity gradients are the largest, to their minimum value at the water surface in a linear manner. The spanwise component followed a similar trend, but started to decrease in the near-bed region. Other flume (Song and Graf, 1994) and *in situ* (Sukhodolov *et al.*, 1998) studies revealed similar trends for the RMS of velocity fluctuations, although the latter displayed far more scatter, presumably due to the influence of complex bed topography. Moreover, Reynolds shear stress patterns were quite different under complicated topography, with some studies suggesting that maximum turbulence production occurring at 0.1 of the flow depth and others showing a maximum value at 0.5 of the flow depth (Sukhodolov *et al.*, 1998). This could arise from the flow undergoing local acceleration or deceleration, which can serve to decrease or increase point values of Reynolds shear stress (Song and Chiew, 2001), or the flow being deflected in the vertical direction, which would modify its vertical distribution. An alternative possibility for these inconsistencies is that "typical" eddies can be formed in areas other than the near-bed region since strong velocity gradients can exist at heights up to half of the flow depth (ex: Kim *et al.*, 1971) (Figure 12). However, in the absence

of the vertical flow component, it is difficult to ascertain whether these gradients are a precursor to eddie generation or simply a velocity signature of the busting cycle.

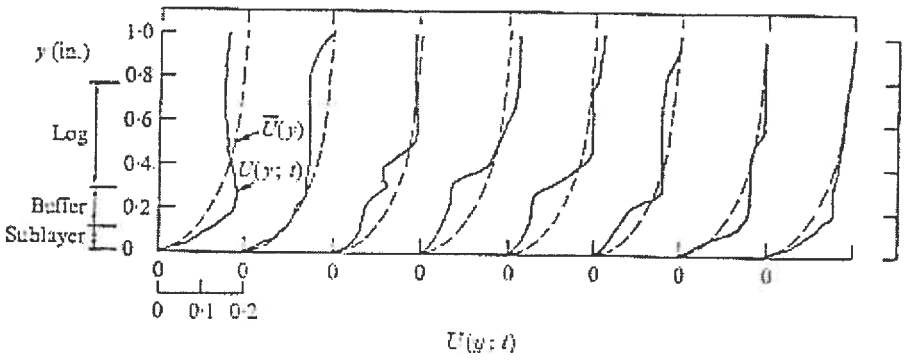

Figure 12: Instantaneous (black line) and average (dashed line) velocity profiles (Kim et al., 1971).

2.2.2. Secondary Circulation

Secondary circulation cells are features that have been observed in straight (Sukhodolov *et al.*, 1998; Rodriguez *at al.*, 2002), braided (Richardson and Thorne, 1998), meandering channels (ex: Rhoads and Welford, 1991) and at river confluences (Rhoads and Kenworthy, 1998), although the mechanisms that drive them are quite different. While those in the two former cases are driven primarily by turbulence (Sukhodolov *et al.*, 1998), secondary currents in river bends are driven by centrifugal force, and are therefore relatively strong (Rhoads and Welford, 1991). Considering that Demuren (1991) found the strength of secondary currents to range between 10% and 40% of the downstream component, it suggests that the lateral component of shear stress should display a similar variability.

2.2.2.1. Mean Velocity

Under the simplest of conditions, secondary currents develop along river bends as the flow is progressively deflected towards the outer bank through a combination of

centrifugal force (Rhoads and Welford, 1991) and topographic steering (Whiting and Dietrich, 1991). While the strength of lateral forces is determined by the plan geometry and stage of the channel, any amount of deflection will affect the flow structure in two distinct ways. Firstly, it displaces the high velocity core towards the outer bank (Dietrich and Whiting, 1989). Secondly, it causes the river to develop a transverse slope along the water surface (Chang, 2002), thereby creating an inwardly directed pressure gradient. As such, the magnitude and orientation of cross-stream flow is governed by the balance between the outwardly directed centrifugal force and the inwardly directed pressure gradient. Centripetal acceleration is proportional to water velocity whereas pressure force at a point is determined by the depth of the overlying water. Therefore, centrifugal forces dominate the upper portion of the profile, resulting in an outward motion whose intensity increases towards the surface, while the lower portion is dominated by pressure forces and the inward motion strengthens towards the bed. By virtue of the relationship between flow velocity and bed shear stress, the outer half of river bends are preferentially eroded and the bed sediments are transported towards the inner bank (Dietrich and Smith, 1984). This creates the typical deep concave scour pool next to the outer bank and shallow convex point bars next to the inner bank seen in meander loops (Figure 13).

Indeed, previous research has implied that secondary currents can make a significant contribution to the overall magnitude of bed shear stress. While studying sediment transport along a sand bedded meander, Dietrich and Whiting (1989) noted that its sediments were mobile, yet estimates of shear stress were below the threshold value. This discrepancy was attributed to the contribution of the cross-stream component to the

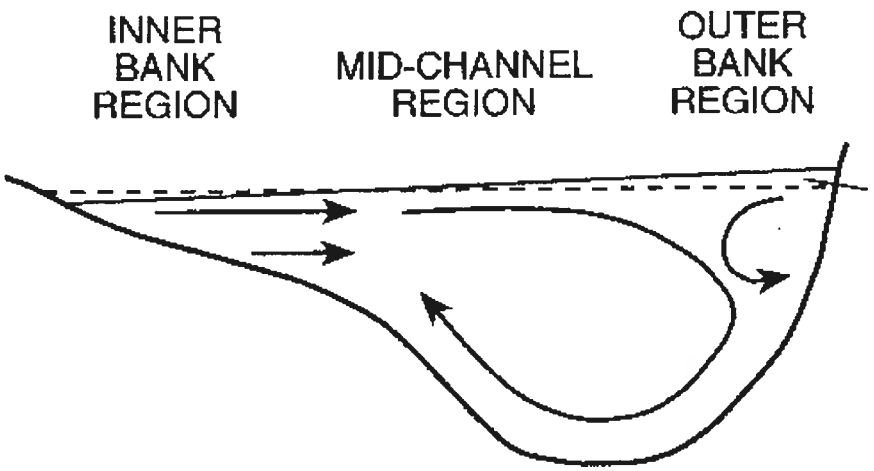

Figure 13: Secondary currents in river bends from Knighton (1998).

overall magnitude of stress levels, which was omitted from their calculations as it was treated as a second order term.

Moreover, there can be a great deal of variation in the structure of secondary currents in river bends. Both field (Frothingham and Rhoads, 2003) and modelling studies (Ferguson *et al.*, 2003) have demonstrated that the lateral extent of circulation cells will vary along a single meander loop, and they occasionally decay completely. Furthermore, researchers have sometimes detected the presence of an additional weaker cell along the outer bank circulating in the opposite direction (Blankaert and Graf, 2001). In the context of bank stability analysis, this has important implications as the second cell displaces the high velocity core, hence the zone of maximum bed scour, towards the center of the channel. Therefore, these additional cells reduce the lateral migration rate of a river.

It has been noted that flow can also become constricted in sharply curved bends due to the development of large recirculation eddies downstream of the point bar (Ferguson *et al.*, 2003) (Figure 14). Acting as a flow obstruction, the lateral extent of these recirculation zones will not only modify the pattern of secondary currents, but can also intensify bed shear stress by concentrating flow along the outer portion of the channel.

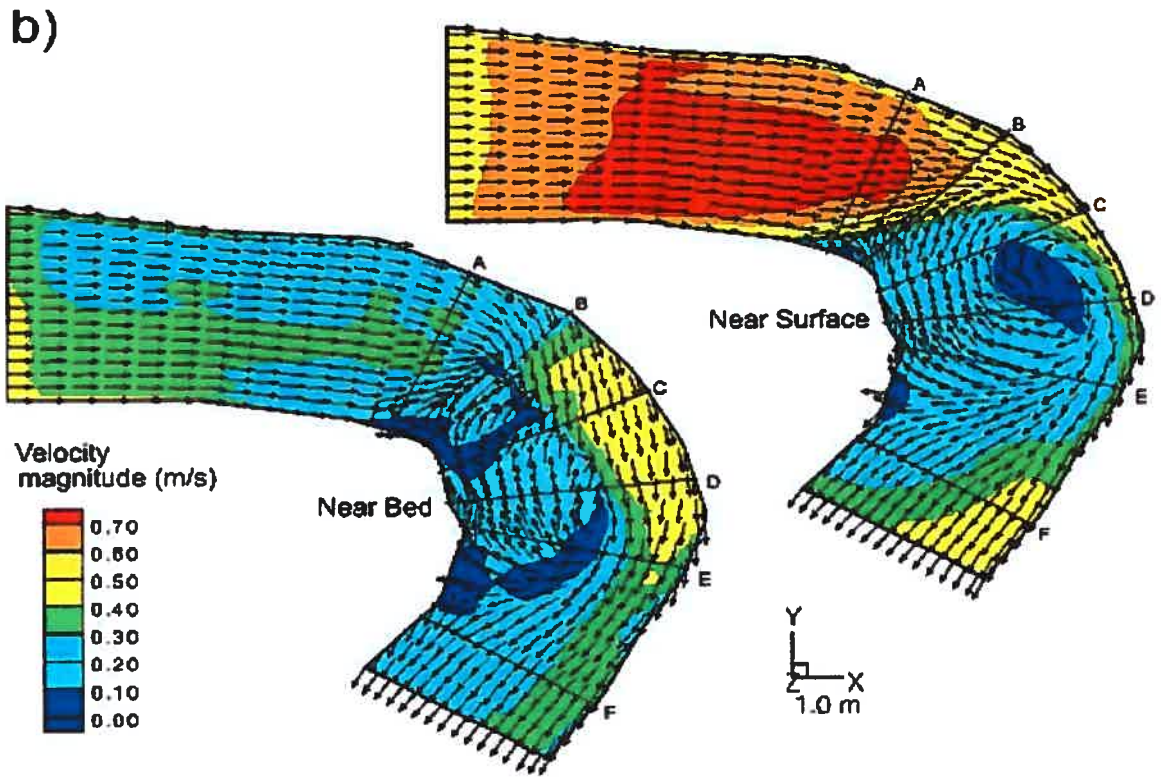

Figure 14: Flow recirculation in river bends (Ferguson et al., 2003).

2.2.2.2. Turbulence Distribution

While there are no *in situ* studies examining turbulence distributions in river bends, a great deal of research has focused on identifying the various sources of turbulence and their distributions along straight reaches. Based on this and the

characteristic flow patterns in river bends, it is possible to make inferences on the spatial distribution of turbulence intensities along meander loops.

The region upstream of the bend entrance is characterized by high flow velocities with respect to that observed in pools. These riffle regions typically contain symmetrical cross-sections compared to pools, and therefore one would expect a linear decrease in turbulence intensities towards the water surface like that observed by Song and Graf (1994). Yet natural flows are likely to exhibit slightly different patterns due to increased roughness. Previous studies have illustrated that intensities increase with the presence of roughness elements (Grass, 1971); moreover, riffle sections in sand bedded reaches often contain bedforms, which further increase turbulence driven events (Sukhodolov *et al.*, 1998; Rodriguez *et al.*, 2002). Therefore one would expect the downstream values of turbulence intensities to be higher than those seen in flumes. Moreover the vertical turbulence distribution may take the form of an exponential decrease (Sukhodolov *et al.*, 1998; Blanckaert and Graf, 2001) rather that the linear trend reported by Song and Graf (1994). Additionally, this decrease in turbulence associated with bed distance may only be valid for the central region of the channel. Since turbulence intensities are proportional to local velocity gradient, which is related to boundary distance, near bank vertical distributions may be characterized as uniform or even display an increase towards the surface as the bank becomes the dominant boundary affecting flow. Cross-stream and vertical components of turbulence are generally weak compared to downstream values in these regions (Sukhodolov *et al.*, 1998).

Unlike the case of straight reaches, the flow in river bends display strong secondary currents as well as large accelerations and decelerations due to rapid changes in bed topography. Given that both of these factors influence turbulence, turbulence distributions in meander loops will resemble distorted versions of those seen along straight reaches.

As the flow travels through the bend, a separation zone may form at the pool entrance similar to that observed over a backward step by Nelson *et al.* (1995) and beyond dune crests (Bennett and Best, 1995). Upon entering the pool, the flow will decelerate due to an increasing cross-sectional area; recent research has highlighted that flow deceleration is associated with increased turbulence activity (Song and Chiew, 2001; Thompson, 2004). Conversely, the pool exit is likely to be the site of lower turbulence activity due to flow acceleration as well as intense sweep events like that observed on dune faces by Bennett and Best (1995). While this describes topographically induced turbulence distributions for single pool river bends, laboratory studies suggest that meander loops can contain multiple points of flow separation. In their flume study of bed development in meanders, Whiting and Dietrich (1993a) found that multiple pools tend to develop along the outer bank under large amplitude bend configurations, which would result in multiple shear layers. While numerical simulations using their data were unable to reproduce the observed bed topography (Wu *et al.*, 2000), other flume (Blanckaert and Graf, 2001) as well as *in situ* studies (Whiting and Dietrich, 1991) have observed multi-pool development in much tighter bends.

Moreover, cross-stream and vertical turbulence patterns are further complicated by the presence of strong secondary currents. Circulation cells are characterized by

outwardly directed near-surface currents and inwardly direct near-bed currents with regions of downwelling and upwelling next to the outer and inner banks, but little research has focused on cross-sectional distributions of turbulence in river bends; those that have show a far more complex pattern than in straight reaches. In their meander experiment involving a flume, also with smooth boundaries, Shiono and Muto (1998) found similar trends in turbulence intensities as those of Song and Chiew (2001). However, Blanckaert and Graf (2001) showed that the turbulence intensities vary with bank distance – cross-stream fluctuations were stronger in the center of the channel whereas the converse is true towards the banks. The literature also reveals that while there are no shortage of studies indicating that bed shear stress increases towards the outer bank (Song and Chiew, 2001), there are also instances where the opposite is true (Shiono and Muto, 1998; Blanckaert and Graf, 2001). This pattern cannot have resulted from flow separation along the outer bank as both of these studies were performed in flumes with smooth plexi-glass banks, but neither set of authors propose an explanation for such a trend.

Further complexities to turbulence patterns are introduced by the presence of obstructions and planform geometry of the reach since both of these factors can drastically modify the systems flow dynamics. Researchers have noted that densely vegetated banks (Thorne and Furbish, 1995) and large woody debris (LWD) (Daniels and Rhoads, 2003; Daniels and Rhoads, 2004) tend to inhibit circulation cells, which will modify cross-stream and vertical components of turbulence so as to resemble that of a straight reach. Moreover, LWD along river banks tend to redirect the flow towards the center of the channel (Daniels and Rhoads, 2003) much like the case of flow over fences

(Lee and Kim, 1999) and flow deflectors (Biron *et al.*, 2004a); this creates vertical shear layers, which are the sites of intense turbulence activity. Similar vertically oriented regions of flow separation can be produced in tight river bends (Andrle, 1994; Ferguson *et al.*, 2003), yet the strength of this shear layer is highly dependent on upstream geometry. Numerical simulations have demonstrated that the extent of flow separation is increased if the upstream reach is curved opposite to the river bend and reduced if curved in the same manner as the bend compared to a straight upstream section (Hodskinson and Ferguson, 1998) (Figure 15). Similar recirculation zones have been observed downstream of the point bar along sharply curved meander loops in the absence of an upstream bend (Ferguson *et al.*, 2003).

Turbulent processes have clear theoretical implications for meander evolution in a sand bedded river, but research into this subject has been completely confined to laboratory settings, with most studies involving a trapezoidal channel. Due to variable bed topography, flow structure, planform geometry and obstructions, turbulence patterns in natural rivers are inherently far more complicated than those observed in flume experiments. Yet, considering the strong link between turbulent structures and sediment transport, all studies attempting to predict channel evolution should not neglect this phenomenon

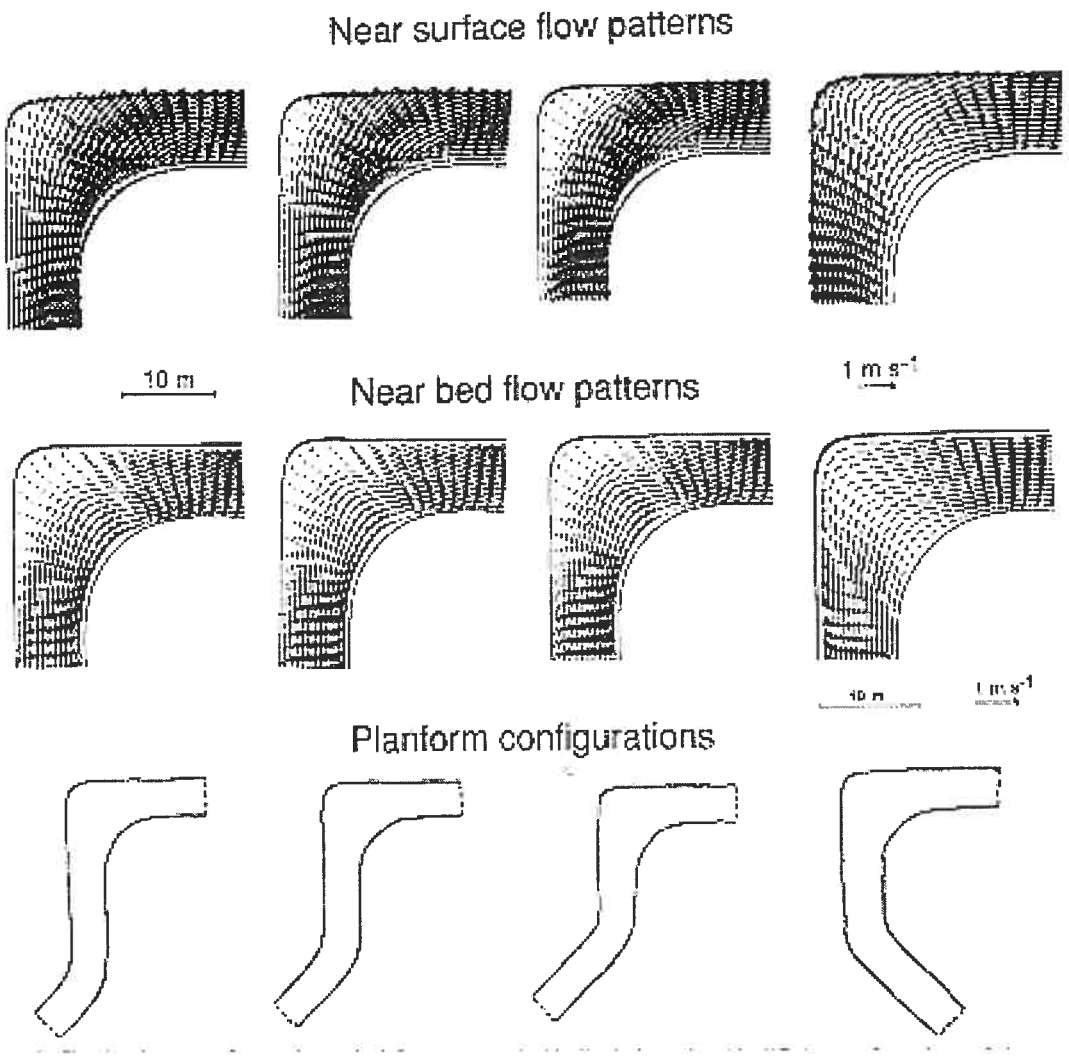

Figure 15: Effects of upstream geometry on extent of flow separation along the outer bank (Hodskinson and Ferguson, 1998).

2.3. Bed Shear Stress Estimation

Despite the fundamental role of bed shear stress in fluvial processes, obtaining accurate estimates of this variable in natural rivers with fully developed flow has proven difficult even in straight reaches. This can be attributed to either the lack of consensus on the proper technique to calculate this variable, different measuring devices used in field studies, or to the lack of an adequate theory in non-uniform flows.

River engineering projects have traditionally quantified this variable using various techniques that assume the flow is uniform, steady and one-dimensional (Chang, 2002). In spite of their success, the aim of such projects is often to maintain a stable channel under bank full or flood conditions. Hence, their bed shear stress estimates are padded by a safety factor to ensure channel stability, which is inappropriate when attempting to evaluate patterns of bed scour by comparing the hydraulic forces of the flow against the critical value needed to initiate sediment transport.

While Dietrich and Whiting (1989) and Biron *et al.* (2004b) have assessed the relative accuracy of the various methods in field and laboratory studies respectively, further investigation is required to resolve under which conditions each method can be applied. In general, it appears as though the appropriate calculation technique depends on both the scale of the project at hand and the channel flow conditions.

2.3.1. Mean Flow Techniques

The most widely applied approach in determining boundary shear stress is the reach-averaged stress method (Dietrich and Whiting, 1989, Petit, 1990), where:

$$\tau_o = \rho g R S_f \qquad (1)$$

where τ_o is bed shear stress, ρ is mass density of water, g is acceleration due to gravity, R is hydraulic radius and S_f is the energy slope. While this method is well suited for studies focusing on shear stress distributions at the reach or watershed scales where obtaining a detailed velocity dataset is problematic, it masks the spatial differences in stress patterns required for projects operating at the bend scale.

The next most common approach to deriving shear stress is based on the assumption that the vertical velocity distribution will follow a logarithmic profile (Prandtl, 1935). Here, the equation is:

$$\tau_o = \frac{\rho(u\kappa)^2}{\left(\ln\left(\frac{z}{z_o}\right)\right)^2} \qquad (2)$$

where u is velocity at a given height above the bed, κ is Von Karman's constant (~0.4), and z_o is the characteristic roughness length. While this method has been used often in smaller scale studies (Petit, 1990; Whiting and Dietrich, 1991; Biron *et al.*, 1998; Kim *et al.*, 2000; Biron *et al.*, 2004b), Kabir and Torfs (1992) highlighted the difficulty in deriving the correct value of z_o over mobile beds. Moreover, obtaining velocity profiles at many locations is impractical for many field studies since time is a major constraint.

While flume experiments have indeed validated the log-law assumption (eg: Song and Chiew, 2001), there is ample evidence that natural bed topography acts as a source of profile distortion. Both laboratory and field studies over gravel (Roy and Buffin-Bélanger, 2001) and sand (Bridge and Best, 1988; Bennett and Best, 1995) have detected zones of recirculation (Figure 10i). Furthermore, Blanckaert and Graf (2001) found that the high speed core of the flow became submerged along river bends, and therefore the assumption of a logarithmic velocity profile is not valid.

More importantly, studies of channel migration pose unique difficulties as they inherently require estimates of bed shear stress at the toe of a bank to evaluate their stability. However, velocity profiles are even more likely to deviate from their expected pattern in these areas since the log-law theory incorporates the bed contribution to flow

resistance, but not the bank component. In their study of the flow structure within a straight reach of a sand-bedded river, Sukhodolov *et al.* (1998) found that the logarithmic assumption is only valid for profiles in the central portion of the channel; measurements in region beyond 0.3 to 0.7 of the flow depth and those where bank proximity is under 0.3 of the channel width deviate greatly from their expected values.

For theoretical estimations the drag coefficient method is often used, which relates the boundary shear stress to the square of water velocity (U). It is defined as:

$$\tau_o = \rho \frac{C_D U^2}{2} \tag{3}$$

where C_D is the drag coefficient. While this method is advantageous in that it requires a single velocity measurement, obtaining accurate results is problematic due to the variability of, and the difficulties of estimating C_D throughout the reach.

A final approach involving mean velocity is to modify equation 2 so it requires a single velocity measurement at any above the bed, which can be done through an argument for boundary roughness. Here, z_o can be estimated through the equation:

$$z_o = \frac{AD_x}{f(R_*)} \tag{4}$$

where A is an empirical constant, D is a length scale of grains controlling resistance where x is the percent finer than that size fraction, and R_* is the Reynolds roughness number (Dietrich and Whiting, 1989), which can be reduced to:

$$z_o \approx 0.1 D_{84} \tag{5}$$

where D_{84} is the sediment size where 84% of all bed sediments are finer.

In spite of these equations having been applied in a range of fluvial research, previous studies on the varying shape of velocity profiles, the contribution of secondary currents and impacts of turbulent processes on stress levels bring the validity of these techniques into question.

2.3.2. Turbulent Flow Techniques

Previous studies have assessed the differences between mean flow and turbulence based approaches to estimate bed shear stress (Dietrich and Whiting, 1989; Kabir and Torfs, 1992; Kim *et al.*, 2000; Huthnance *et al.*, 2002; Biron *et al.*, 2004b). Although a universal method remains elusive, the results of the turbulence based techniques are very promising. Considering the implications of perfecting the link between turbulence and shear stress on our current models of sediment transport and channel evolution, this should be the focus of intensive research. Therefore it is somewhat disconcerting to note that despite the availability of high frequency velocity sampling devices, this topic has never been investigated along natural rivers. Although an experiment was performed in a straight flume tank to evaluate the different turbulence based techniques (Biron *et al.*, 2004b), the authors cautioned that the findings of similar field studies may be inconsistent with theirs due to irregularities in the structure of the flow in rivers. Yet, since no such comparative studies exist, this issue clearly merits further attention.

To analyse a turbulent signal the downstream (u), cross-stream (v) and vertical (w) components of velocity at time t must be broken down into their time averaged values and their instantaneous deviations. They can be written as:

$$u(t) = \overline{u} + u'(t) \tag{6}$$

$$v(t) = \overline{v} + v'(t) \tag{7}$$

$$w(t) = \overline{w} + w'(t) \tag{8}$$

where the overbar denotes the time averaged quantity and the prime, the instantaneous deviation (Clifford and French, 1993).

Using turbulence data, there are three general techniques available to obtain shear stress. The first approach is the Reynolds shear stress technique, whose equation in the downstream-vertical plane (τ_{xz}) is defined as:

$$\tau_{xz} = -\rho\overline{u'w'} \tag{9}$$

where $\overline{u'w'}$ is the time averaged product of the instantaneous deviations of velocity in the downstream-vertical plane (Clifford and French, 1993). This method has been widely applied in both flume studies (ex: Shiono and Muto, 1998; Shiono *et al.*, 1999; Blankaert and Graf, 2001; Song and Chiew, 2001) and natural river studies (ex: Roy *et al.*, 1996; Sukhodolov *et al.,* 1998; Buffin-Bélanger *et al.*, 2000b).

Fluctuations of velocity that contribute positively to Reynolds shear stress are located in quadrants 2 and 4 (Roy *et al.*, 1996) (Figure 16), which are referred to as ejection (quadrant 2) and sweep (quadrant 4) events. By contrast, events lying within quadrants one and three lower the local shear stress value. Previous studies in the boundary layer flow involving quadrant analysis have shown that bursts and sweeps make a larger contribution than quadrants 1 and 3 events (ex: Bogard and Tiederman, 1986).

Despite its prevalence, it has been suggested that equation 9 does not include all the sources of stress (Corrsin, 1957) and that the Reynolds shear stress should actually take the form of:

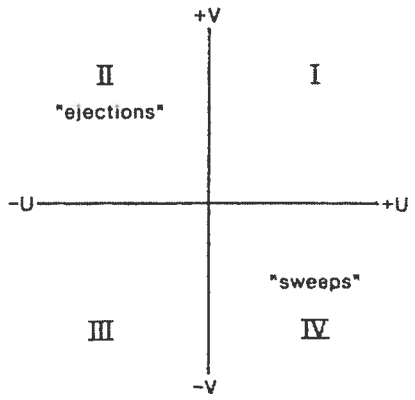

Figure 16: Quadrant description in a eularian frame of reference (Roy et al., 1996).

$$\tau_{xz} = -\rho < \overline{u}w' + u'\overline{w} + u'w' > \qquad (10)$$

Yet it appears as though only one study has attempted to use this technique (Boyer *et al.*, in review).

A fundamental problem with equations 9 and 10 pertains to the orientation of the velocity vectors prior to analysis. The majority of studies to date have defined u' as being parallel to the banks and w' as being perpendicular to the bed (Whiting and Dietrich, 1991, Zhou and Antonia, 1994, Roy *et al.*, 1996, Lee and Kim, 1999, Blanckaert and Graf, 2001). However in the case of meandering rivers where near-bed velocity vectors are strongly skewed towards the inner bank due to secondary currents (Rhoads and Welford, 1991), it may be more appropriate to rotate the data so that the downstream direction is parallel to the streamline. Given that there is a positive relationship between velocity deviations and time averaged magnitudes, it is possible that calculated Reynolds shear stress values may be significantly larger in this frame of reference versus the parallel to banks system. Following this logic, it may also be useful

to rotate the velocity data so as to eliminate both the cross-stream and vertical components since many previous studies have indicated that near bank velocity vectors have a relatively strong vertical component (ex: Shiono and Muto, 1998). By definition, a shear stress is a force that is directed parallel to the object which it is acting on (Chang, 2002). This has led some authors to conclude that velocity data must be rotated in such a manner that the "downstream" and "vertical" components of velocity are oriented parallel and perpendicular to the surface over which they are flowing (Maurizi *et al.*, 1997). Such a method, however, has not been applied to fluvial geomorphology studies. Moreover, Roy *et al.* (1996) made the argument that maintaining a consistent frame of reference is necessary as this is a systematic way of analyzing turbulent data, thereby allowing one to compare signals at different locations and draw valid conclusions about the distribution of shear stress.

While the bursting cycle provides valuable insight into the mechanisms of momentum transfer in turbulent flows, its application to bed scour is somewhat limited (Nelson *et al.*, 1995). Although studies have shown that bursts act to maintain the suspension of sediments (Lapointe, 1992) and sweeps induce bedload transport (Drake *et al.*, 1988; Williams *et al.*, 1989), Nelson *et al.* (1995) demonstrated that quadrant 1 events are just as capable of transporting bed sediments as sweeps of similar magnitude, yet quadrant 1 events act to lower the Reynolds shear stress value. Moreover, roughly half of the contribution to the Reynolds shear stress arises from bursting, which should have no impact on scour. These inconsistencies are yet to be resolved. Additionally, it is well documented that instantaneous Reynolds shear stresses can be many orders of magnitude higher that the time-averaged product (ex: Grass, 1971), and hence sediments

may be entrained when the time-averaged product would indicate otherwise. It is possible to employ techniques such as hole-size analysis to isolate strong events (ex: Luchik and Tiederman, 1987), but there is no consensus on what hole size to use. Clearly the uncertainties about proper hole size have serious implications for predicting absolute scour, yet this issue is far less problematic in the context of relative turbulence distributions. The more prominent issue is under what conditions one can expect to find high turbulence intensities.

Turbulence is inherently a three-dimensional phenomenon, yet the majority of studies to date involving Reynolds shear stresses have only examined the effects of turbulence in the downstream-vertical plane. For the case of bank erosion studies in tight meander bends, where secondary currents are relatively strong (Rhoads and Welford, 1991), it may be more appropriate to sum the Reynolds shear stress in the downstream-vertical and cross-stream vertical planes to obtain an accurate value of shear stress. Such an approach was adopted by Huthnance *et al.* (2002), who used the equation:

$$\tau_o = \rho[\overline{u'w'}^2 + \overline{v'w'}^2]^{0.5} \qquad (11)$$

where $\overline{v'w'}$ is the time averaged product of the instantaneous deviations of velocity in the cross-stream-vertical plane. Their use of the Pythagorean theory may be inappropriate, however. Previous studies have displayed that the Reynolds shear stress in the downstream-vertical plane can indeed be negative (Roy *et al.*, 1996; Blanckaert and Graf, 2001), yet the technique used by Huthnance *et al.* (2002) would assign a positive value to the Reynolds shear stress under all conditions.

It is due to the uncertainties about a varying frame of reference and the quadrants that contribute to sediment transport rates that the aforementioned techniques of estimating bed shear stress are difficult to apply in river bends where flow is highly three dimensional. Other turbulent techniques based on turbulent kinetic energy are insensitive to orientation. The first assumes that the shear stress is related to turbulent kinetic energy, and is defined as:

$$\tau_o = c_1 * \frac{1}{2}\rho(u'^2 + v'^2 + w'^2) \qquad (12)$$

where c_1 is a conversion coefficient with a value of around 0.19 (Soulsby, 1983). While turbulent kinetic energy is often calculated in fluvial research when three-dimensional flow data is available (Shiono and Muto, 1998; Sukhodolov *et al.,* 1998; Shiono *et al.*, 1999; Blankaert and Graf, 2001), the use of this variable to calculate shear stress appears to be limited primarily to oceanographic studies with the sole exception of Biron *et al.* (2004b). The obvious advantage of the technique is that it is the only method that incorporates all three components of the flow. Moreover, it does not suffer from the same drawbacks as the Reynolds shear stress approach: it is insensitive to the orientation of the frame of reference. Yet, it is only recently that instruments capable of recording turbulent properties of a flow in three dimensions have become available. As such, and also due to the lower error in the vertical component compared to the horizontal components in these new instruments, an alternative technique of calculating bed shear stress from turbulent kinetic energy has been developed. Here, bed shear stress is defined as:

$$\tau_o = c_2 * \rho \overline{w'^2} \quad (13)$$

where c_2 is a coefficient with a value of 0.9, which is used to convert vertical velocity fluctuations into shear stress as outlined in Kim *et al.* (2000). The application of this equation to fluvial geomorphology research appears to be limited to a single study involving flow deflectors in a straight flume (Biron *et al.*, 2004b). Moreover, it requires a constant relationship of the vertical fluctuations with those in the downstream and cross-stream planes, which may not always be the case. Blanckaert and Graf (2001) demonstrated that within a cross-section, boundary conditions necessitate that the vertical fluctuations are larger than the cross-stream fluctuations in the near bank region whereas the converse is true towards the center of the channel. This highlights the need to include the effects of fluctuations in the three components of velocity when analyzing turbulent data.

3. Methodology

Recall that the objectives of this thesis are to: (1) assess the performance of a pulse-coherent acoustic Doppler profiler (PC-ADP) against an acoustic Doppler velocimeter (ADV), (2) investigate the three-dimensional flow dynamics of a meander loop, and (3) examine the link between turbulence, shear stress and bank failure. The following chapter presents the study site, as well as the data collection and treatment procedures used in order to fulfil these objectives.

3.1. Study Site

The reach being investigated in this study is a section of the Petite Barbue River, located just outside of St. Césaire, Québec, approximately 60 km to the east of Montréal (Figure 17). The bend length is 70 meters along the channel centerline with a depth of 3.2 meters at bank full conditions. Given a radius of curvature of 18.5 meters and a width of 11.5 meters yields a ratio of 1.6, which represents a relatively sharp 180 degree bend. Bed sediments are generally sandy with a D_{50} of 0.38 mm and a D_{84} of 0.92 mm and contained ripples throughout the reach, especially towards the bend entrance. Bank material is highly uniform throughout the bend in both the downstream and vertical directions, and consists of a cohesive mixture of clay and silt.

The site is ideally suited for this project for two reasons. Firstly, variations in flow stage are limited by a small, decommissioned dam located approximately 650 meters upstream of the study bend, thereby maintaining a relatively constant discharge throughout the majority of the data collection period, which extended from May, 2001 to October, 2004 (Figure 18). Such conditions are favourable since constant flow stages allow for a rigorous examination of the interaction between flow structure, turbulence

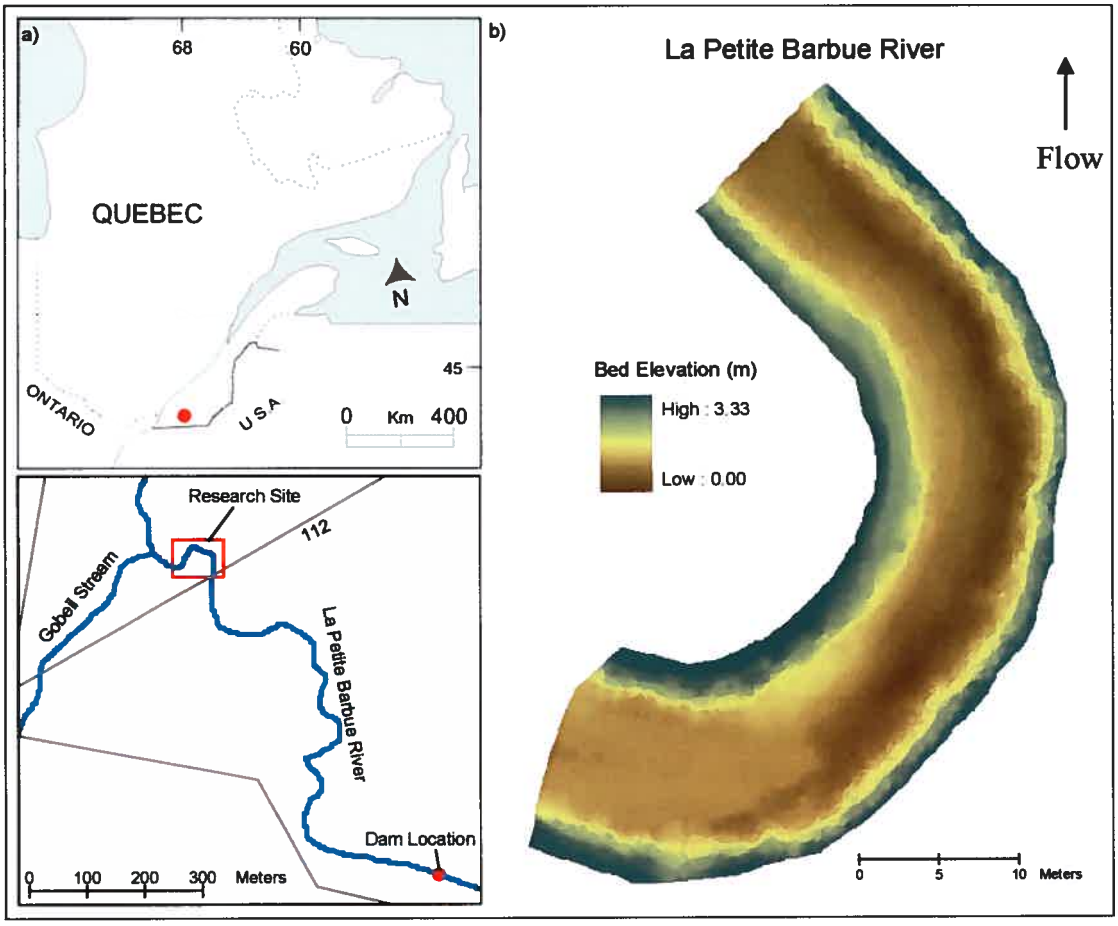

Figure 17: a) Location of study bend, b) Bed topography of the study reach.

characteristics and bank failure in isolation from the extreme flood events that typically dominate patterns in channel evolution. Additionally, it has been suggested that turbulence plays an important role in erosion and sediment transport if the channel's flow is in equilibrium with its sediments (Drake *et al.*, 1988). Another interesting aspect of this site is how a decommissioned dam will affect channel evolution. On the one hand, bankfull flow stages typically correspond with the channel forming discharge. However, bankfull levels are rarely achieved at this site, presumably due to the presence of the decommissioned dam. It is conceivable that channel evolution is controlled by low-flow processes in this type of scenario if nick point develop along the banks under

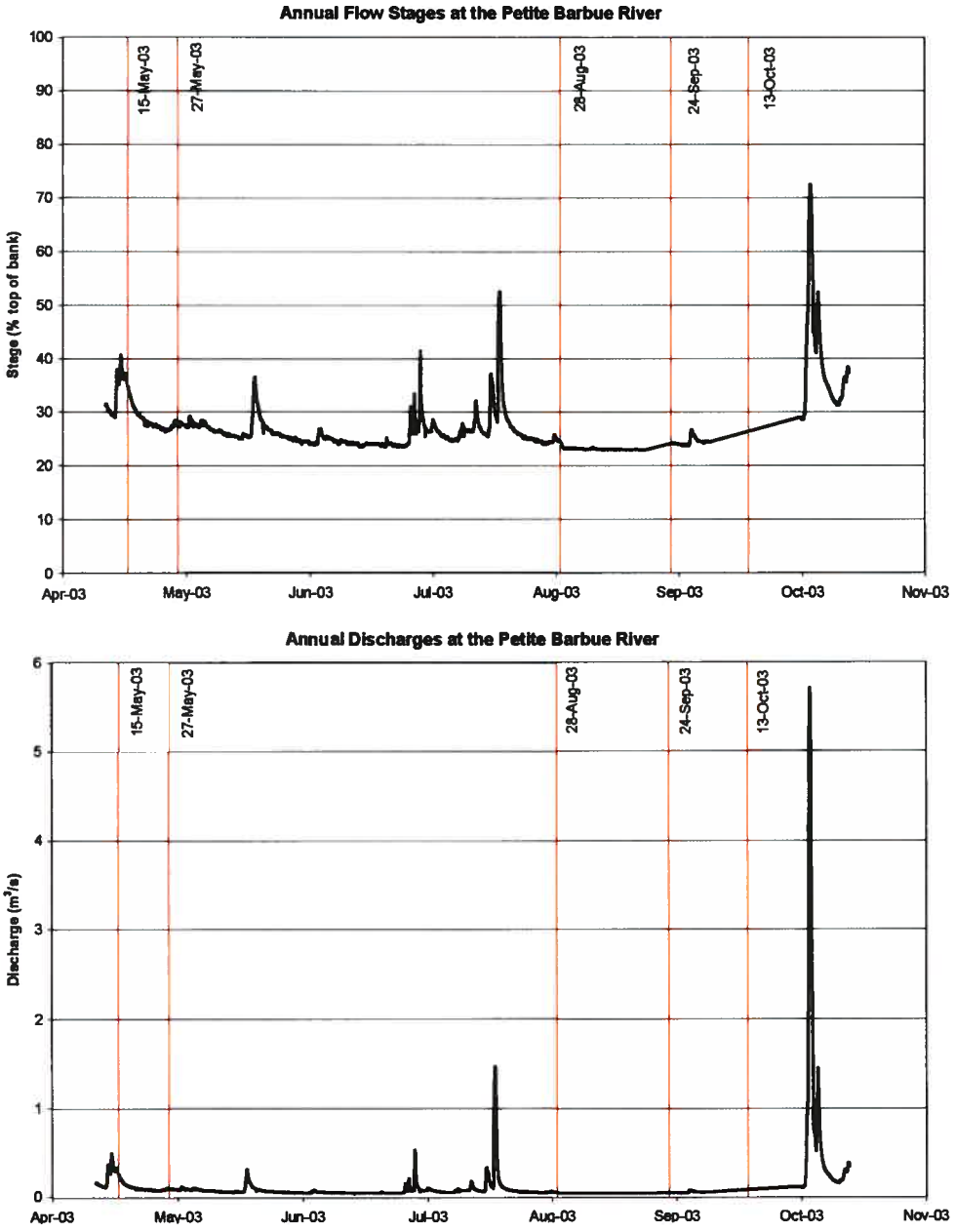

Figure 18: Examples of annual variations in flow stage (a) and discharge (b), based on a rating curve, at the study bend.

these conditions. This would ultimately modify the flow structure at the bank toe at bankfull levels, hence large-scale failure events; the validity of this theory will depend on how well the shear stress patterns at low flow conditions match the spatial pattern of bank failure events. But if this hypothesis is true, the constant discharge levels

maintained by the dam allow one to gain new insights into turbulence driven channel development.

Secondly, the study site is a text book example of a near perfect 180 degree meander loop that displays evidence of multiple bank failure events (Figure 19). Yet, unlike the classical models that predict bank erosion to be most prevalent downstream of the bend apex, reconnaissance trips have shown that failure events are largely restricted to two distinct zones: the bend entrance and exit. In order to prevent any further migration of the channel, stabilization measures were put in place during the first two weeks of June 2003 along the entire length of the bend. Unlike the majority of stabilization projects to date which typically employ "hard engineering" techniques such as rip-rap (Figure 2), this project adopted a "soft engineering" approach. Here, the bank

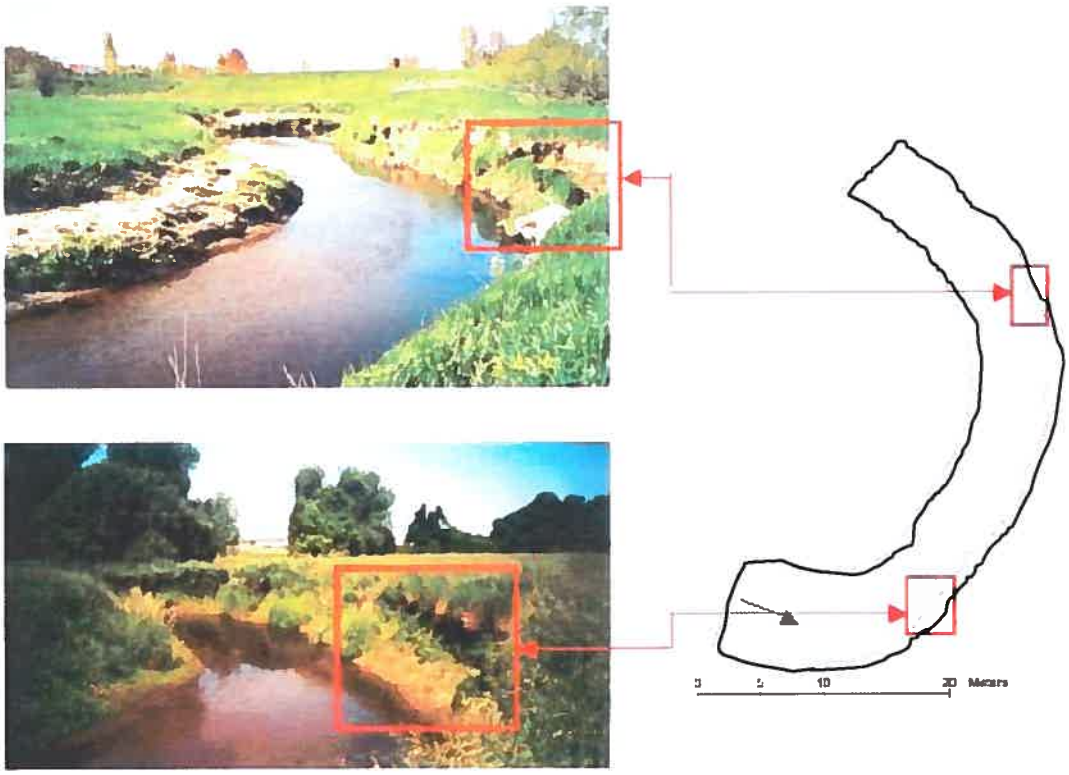

Figure 19: Location of recent bank failure events.

slope was reduced to 30 degrees and its sediments were reinforced by planting woody, water-resistant vegetation between the bank top and the low water line (Figure 3).

3.2. Data Collection

The data used in this project was collected over a period of 3.5 years, 2.5 years of which was obtained while the channel was in its natural state (May 2001 to June 2003) and the remaining year after the banks were stabilized (June 2003 to October 2004). During this time, three types of measurements were collected repeatedly: bed and bank topography, sediment characteristics and three-dimensional velocity measurements.

3.2.1. Bed and Bank Topography

Figure 20: Leica total station.

Measurements of the rivers bed and bank topography were taken using a Leica total station (Figure 20). In order to examine the evolution of the reach over the course of four years, a consistent frame of reference was maintained using permanent benchmarks.

The sampling scheme aimed at obtaining the maximum density of points that time permitted while focusing on regions where there was a significant change in slope. Measurement density varied, but was in the order of $1.06/m^2$ for collection days dealing specifically with topography and $0.81/m^2$ if velocity measurements were also taken.

A total of 11 bed and four bank surveys were performed for this project. Of these, nine bed and two bank surveys were taken while the river was in its natural state, with the remaining two bed and two bank surveys were done after the stabilization measures had been implemented. Although it would have been desirable to present the timing of these surveys with respect to the flood hydrographs to better understand the effects of flow regime on reach dynamics, a combination of instrument problems and data corruption issues prior to 2003 have prevented such an analysis.

3.2.2. Bed and Bank Sediments

Samples of the bed and bank material were collected to characterize the reach and to quantify and map the spatial distribution of critical shear stress through the bend. Such information is crucial not only for identifying zones that are likely to experience a significant degree of bank failure, but also in providing baseline stress levels which can be used to assess the values estimated from the various methods to compute bed shear stress.

Unlike the other variables being monitored for this project, data on the channel's sediment distribution were collected once during the course of this study. However, it is unlikely that this variable would have changed markedly with time since the dam has been present for decades, which is a sufficient amount of time for the channel to have adapted to the changes in flow regime and sediment supply associated with this structure. Additionally, there were no disturbances to the reach that would modify sediment sources or affect the sediment supply between the study site and the dam (Figure 17).

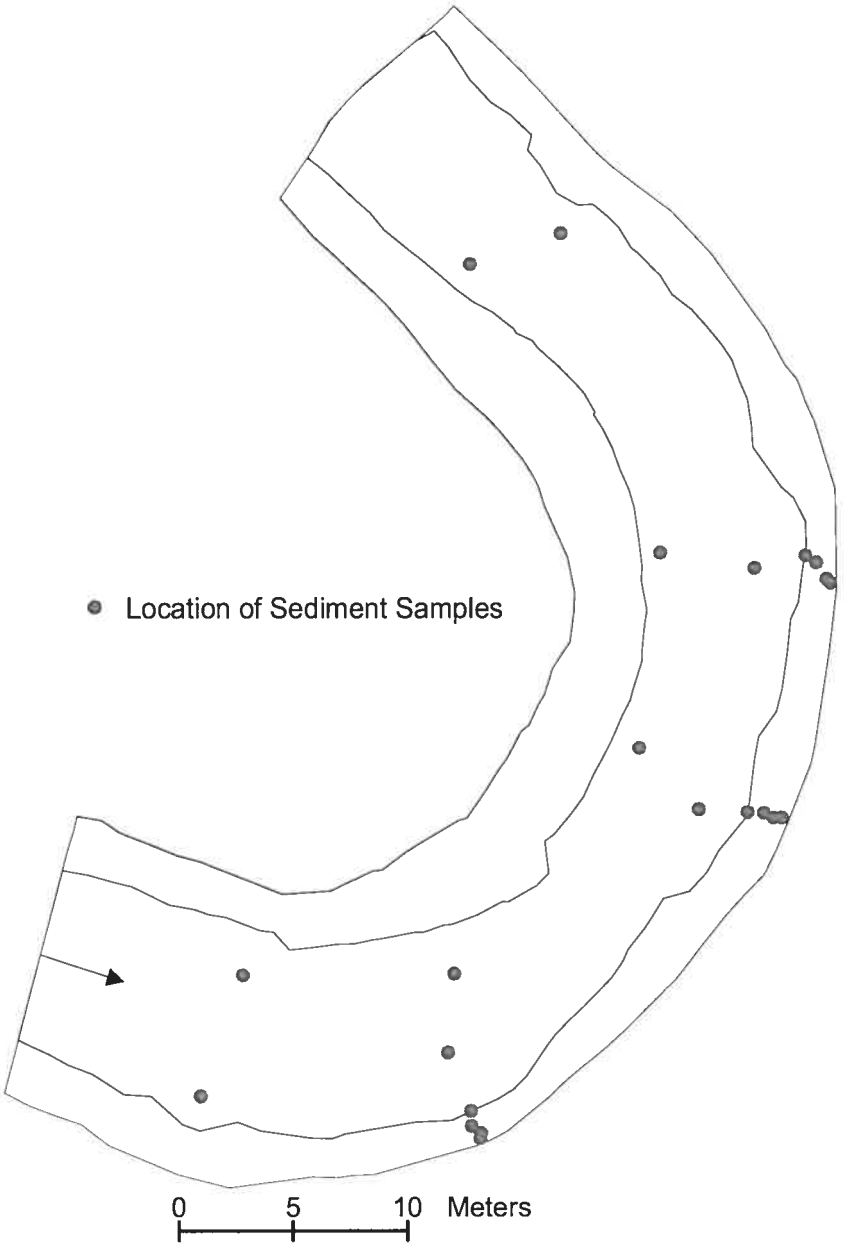

Figure 21: Location of sediment samples.

Bed sediment sampling was conducted at five cross-sections spaced evenly between the bend entrance and exit (Figure 21). A total of six samples were collected per transect; since there was little variation in sediment size between the inner and outer banks, two of the samples were from the bed and the remaining four from the bank face.

After drying and removing any organic compounds from the sample, the sediment size and mass were obtained by hydrometery for the finer fraction and by dry-sieving for the coarser fraction. This information was subsequently used to plot cumulative frequency distributions, from which the D_{84} value is used to calculate the critical shear stress (Petit, 1990).

3.2.3. Flow Velocity

In this project, velocity measurements were taken using two separate instruments: a Sontek acoustic Doppler velocimeter (ADV), and a Sontek pulse-coherent acoustic Doppler profiler (PC-ADP) (Figure 22). Each of these devices is able to take

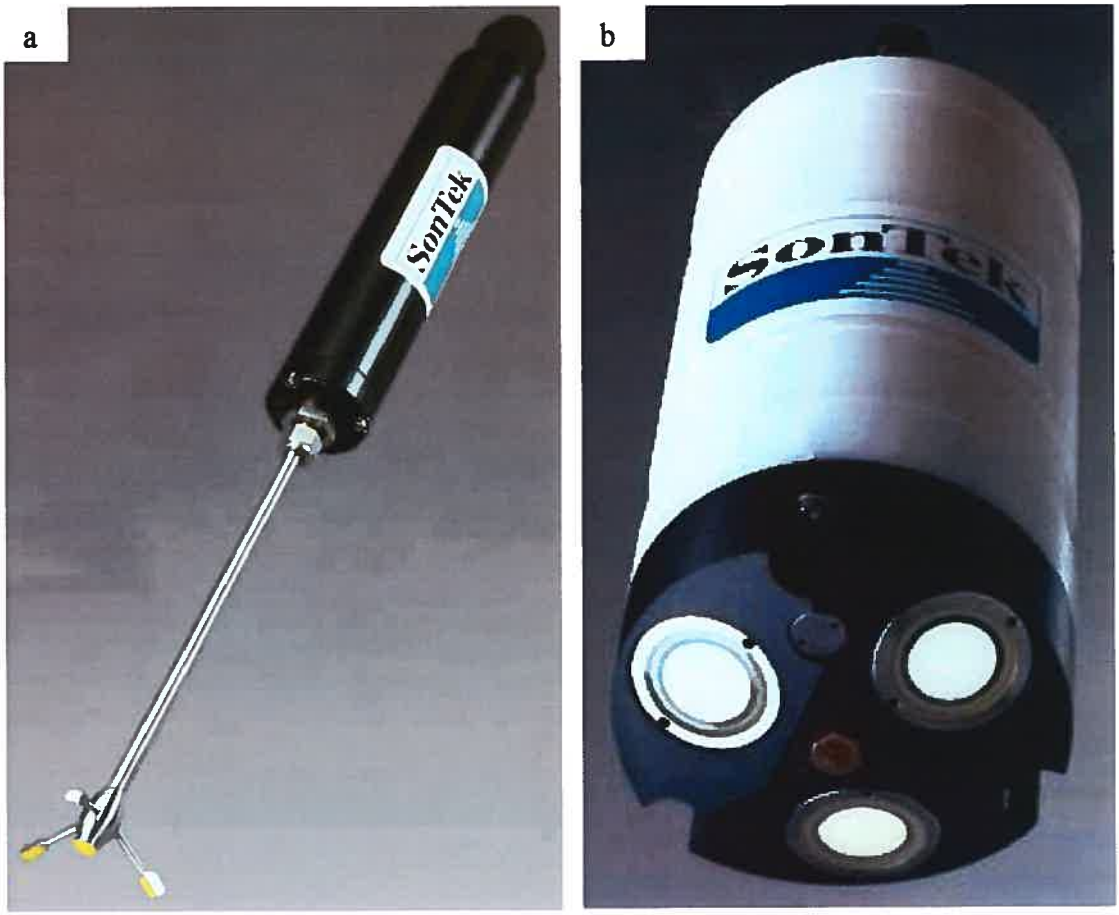

Figure 22: a) Sontek acoustic Doppler velocimeter (ADV), b) Sontek pulse-coherent acoustic Doppler profiler (PC-ADP).

three-dimensional samples of velocity by using the principle of "Doppler shift". The instrument emits an acoustic signal of a given frequency into the flow, which is reflected back to the device by the suspended sediments passing through the sampling volume. Assuming that the water is not stagnant, the frequency of the reflected signal will differ from its initial value. For simplicity sake, consider the flow moving towards or away from the device only. If the motion of suspended sediments is directed towards the device, the reflected signal will have a higher frequency (or shorter wavelength) than its initial value, whereas the converse is true if sediments are moving away from the instrument (Figure 23). Since the receiver that measures the reflected signal on each of

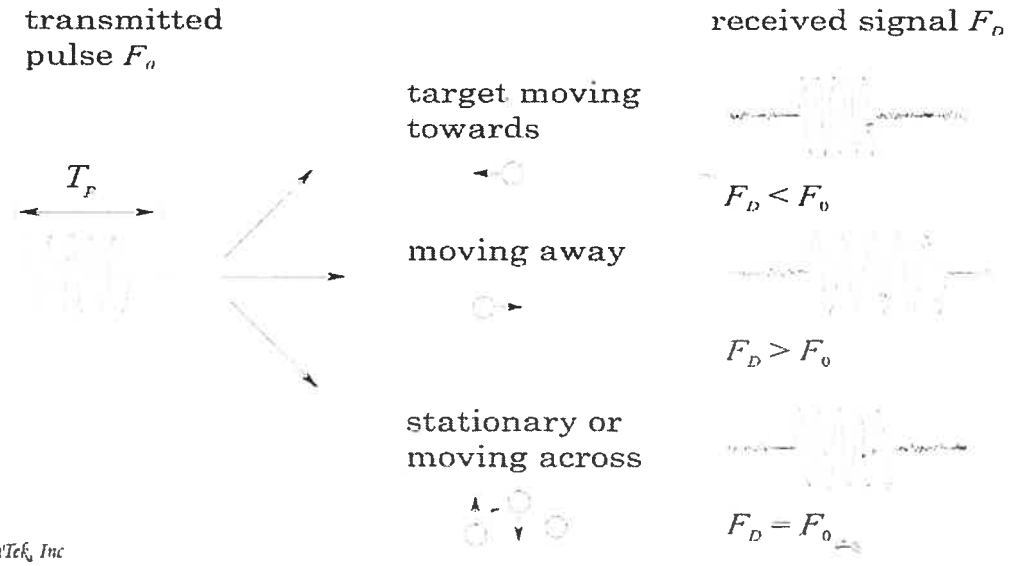

Figure 23: Frequency shift between emitted and reflected signal (From Sontek manual).

these devices consists of three angled sensors, they are able to determine the three components of velocity. Yet, despite the similarities in what is measured and how it is accomplished, these two instruments are different in many respects.

The ADV is used to take single point measurements of flow speed. While this device emits acoustic signals at a rate of 100 Hz, it uses the average of four successive emissions for each instantaneous velocity measurement to improve the quality of the data, yielding a sampling rate of 25 Hz. By virtue of its high sampling frequency and small sampling volume (about 1 cm^3), the effects of spatial and temporal averaging are minimal. Moreover, it is less likely to disturb the flow than more traditional instruments since the sampling volume is located 5 cm from the tip of the probe (Figure 24a). As such, it has become the instrument of choice for *in situ* studies pertaining to turbulence (e.g. Lane *et al.*, 1998; Sukhodolov *et al.*, 1998).

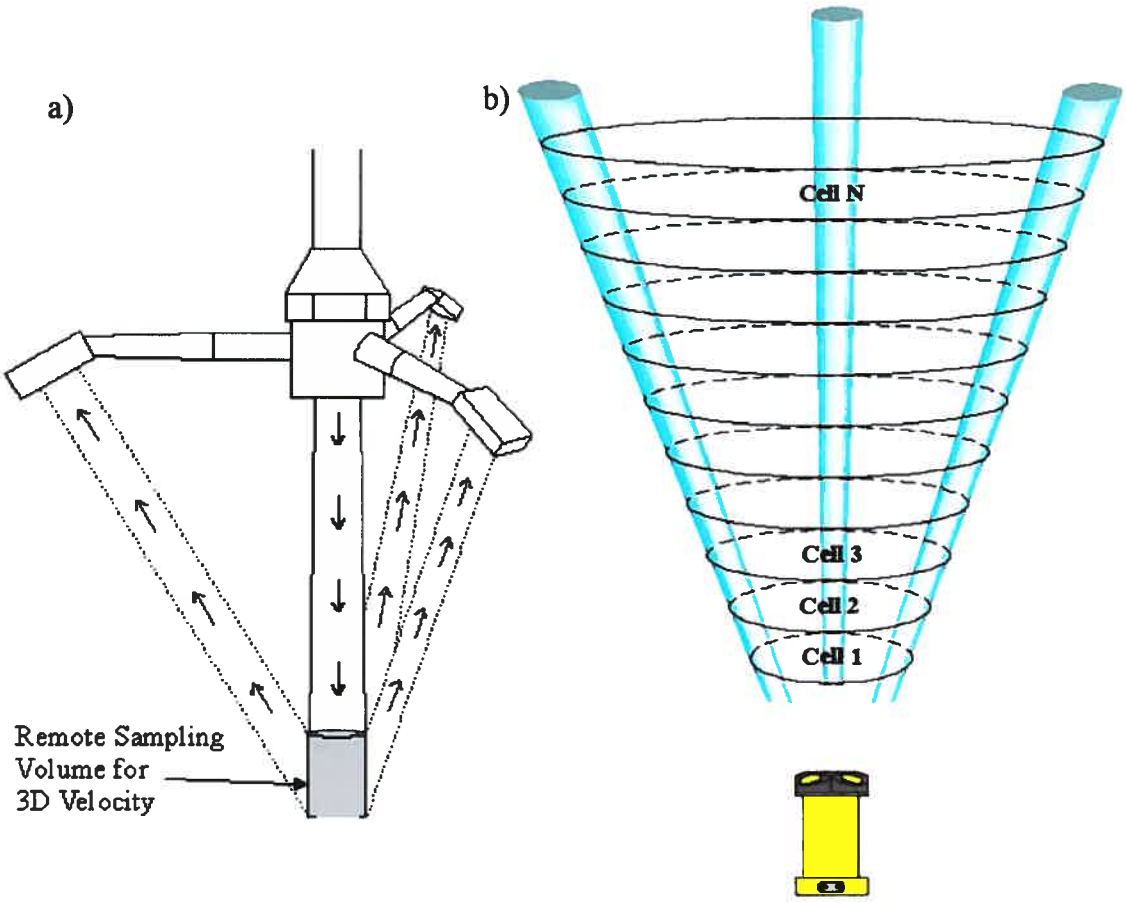

Figure 24: Sampling volumes of ADV (a) and PC-ADP (b).

By contrast, the PC-ADP is used to record instantaneous velocity profiles. This instrument emits acoustic signals at a rate of 4 Hz and uses the average of two emissions per instantaneous profile, yielding a sampling rate of 2 Hz. The width of the acoustic signal emitted by this device from the center to the edge of the beam is 15 degrees. So while the vertical dimension of the sampling volume is defined by the user, its planform area, and hence sampling volume, will increase as the measurement location gets further away from the instrument (Figure 24b). Despite the increased effects of spatial and temporal averaging of flow statistics compared to the ADV, the PC-ADP has one distinct advantage: by recording profiles rather than point measurements, it is possible to identify and study large scale turbulent structures that exist in natural flows.

A custom mounting apparatus similar to that used by Lane *et al.* (1998) was fabricated to deploy these instruments. In this setup, the measuring device is attached to a U-shaped bracket that can slide vertically on a surveying rod (Figure 25). The dimensions of the bracket are chosen so as to displace the sampling instruments by a distance that is sufficient to avoid contaminating the measurements with any rod induced wake effects. Finally, two prisms are mounted on top of the surveying rod at an angle normal to the bracket so that the instruments location in the local coordinate system can be recorded with the total station (Figure 26).

Figure 25: Mounting system of ADV and PC-ADP.

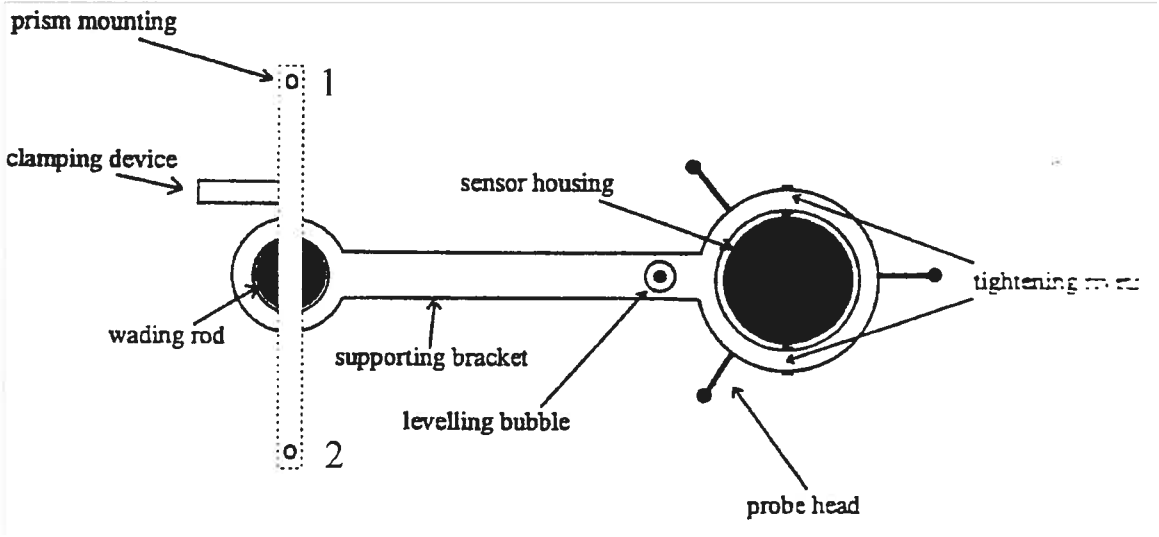

Figure 26: Top view of mounting device (Lane et al. 1998).

The sampling scheme used for collecting data with the ADV consisted of recording measurements at five to seven cross-sections distributed evenly between the entrance and exit of the bend (Figure 27a). Velocity values were recorded at five lateral positions at two or three different depths within each cross-section. In order to perform an accurate analysis of the flow turbulence characteristics, a sampling interval of two minutes was used to obtain a statistically significant measurement, which is equal to three-thousand instantaneous velocity readings (Buffin-Bélanger and Roy, 2005). A total of 6 velocity datasets were obtained over flow stages that ranged from 22 % to 41 % of the bankfull level (Figure 28a). This range should be sufficient for bank erosion purposes since failure occurs due to scour at the bank toe, and sediment transport events were observed during these flow stages. Table I presents the general flow characteristics for each of the collection dates.

A sampling scheme similar to that used with the ADV was adopted for the PC-ADP measurements. Samples were recorded at three locations: at the entrance, apex and exit of the bend (Figure 27b). Measurements were taken at five to seven positions spaced laterally

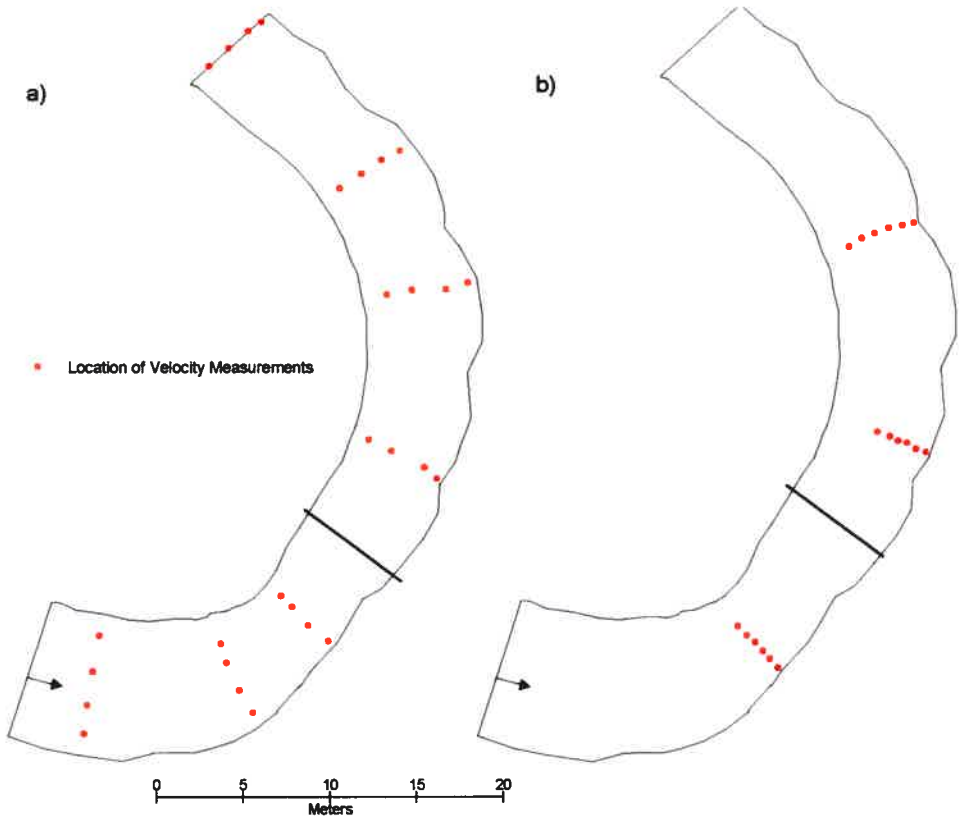

Figure 27: Location of (a) ADV and (b) PC-ADP samples.

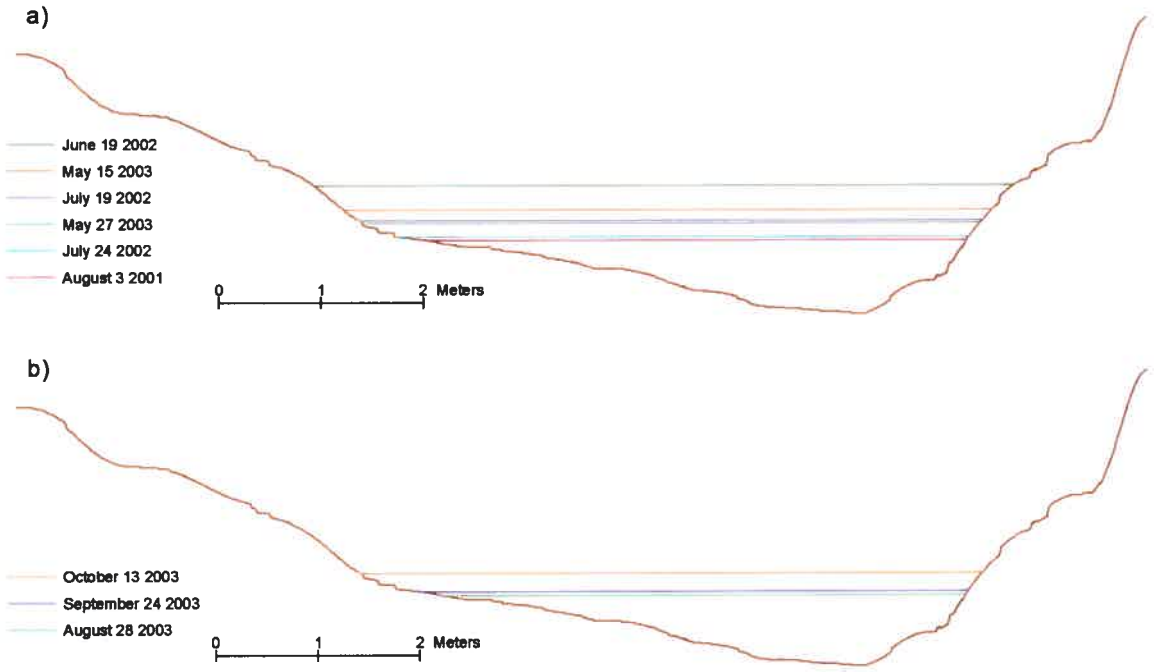

Figure 28: Flow stages of ADV (a) and PC-ADP (b) surveys (location displayed in black on Figure 27).

Date	% of Bankfull	Discharge (m^3/s)	Average Width (m)	Average Depth (m)	Average Velocity (m/s)	Reynolds #	Froude #
August 3, 2001	22.2%	0.12	4.90	0.32	0.08	169.26	0.07
July 24, 2002	23.3%	0.19	5.98	0.31	0.10	224.45	0.09
May 27, 2003	28.1%	0.64	6.46	0.38	0.26	560.05	0.21
July 19, 2002	29.0%	0.62	6.13	0.40	0.25	544.00	0.20
May 15, 2003	32.8%	1.24	7.11	0.54	0.32	651.13	0.22
June 19, 2002	41.2%	2.04	7.58	0.53	0.51	1028.78	0.35

Table I: General flow characteristics of ADV datasets

along each cross-section for a period of fifteen minutes, which is equal to 1800 instantaneous profiles per location. The PC-ADP's sampling volume's vertical dimension was held constant at 4.5 cm; hence the number of measurements in each profile is entirely dependent on local flow depth. A total of three velocity datasets were obtained in this manner over flow stages that ranged from 21 % to 29 % of the bankfull level (Figure 28b).

3.3. Data Processing

Given the experimental setup and the type of equipment used to collect velocity measurements for this project, some processing procedures must be carried out before analyzing the data. In general, they can be summarized as follows: determining instrument location, rotating the components of velocity, and treating the velocity signal.

3.3.1. Instrument Location

While the location of the two prisms on top of the surveying rod does not explicitly give the instruments coordinates, it is possible to derive their location with the aid of a few trigonometric formulas (Lane *et al.*, 1998).

As can be seen in Figure 29, the two prisms are positioned at equal distances from the center of the mounting plate, which is threaded onto the top of the surveying rod. Using a Cartesian coordinate system, the location of the rod (x_3, y_3) corresponds to the

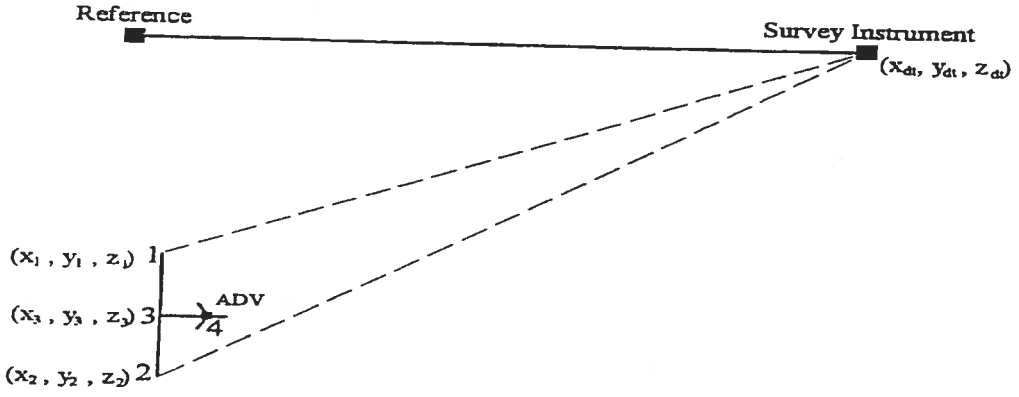

Figure 29: Location of ADV with respect to the surveying prisms (Lane et al. 1998).

average position of the two prisms, which can be calculated by applying the following equations

$$x_3 = \frac{x_1 + x_2}{2}; \quad y_3 = \frac{y_1 + y_2}{2} \tag{14}$$

Here, x_1 and y_1 are the coordinates of the prism closest to the inner bank, while x_2 and y_2 are the coordinates of the prism nearest to the outer bank.

To determine the location of the velocity device, it requires knowledge of both the distance by which they are displaced from the rod and the angle of displacement with respect to the local coordinate system. While the mounting bracket spaces the ADV and PC-ADP from the surveying rod by a fixed distance, the contribution of this displacement to the rod coordinates will depend on the orientation of the mounting system at the time of measurement. The first step is to obtain the angle of the prisms (β_{12}) which can be derived by applying the equation

$$\beta_{12} = \text{ATAN2}(\Delta y_{21}, \Delta x_{21}) \tag{15}$$

In this case, Δx_{21} and Δy_{21} are equal to the difference between the x and y values of the two prisms and the ATAN2 (arctangent) function serves to calculate the circular bearing of the prisms in radians, the values of which will range between $-\pi$ and $+\pi$. Unlike the traditional system where 0^0 is found on the x-axis and the angle increases with a counter clockwise rotation, 0^0 is found on the y-axis and increases with a clockwise rotation in circular bearings. Given that the mounting bracket is perpendicular to the prisms, the bearing of the ADV and PC-ADP (β_{34}) can be obtained using the equation

$$\beta_{34} = \beta_{12} \pm \frac{\pi}{2} \tag{16}$$

Depending on which prism is assigned to location 1, an angle of $\frac{\pi}{2}$ will be either added to or subtracted from the initial value of β_{12}. For this project, the inner bank prism is at location 1, and therefore $\frac{\pi}{2}$ is subtracted from the initial value of β_{12}.

Having calculated the bearing of the instruments, their Cartesian coordinates (x_4, y_4) can be obtained using the following equations

$$\begin{aligned} x_4 &= x_3 + d\sin(\beta_{34}) \\ y_4 &= y_3 + d\cos(\beta_{34}) \end{aligned} \tag{17}$$

Here, d represents the distance between the centre of the rod and the centre of the ADV or PC-ADP in meters.

3.3.2. Velocity Rotation

While attempts were made to ensure that the instruments were parallel to the banks for each measurement, misalignments of a few degrees were inevitable. This is a noteworthy

point since previous studies have highlighted the importance of maintaining a consistent frame of reference when analyzing three-dimensional flow fields (Roy *et al.*, 1996). Even slight variations in sensor alignment can produce significant misrepresentations of the channel's flow structure since both turbulence properties and evidence of circulation cells are highly sensitive to instrument orientation, especially the Reynolds shear stress (Stapleton and Huntley, 1995; Kim *et al.*, 2000). As such, Lane *et al.* (1998) developed a technique that aligns the downstream and cross-stream components of the entire dataset with a common frame of reference: the axes of the Cartesian coordinate system at the site (Figure 30).

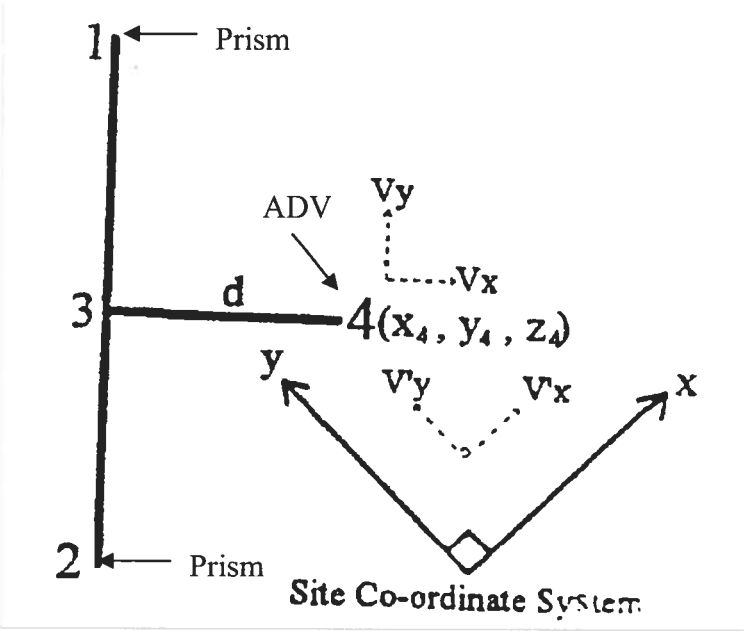

Figure 30: Rotation of velocity components into the local co-ordinate system (Lane et al., 1998).

It should be noted that the Lane *et al.* (1998) approach is not particularly useful for river bends. Since downstream and cross-stream components of velocity are typically defined as running parallel and perpendicular to the streamline (Rhoads and Kenworthy, 1999) or its banks (Roy *et al.*, 1996), the frame of reference for the flow will rotate within the

site coordinate system. Consequently, the Lane *et al.* (1998) technique has been modified for this project.

In this study, the ADV is used to examine the distribution of the turbulent properties of the flow. For this type of spatial analysis, it has been suggested that a consistent frame of reference should be used (Roy *et al.*, 1996). Therefore the downstream and cross-stream components of stress were rotated to be parallel and perpendicular to the banks.

As noted in Lane *et al.* (1998), the rotated downstream (u_{corr}) and cross-stream (v_{corr}) components of velocity can be derived by applying the following equations

$$\begin{aligned} u_{corr} &= u \sin(\beta_{corr}) - v \cos(\beta_{corr}) \\ v_{corr} &= u \cos(\beta_{corr}) + v \sin(\beta_{corr}) \end{aligned} \tag{18}$$

Here, u and v are the initial magnitudes of the downstream and cross-stream components of flow, and β_{corr} is the angle of rotation in whole circle bearings. As can be seen in Figure 30, the value of β_{corr} is equal to the difference between the bearings of the flow measurement (β_{12}) and its corresponding cross-section (I), which can be obtained with the following equation:

$$\beta_{corr} = \beta_{12} - \beta_{x\text{-sect I}} \tag{19}$$

Here, $\beta_{x\text{-sect I}}$ is the bearing of a given cross-section (I) with respect to the local coordinate system. This can be determined by applying the formula

$$\beta_{x\text{-sect I}} = \text{ATAN2}\,(\Delta y_{x\text{-sect I 21}}, \Delta x_{x\text{-sect I 21}}) \tag{20}$$

where $\Delta x_{x\text{-sect I 21}}$ and $\Delta y_{x\text{-sect I 21}}$ are equal to the difference in transect coordinates between the inner (1) and outer (2) banks.

Unlike ADV data, the aim of collecting measurements with the PC-ADP is to investigate the character of secondary circulation cells along river bends. For this type of analysis, Rhoads and Kenworthy (1998) suggest rotating the downstream and cross-stream velocity components so as to run parallel and normal to the mean flow direction of the transect. Considering that circulation cells cause the orientation of a streamline to vary with depth, a Rozovskii-based approach is used to determine the mean flow direction of a transect. Here, proper alignment is said to be achieved when cross-sections display no net lateral discharge. While it has been suggested that such an approach will exaggerate the extent of helical motion along a channel (Lane *et al.*, 1999), Rhoads and Kenworthy (1999) contend that since circulation cells are defined as being features acting along a plane running normal to the direction of mean flow, their technique is not flawed. Moreover, they argue that their technique is superior since circulation cells may not be detected while using a channel line based coordinate system unless the flow is running parallel to the banks. Therefore, multiple iterations are performed on the values of $\beta_{\text{x-sect}}$ in equation 20 until the alignment criterion is satisfied.

3.3.3. Signal Treatment

Prior to analyzing the ADV data, the raw velocity signals must be treated for instrument error. In general, these errors result from low correlation values, instantaneous spikes in the signal, and contamination by Doppler noise (Figure 31).

To determine signal correlation levels, the ADV takes 4 samples for each instantaneous measurement. However, a variety of factors can cause the signal to lose its coherence over this period, thereby creating errors in flow speed. Therefore, each velocity

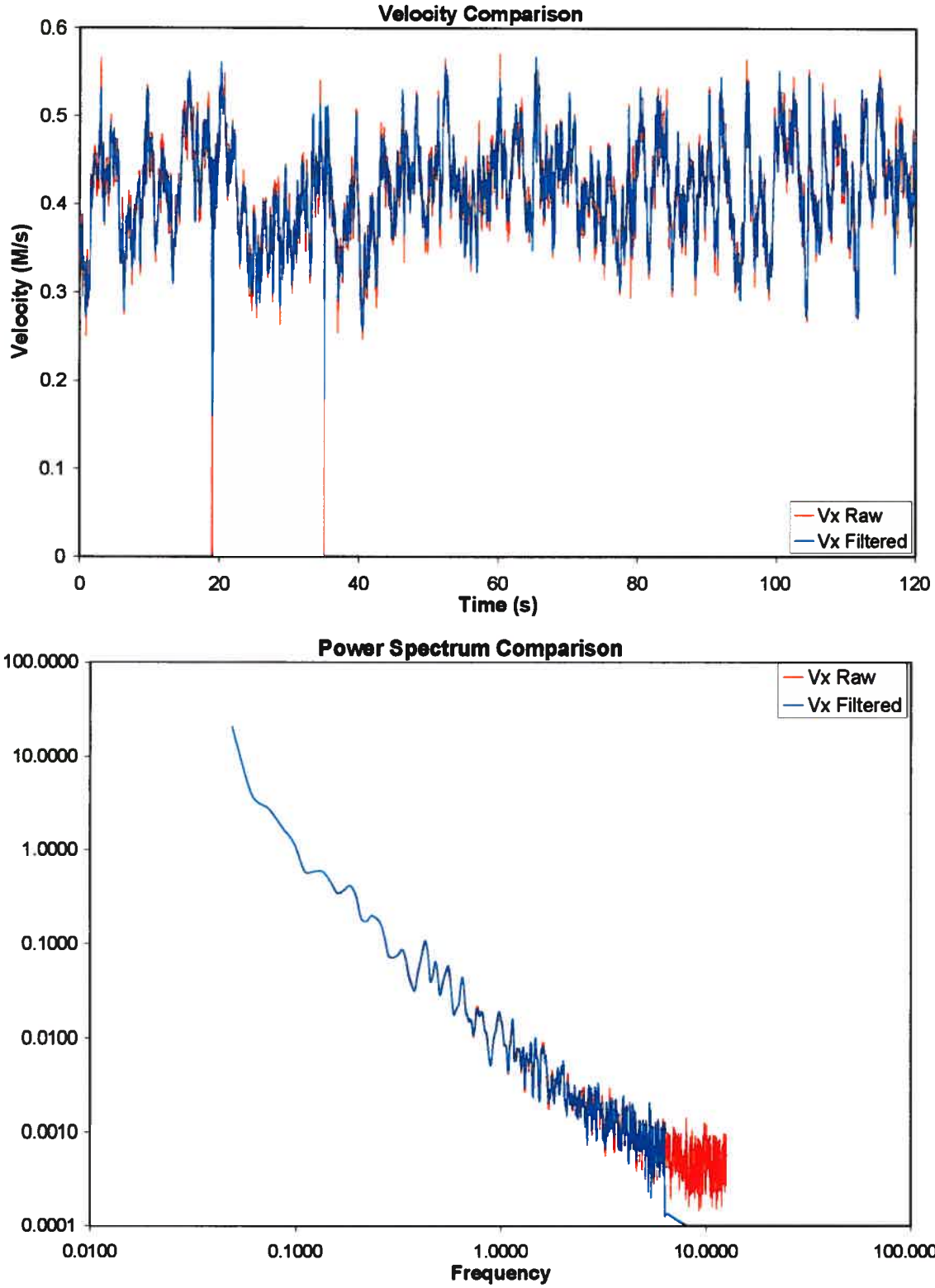

Figure 31: Effect of applying Chebyshev (type 1) filter on (a) velocity signal and (b) power spectrum. Red represents the original signal and blue is the filtered one.

measurement underwent a visual inspection prior to treatment for evidence of signal drift or an excessive number of spikes; this was not an issue in any of the measurements, which is expected given the low energy of the system. Measurements were also checked for low correlation levels and, as suggested by Lane *et al.* (1998), were removed from the survey if their values were below 70%. Out of all the velocity data collected for this project, only three measurements had to be discarded and there was never more than one corrupted signal per collection date. Signal treatment itself consisted of spike removal and applying a low pass filter to the measurements. While there are many ways to detect spikes, Goring and Nikora (2002) demonstrated that their phase-space threshold technique performed the best and was therefore used here. ADV signals are also inherently contaminated by Doppler noise in the high frequency portion of their power spectrums (McLelland and Nicholas, 2000). As such, velocity measurements are corrected by applying a Chebyshev (type 1) low pass filter (Nicholas, 2001) (Figure 31).

3.4. Analysis and Presentation

The initial step in analysis is to assess the performance of the PC-ADP against the ADV for collecting mean and turbulent flow properties to determine the limitations of its application. For this test, measurements were taken in regions of normal (Location 1) and separated (Location 2) flow (Figure 32) using both the devices. Next, the PC-ADP is used to detect large-scale coherent flow structures and illustrate the difference seen in areas of normal and separated flow. The PC-ADP is then used to characterize the helical flow cells along the bend at different flow stages. Subsequently, the ADV data from the main and separated flow regions is used to determine the appropriate technique for estimating bed

shear stress. Finally, a GIS software (ArcGIS 8.2) was used to map the bed topography, water speed, stress distributions and to identify zones of erosion and deposition.

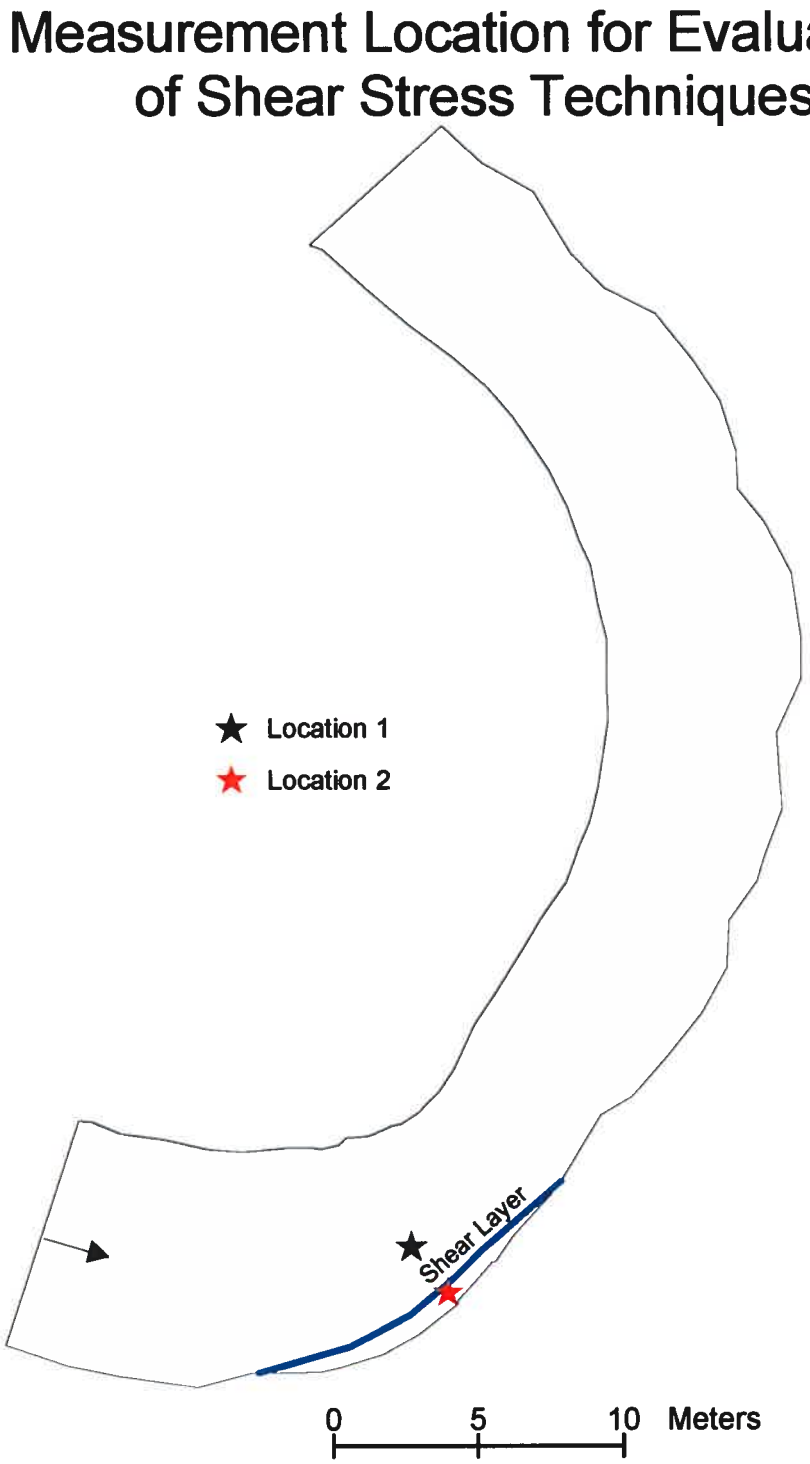

Figure 32: Locations for evaluating shear stress estimation techniques.

4. Results

4.1 Instrument Evaluation

The PC-ADP technology has just recently been available to study fluvial processes in shallow rivers (Vallée, 2003), and there appears to be no definitive conclusion in the literature as to how its measurements are affected by spatial and temporal averaging. As such, the initial section of the results section is dedicated to evaluating its capabilities in terms of measuring mean flow properties, turbulence statistics and identifying turbulence driven processes (Vallée, 2003). To accomplish this, its results are compared against those obtained using an ADV, a standard piece of equipment that uses a similar technology (Doppler shift) as the PC-ADP. In order to bolster the strength of this evaluation, velocity profiles were taken at two locations: in the region of the main flow adjacent to a vertical shear layer where the flow depth is 0.86 m, and one in the region of flow separation where the flow depth is 0.66 m (Figure 32). PC-ADP profiles consist of 16 and 12 vertical points respectively, collected over a span of 905.5 seconds in the regions of the main and separated flow, respectively, while ADV profiles consist of 12 and 11 vertical points collected over a span of 140 seconds.

4.1.1 Comparison of Mean Flow Measurements

Figure 33 presents the three-dimensional velocity profiles obtained with the ADV and PC-ADP in the region of main (a) and separated (b) flow. Samples were first taken with the ADV, then the PC-ADP before changing locations so as to minimize the difference in sampling time between the two instruments while maintaining the same positioning. As for the region of main flow (Figure 33a), the velocity profiles clearly display a logarithmic trend

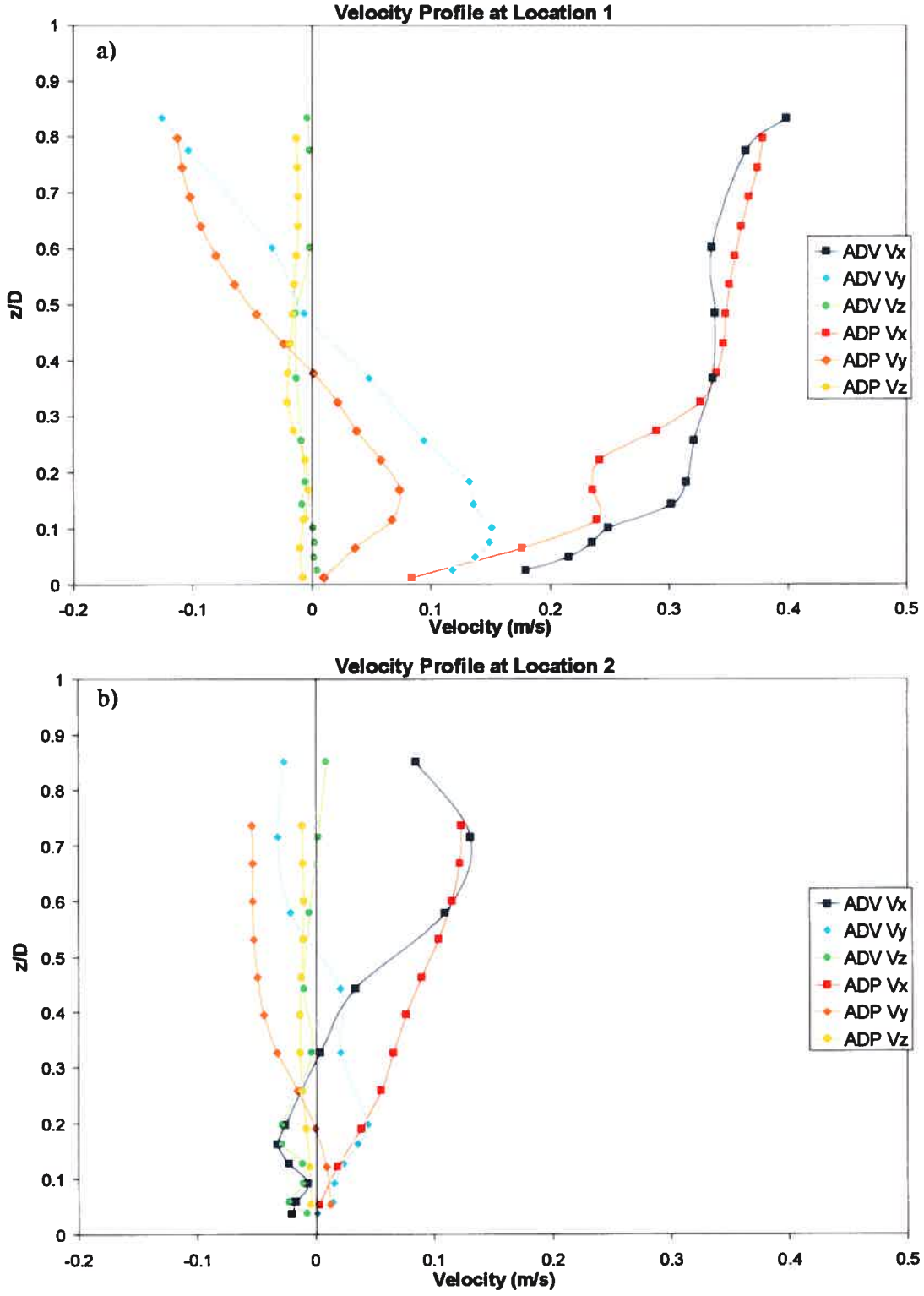

Figure 33: Three-dimensional velocity profiles obtained with the ADV and PC-ADP in the areas of main (a) and separated (b) flow.

irrespective of the sampling device. Moreover, secondary currents are consistently characterized by outwardly directed flow at the water surface (negative lateral component, Vy), mild downwelling towards the outer bank (negative vertical velocity, Vz) and an inward orientation (positive Vy) closer to the channel bed. While the results show that the two devices yield similar results in the upper 70% of the profile, discrepancies in measurements increase towards the bed, resulting in non-zero y-intercepts and slope values that are not equal to one. In the region of main flow, the PC-ADP under-estimates near-bed downstream velocities with respect to the ADV; this produces a negative y-intercept and a slope greater than one in the regression analysis. Presumably, this is due to the larger near-bed spatial averaging effects. In effect, this skews the regression analysis, resulting in a negative y-intercept and a slope greater than one. By contrast, the PC-ADP over-estimates near-bed downstream velocities in the separation zone since the sampling volume extends across the vertical shear layer to include part of the main flow. Hence regression analysis yields a positive y-intercept and a slope that is less than one (Table II). Nonetheless, the high correlation coefficients of the downstream and lateral components of flow (0.905 and 0.975 respectively), and the profiles presented in Figure 33 indicate that the two devices yield similar measurements (Table II). Although the correlation coefficient of the vertical component is lower (0.597), qualitative inspection shows that their values and trends are quite similar.

By contrast, measurements from the region of separated flow highlight that such areas are characterized by atypical, complex flow features, which can have significant impacts on the agreement between the two devices (Figure 33b). Although the correlation of the

		Y-Intercept	Slope	R^2	Correlation Coefficient	Slope (y-Int=0)	R^2
Main Flow	Vx	-0.1505	1.4294	0.8193	0.905	0.9560	0.7277
	Vy	-0.0416	0.7211	0.9500	0.975	0.5110	0.6519
	Vz	-0.0094	0.5455	0.3566	0.597	1.3639	-1.3727
	RMS Vx	0.0485	0.5907	0.3381	0.582	1.2539	-0.1951
	RMS Vy	0.0915	-1.0291	0.4738	-0.688	0.8722	-1.2039
	RMS Vz	0.0090	0.1721	0.5551	0.745	0.3994	-0.5325
Separated Flow	Vx	0.0446	0.6623	0.8386	0.916	0.9598	0.0014
	Vy	-0.0313	0.7401	0.4407	0.664	0.3091	-0.6594
	Vz	-0.0117	-0.2141	0.4590	-0.678	0.3556	-5.4141
	RMS Vx	0.0789	0.2712	0.1835	0.428	1.0893	-1.9592
	RMS Vy	0.0681	0.7009	0.1386	0.372	2.0143	-0.3636
	RMS Vz	0.0045	0.3923	0.7985	0.894	0.4918	0.7434

Table II: Linear regression of mean and turbulent flow properties of PC-ADP versus ADV data.

downstream flow speeds remain high (0.916), it is greatly reduced for the lateral and vertical components (0.664 and -0.678 respectively) (Table II). Moreover, the qualitative agreement between the two devices is limited to the upper 25% of the measurements; whereas the ADV suggests an upstream flow orientation over the bottom 30% of the profile, the PC-ADP indicates that velocity decreases linearly towards the bed, but that it remains oriented downstream (Figure 33b). While attempts were made to minimize sensor misalignment, this is certainly one of the factors contributing to these findings. Although this is not as big of an issue in high energy environments, it can be problematic when dealing with low flow speeds; there are no obvious measures that can be taken to reduce this problem that were not already used in this study. Spatial averaging is certainly another factor contributing to these discrepancies, especially in the near-bed region. The sampling volume of the PC-ADP increases towards the bed to such a degree that its measurements may become contaminated if they either extend across the vertical shear layer or intersect the outer bank. However,

there is a higher qualitative match between secondary currents, which display outwardly directed currents near the water surface, downwelling and an inwardly directed current near the bed as seen in the main flow. Again, there appears to be a constant skew in the lateral component of flow, further indicating that the discrepancy results from sensor misalignment and spatial averaging within the signal rather than an actual difference in the performance of the two instruments.

4.1.2 Comparison of Turbulence Statistics

Figure 34 presents the three-dimensional turbulence statistics of the ADV and PC-ADP measurements in the areas of main (a) and separated (b) flow. In the region of main flow (Figure 34a), maximum downstream RMS values were located at roughly 0.2 of the flow depth and decrease towards the free surface with both instruments, which corresponds well with what is expected in pool entrances where the flow is decelerating (Song and Chiew, 2001). As is the case for mean flow properties, the two devices show increased scatter between their turbulence statistics with bed proximity, although the overall agreement is poorer throughout the profile. While this might again result from instrument misalignment, since turbulence statistics are sensitive to changes in orientation, low correlation coefficients suggest that these findings are a reflection of the increased sensitivity of turbulence statistics to the PC-ADP spatial and temporal averaging effects (Table II).

The situation is worse in the region of flow separation (Figure 34b) with virtually no agreement in RMS values for all three components of velocity. This should come as no surprise considering the initial poor agreement in mean flow properties found in this region. Moreover, the impacts of spatial and temporal averaging are likely amplified here if the sampling volume of the PC-ADP should happen to intersect the face of the outer bank or

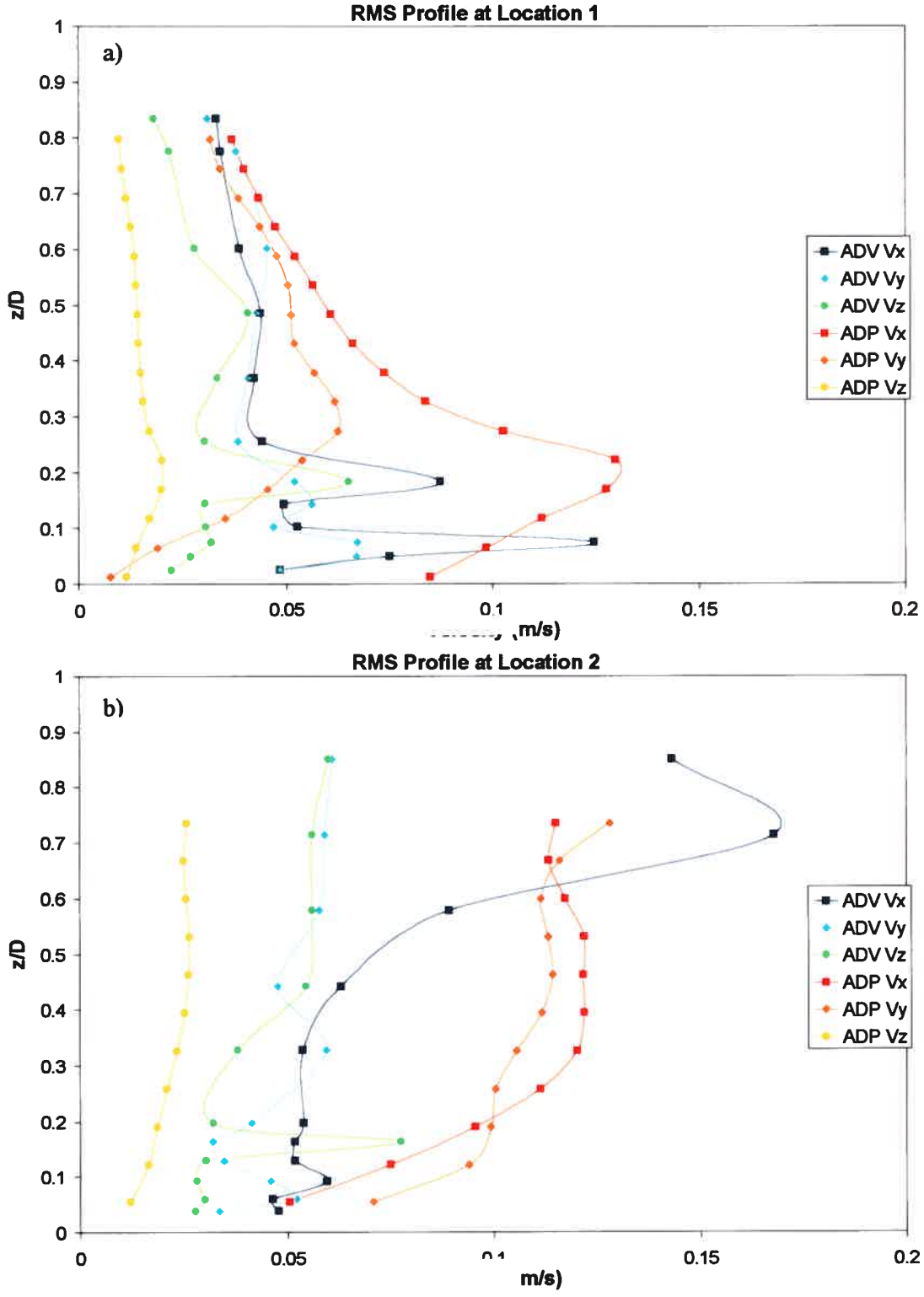

Figure 34: Three-dimensional turbulence statistics obtained with the ADV and PC-ADP in the areas of main (a) and separated (b) flow.

extend across zones. Shear zones generate a high degree of turbulence and their exact location is known to shift with time (De Serres *et al.*, 1999), which could explain the higher RMS values seen in the PC-ADP profile.

4.2 Turbulence Dynamics Across Vertical Shear Layers

Shear layers are a particularly interesting topic in fluvial geomorphology as they are characterized as regions of intense turbulent activity. While many studies have focused on identifying coherent turbulent structures generated in these regions, they have been largely limited to the context of flow separation over the lee side of dunes (eg: Bennett and Best, 1995). Although vertical shear layers have been examined at river confluences (De Serres *et al.*, 1999) and along the inner bank of meander bends (Ferguson *et al.*, 2003), there are no *in situ* investigations on those created by bank irregularities or a non-uniform radius of curvature along the outer half of a channel. As such, this section will focus on the turbulent properties of this particular type of vertical shear layer.

4.2.1 Large Scale Coherent Flow Structures (PC-ADP)

A relatively new development in turbulence-based research is the detection of distinct high and low speed zones in velocity signals that remain structurally coherent throughout the entire depth of the flow (Buffin-Bélanger *et al.*, 2000b). Unfortunately, our knowledge of these features requires further analyses since the published studies relating to this topic have been limited to three (Buffin-Bélanger *et al.*, 2000b), or more recently seven (Roy *et al.*, 2004) vertical measurements using two-dimensional sampling devices. For this reason, it appears as though the PC-ADP provides researchers with an ideal tool to further our understanding of this topic. While questions remain about its ability to yield accurate

turbulence statistics, previous studies using this device in conjunction with flow visualization techniques have confirmed its ability to detect turbulence driven processes (Vallée, 2003), thereby justifying its use in the detection of large scale coherent flow structures.

Due to the increased number of vertical sampling points, the first step is to define what constitutes a large scale flow structure. While no studies have directly addressed this issue, only the events which cover at least 75% of the total flow depth are considered in this analysis.

Figure 35 presents the high and low speed events identified, using the u-level detection technique, from the downstream velocity component i n the region of main (Figure 35a) and separated (Figure 35b) flow respectively. Here, time is represented on the x-axis, relative flow depth along the y-axis and the corresponding thresholds are indicated along the right hand side of the figure; progressively higher thresholds are applied, in increments of 0.5 standard deviations, to identify the particularly strong events. Although distinct coherent structures are visible at both locations under all thresholds, time series analysis of the velocity signals reveal that the high-speed events detected in the main flow measurement initially display a shorter duration and period than low-speed events, but the trend in period is reversed at higher thresholds (Table III). Conversely, the low-speed structures initially display a shorter duration and period in the region of flow separation (standard deviation = 0) after which the trend is reversed. In addition, the absence of high-speed events at thresholds above 2 standard deviations indicates that they are substantially less intense than low-speed structures (Figure 35b). Moreover, all events identified in the area of separated flow are characterized by longer durations and periods than those from the main flow measurements (Table III).

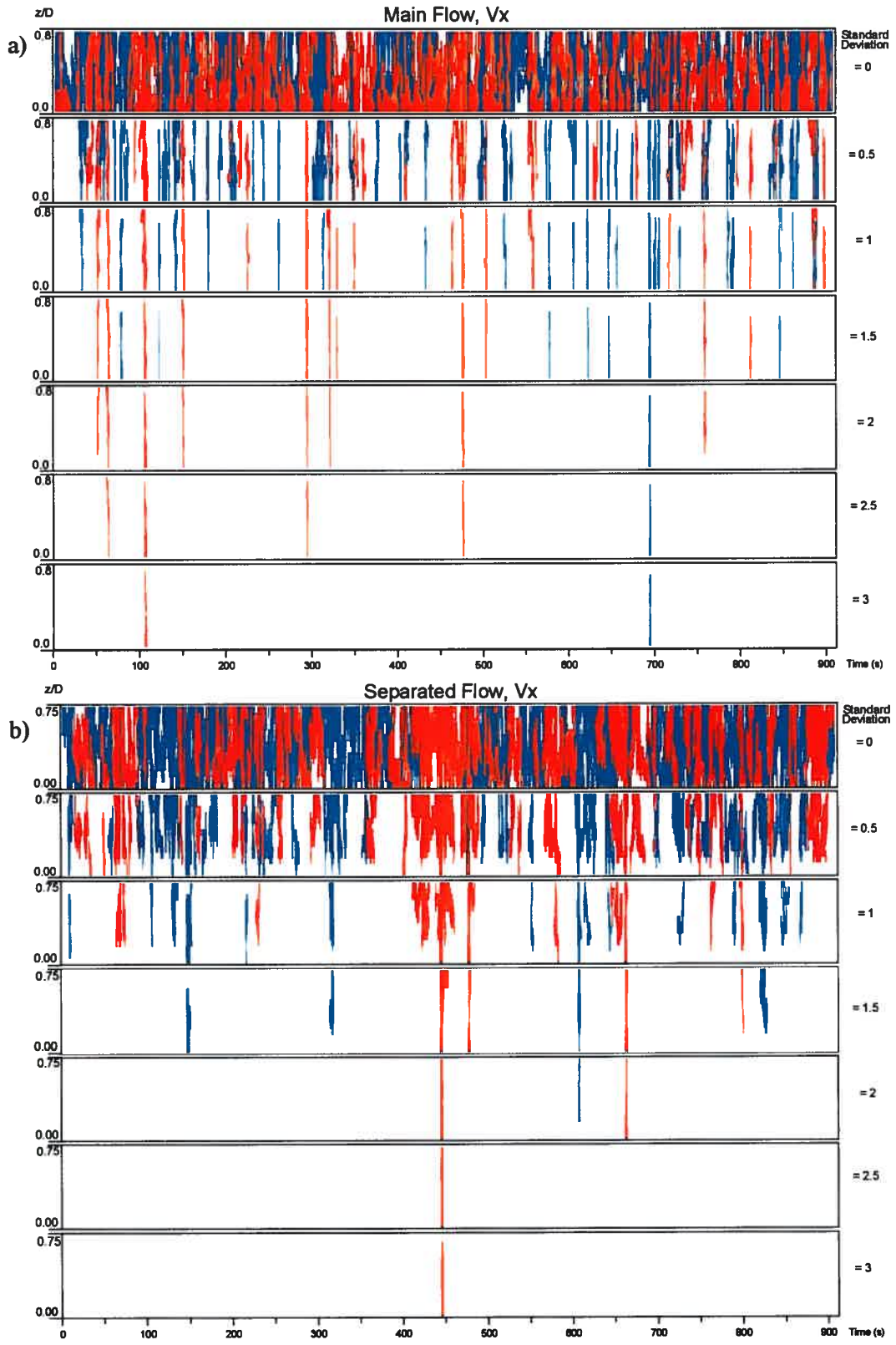

Figure 35: Downstream flow structures identified (via u-level detection technique) using different standard deviations in the areas of main (a) and separated (b) flow (Blue=Fast, Red=Slow).

		Duration (s)				Period (s)			
	# of Standard Deviations	Main Flow		Separated Flow		Main Flow		Separated Flow	
		Fast	Slow	Fast	Slow	Fast	Slow	Fast	Slow
Vx	0	10.3	13.1	15.3	14.1	14.8	16.5	21.1	20.6
	0.5	4.5	4.6	8.2	9.0	18.5	28.3	25.9	25.9
	1	2.2	3.1	5.0	8.7	39.4	50.3	60.4	82.3
	1.5	1.3	2.0	4.9	4.4	129.4	82.3	226.4	226.4
	2	1.5	1.9	1.0	2.5	905.5	113.2	905.5	452.8
	2.5	1.5	1.9		2.5	905.5	226.4		905.5
	3	1.0	2.0		2.5	905.5	905.5		905.5
		Outer Bank	Inner Bank	Outer Bank	Inner Bank	Outer Bank	Inner Bank	Outer Bank	Inner Bank
Vy	0	10.3	16.3	16.7	13.3	14.6	18.5	21.1	18.1
	0.5	6.0	5.6	9.6	8.8	23.8	19.3	29.2	29.2
	1	5.4	4.5	6.5	6.5	90.6	75.5	60.4	75.5
	1.5	2.5	4.3		4.7	452.8	452.8		301.8
	2	1.5			2.5	905.5			452.8
	2.5				2.3				452.8
	3				2.0				452.8
		Bed	Surface	Bed	Surface	Bed	Surface	Bed	Surface
Vz	0	10.6	13.1	12.1	14.8	15.6	17.1	18.5	18.9
	0.5	5.6	6.3	6.8	7.5	18.5	21.6	22.1	21.6
	1	3.6	2.7	5.4	5.1	27.4	60.4	60.4	56.6
	1.5	2.8	1.8	3.6	3.2	82.3	181.1	90.6	301.8
	2	2.0	1.5	2.9		301.8	905.5	226.4	
	2.5	1.5	1.0	2.0		301.8	905.5	452.8	
	3	1.5		2.0		905.5		452.8	

Table III: Summary of average durations and periods for coherent flow structures (identified via u-level detection technique) in the areas of main and separated flow.

Figure 36 presents the structures identified in the lateral velocity component (outwardly and inwardly oriented) of the signals using the same criteria and presentation scheme as previously described. As can be seen in Table III, structures with an outward orientation at low standard deviations display a shorter duration and period than inwardly directed structures, but the trend reverses at higher thresholds (Table III). Overall, the separated flow is much more structured, as was the case with the downstream component. In

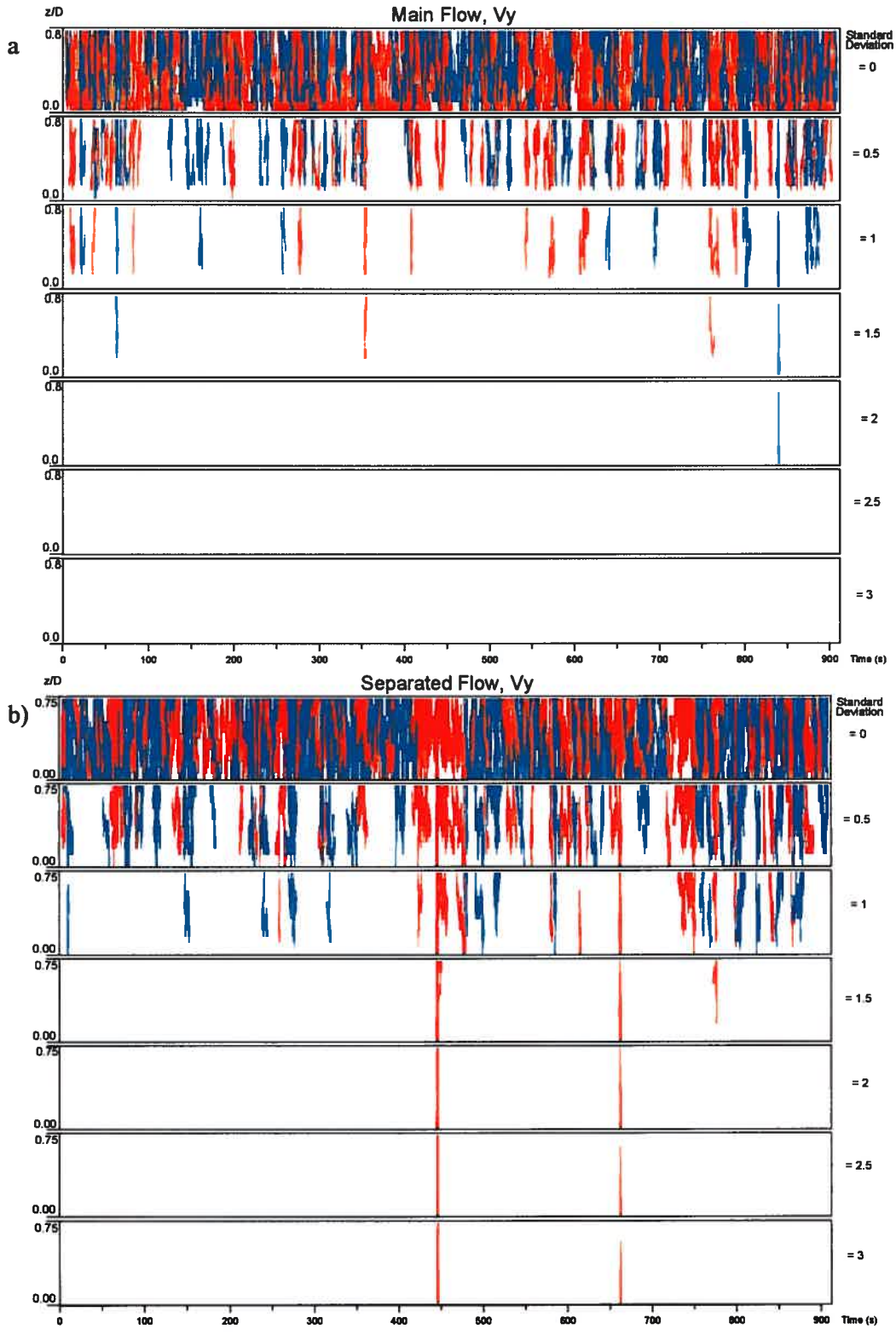

Figure 36: Laterally oriented flow structures identified (via u-level detection technique) using different standard deviations in the areas of main (a) and separated (b) flow (Blue = Outer Bank, Red = Inner Bank).

contrast to the main flow, inwardly oriented events are the stronger of the two in the separation zone (Figure 36b), and while they display shorter durations and periods at low standard deviations, there is a reversal in trends when using the highest threshold at which outwardly oriented structures can still be detected (standard deviation = 1) (Table III). It is interesting to note that the remarkably long inward oriented event lasting from 411.5s to 478.5s in Figure 36b corresponds with an equally long slow moving structure in the downstream velocity component (408s to 473s) (Figure 35b). While the properties of outwardly oriented structures in the main flow are initially similar to the inwardly directed events in the separation zone and vice versa, results obtained under higher thresholds demonstrate that structures oriented towards the outer and inner banks cease to exist in the main flow signal at standard deviations of 2.5 and 2 respectively (Figure 36a), whereas they persist at large threshold values in the separation zone (Figure 36b and Table III).

Figure 37 presents structures identified in the vertical component of the velocity signals that are oriented towards the channel bed and the water surface in the regions of the main (Figure 37a) and separated (Figure 37b) flow. Again, it is evident that the separated flow exhibits a more structured behaviour, although the vertical component is generally less structured than what is seen in either the downstream or lateral velocity components. In general, the bed oriented events have a shorter duration and period, but higher intensity that those directed towards the surface at both locations (Table III). While the main and separated flow measurements display a similar tendency towards higher intensities in bed directed events, this trend is more evident in the shear zone where surface oriented structures cease to persist beyond 1.5 standard deviations (Figure 37b) compared to 2.5 in the main flow signal (Figure 37a).

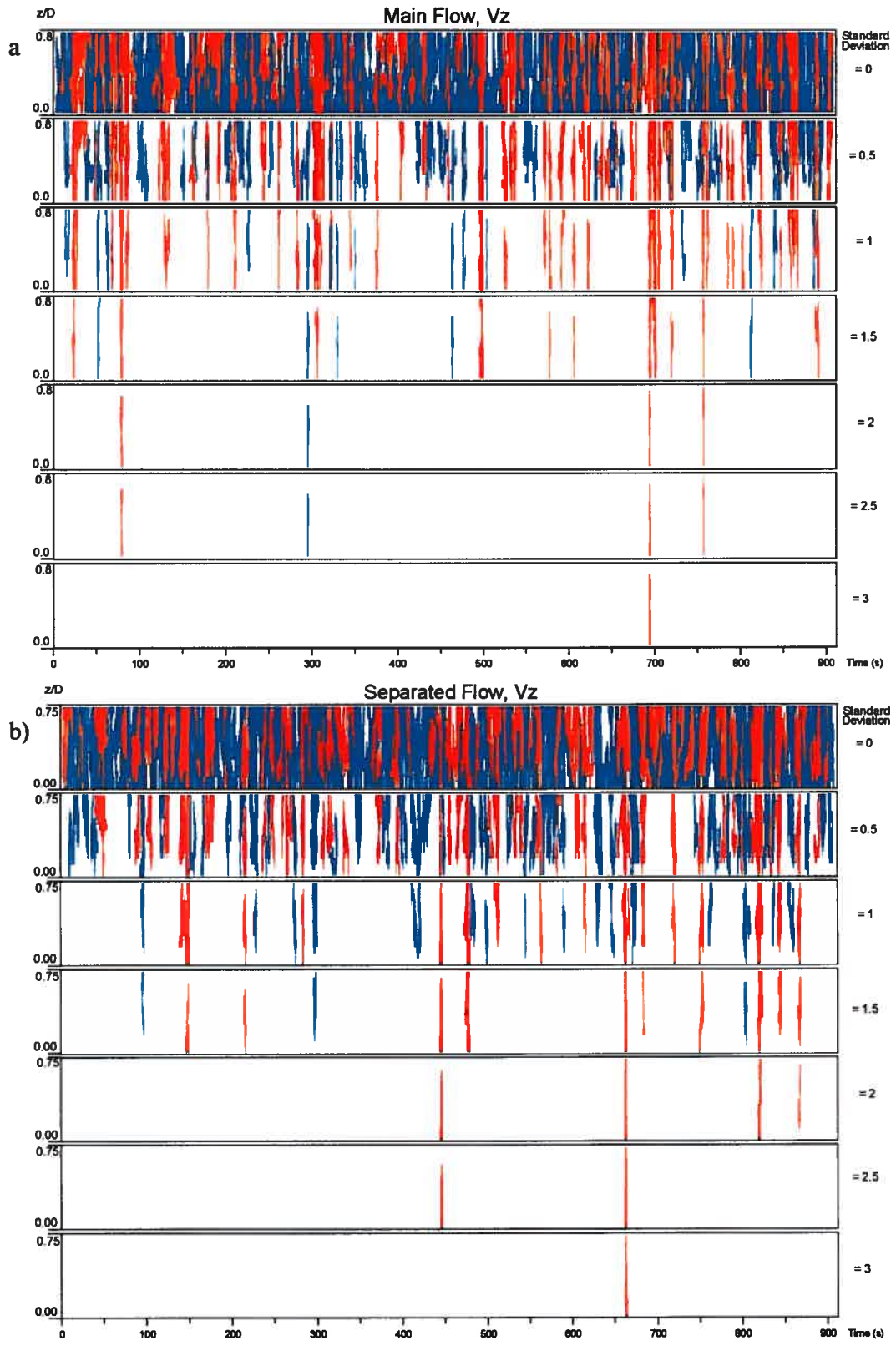

Figure 37: Vertically oriented flow structures identified (via u-level detection technique) using different standard deviations in the areas of main (a) and separated (b) flow (Blue = Surface, Red = Bed).

4.2.2 Burst-Sweep Properties (PC-ADP)

Figure 38 presents the quadrant events identified in the downstream-vertical plane using thresholds of 0 to 3 hole sizes by increments of 0.5 in the region of main (Figure 38a) and separated (Figure 38b) flow. Again, the criterion of structural coherence over 75% of the flow depth for identifying large scale events is retained throughout this section. As can be seen in Figure 38a, quadrant 2 (bursts, in red) and 4 (sweeps, in blue) structures dominate in the main flow. Here, sweeps are consistently more intense and frequent than bursting events, and they display a longer duration for $H > 0$ (Table IV). Conversely, quadrant 1 and 3 structures are characterized by substantially shorter durations, longer periods and lower intensities than either the busting or sweeping events (Table IV). Moreover, quadrant 3 events are by far the weakest of the four structures and cease to persist at a hole size of 0.5. By contrast, there is no clear tendency towards quadrant 2 and 4 dominance in the separated flow (Figure 38b). Although the trend of lower burst intensities under all thresholds relative to sweeps seen in the main flow signal is preserved, quadrant 2 events only display a longer duration than sweeps at lower hole sizes ($H<2$), and actually display a shorter period than sweeping structures at $H = 0$ (Table IV). While the durations and periods of interaction events (Q1 and Q3) remain quite similar under all thresholds, quadrant 3 events are consistently the more intense of the two (Table IV). It is interesting to note that event duration remains similar among all quadrants, yet the periods of interaction structures are substantially shorter than bursts and longer than sweeps at higher thresholds. Additionally, while the intensities of burst and sweep structures are initially higher than the interaction events, those detected in quadrant 3 display the highest intensities at hole sizes greater than 1 (Table IV).

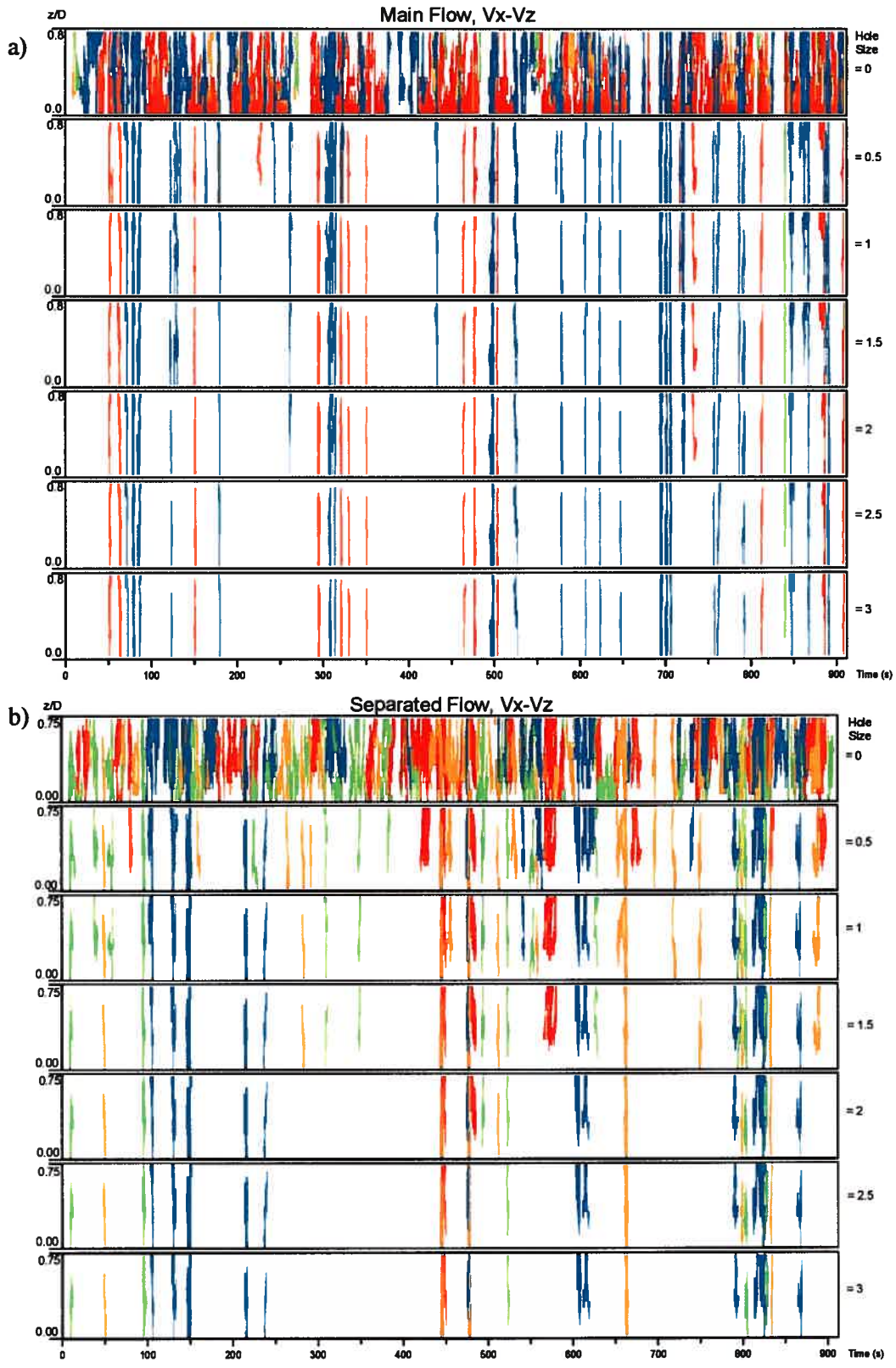

Figure 38: Coherent quadrant structures identified in the downstream-vertical plane using different hole sizes in the areas of main (a) and separated (b) flow (Q1=green, Q2=red, Q3=orange, Q4=blue).

	Duration (s)							
	Main Flow				Separated Flow			
Hole Size	1	2	3	4	1	2	3	4
0	3.8	12.2	4.5	7.1	8.5	7.7	6.2	7.2
0.5	2.0	3.1		3.7	4.7	7.8	4.3	6.3
1	2.0	2.7		3.2	4.3	8.3	4.4	5.5
1.5	2.0	2.6		2.8	3.6	8.3	3.4	5.5
2	1.5	2.3		2.5	3.8	5.0	2.7	5.5
2.5	1.5	2.1		2.5	3.7	3.5	2.8	5.5
3	1.5	2.1		2.3	3.7	3.5	3.0	4.8
	Period (s)							
0	64.7	21.6	90.6	17.8	23.8	27.4	23.8	30.2
0.5	905.5	53.3		27.4	56.6	113.2	50.3	64.7
1	905.5	60.4		31.2	69.7	301.8	69.7	75.5
1.5	905.5	64.7		30.2	90.6	301.8	90.6	82.3
2	905.5	64.7		34.8	150.9	452.8	129.4	82.3
2.5	905.5	69.7		41.2	181.1	905.5	150.9	82.3
3	905.5	69.7		41.2	181.1	905.5	181.1	75.5
	Intensity (N/m^2)							
0	-0.74	2.80	-0.79	4.42	-1.4	3.0	-2.6	4.0
0.5	-3.79	8.41		8.49	-2.6	5.6	-5.7	6.2
1	-4.05	9.41		10.00	-2.9	4.5	-6.8	7.1
1.5	-4.19	9.94		10.31	-3.2	4.8	-9.0	7.6
2	-4.29	10.31		11.52	-3.9	5.4	-12.2	7.8
2.5	-4.33	10.80		13.12	-4.2	4.6	-13.7	7.9
3	-4.40	11.15		13.48	-4.3	4.8	-16.1	7.9

Table IV: Summary of average durations, periods and intensities for coherent quadrant structures in the areas of main and separated flow for Vx-Vz.

Recalling that the lateral velocity component (Vy) is positive towards the inner bank, quadrant 1 and 4 events correspond with structures displaying elevated downstream flow speeds oriented towards the inner and outer banks respectively, whereas quadrant 2 and 3 events contain slower downstream flow speeds that are directed towards the inner and outer banks respectively (Figure 39). As such, bursting and sweeping motions relative to the shear layer's location occur in quadrants 2 and 4 for the main flow measurement, and quadrants 3 and 1 in the separation zone. Figure 40 presents the coherent quadrant events identified in

the downstream-lateral plane for the region of main (Figure 40a) and separated (Figure 40b) flow. Figure 40a clearly illustrates that the downstream-lateral plane contains a broader range of event types than what is seen in the downstream-vertical plane of the main flow signal; coherent structures are distributed relatively evenly among the quadrants at low thresholds, and only a weak trend develops with larger hole sizes. For low hole size values, quadrant 1 and 2 events (oriented away from the shear layer) tend to display slightly longer durations, but this pattern is less distinct at higher threshold values (Table V). While all quadrants display similar periods with a hole size of 0, quadrant 3 and 1 events have the shortest duration once a threshold is applied. It is interesting to note that despite the lack of coherent trends in duration and period, quadrants 3 and 4 (oriented towards the shear layer) display the highest intensity levels at all hole sizes. Moreover, a large number of structures are present under a hole size of three; although higher thresholds were applied to the main flow signal, this eliminated all coherent events in the separated flow signal. Since the aim was to compare coherent flow structures in the two different regions of flow, they

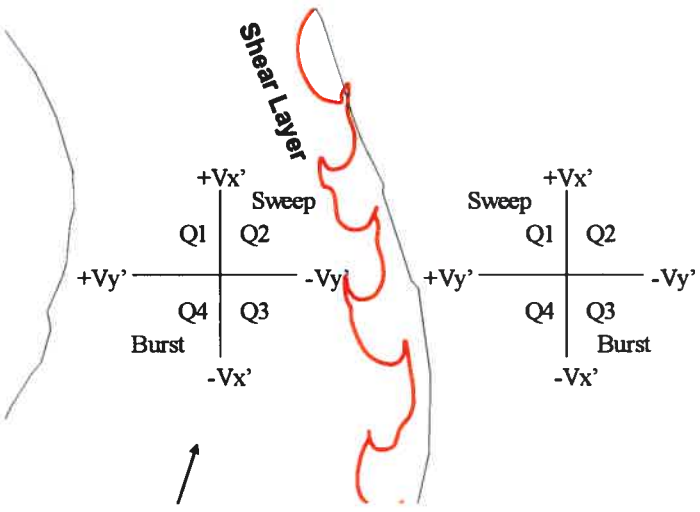

Figure 39: Quadrant location for downstream-lateral plane.

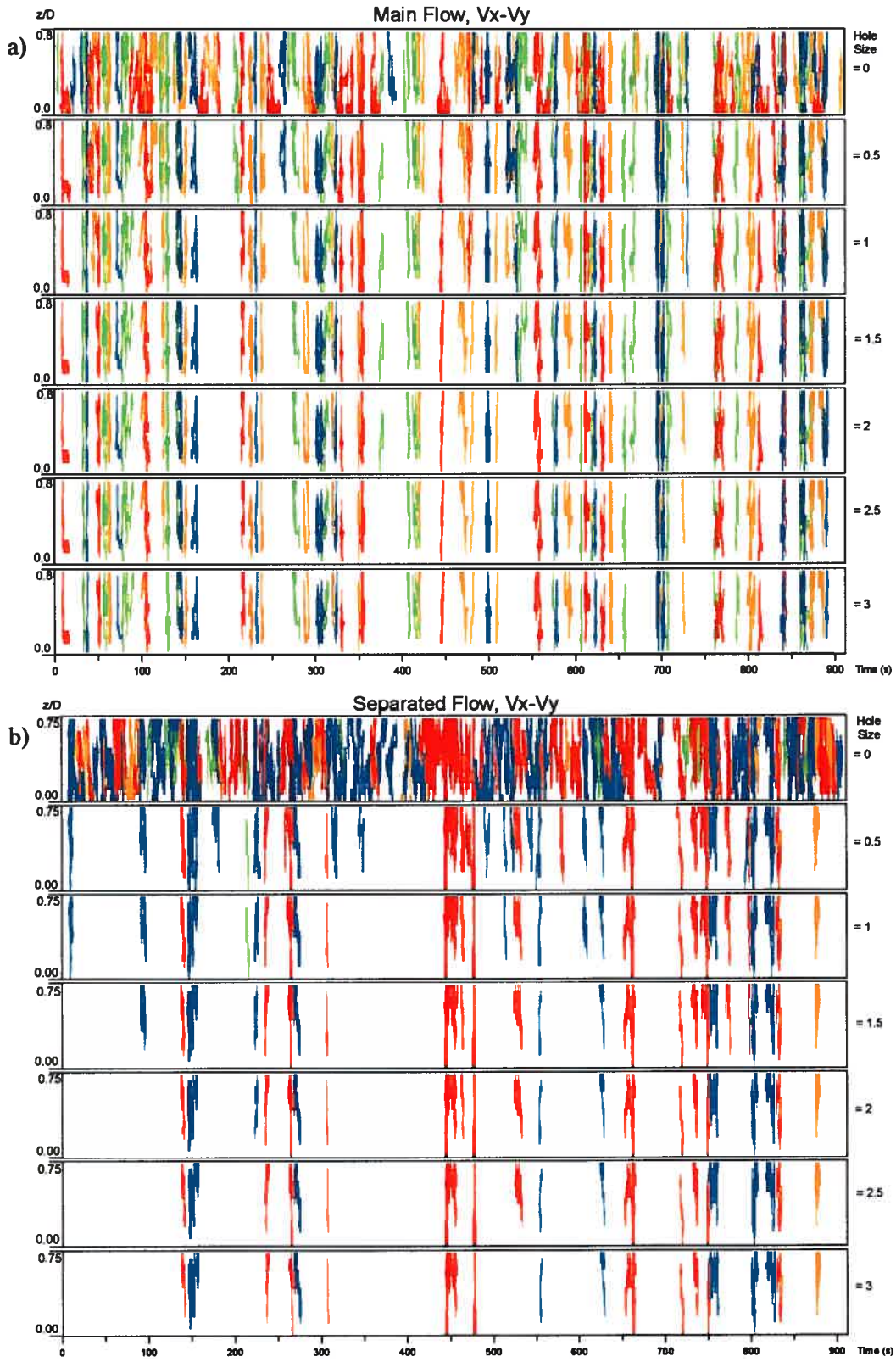

Figure 40: Coherent quadrant structures identified in the downstream-lateral plane using different hole sizes in the areas of main (a) and separated (b) flow (Q1=green, Q2=red, Q3=orange, Q4=blue).

	Duration (s)							
	Main Flow				Separated Flow			
Hole Size	1	2	3	4	1	2	3	4
0	6.7	8.7	5.5	5.4	5.6	9.2	7.2	10.2
0.5	6.2	6.1	5.2	4.6	3.5	6.5	4.0	6.4
1	6.2	5.7	5.0	4.2	3.0	6.6	4.0	6.3
1.5	6.3	5.7	4.8	4.3		6.4	4.0	6.9
2	5.9	5.7	4.8	4.3		5.9	4.0	7.1
2.5	5.2	5.6	4.7	4.2		5.5	4.0	7.5
3	5.1	5.6	4.8	4.2		5.3	4.0	7.4
	Period (s)							
0	29.2	30.2	25.2	36.2	56.6	20.6	75.5	21.1
0.5	37.7	53.3	34.8	47.7	905.5	50.3	452.8	47.7
1	41.2	56.6	37.7	53.3	905.5	60.4	452.8	75.5
1.5	43.1	69.7	43.1	56.6		60.4	452.8	100.6
2	45.3	69.7	43.1	60.4		69.7	452.8	113.2
2.5	47.7	69.7	43.1	60.4		69.7	452.8	129.4
3	50.3	69.7	45.3	60.4		75.5	452.8	129.4
	Intensity (N/m^2)							
0	-4.20	3.01	-5.27	6.99	-7.59	15.94	-9.08	12.32
0.5	-5.10	4.64	-6.31	8.21	-10.45	33.64	-24.31	20.86
1	-5.32	4.76	-6.87	9.06	-10.69	37.62	-24.67	24.17
1.5	-5.55	5.35	-7.61	9.50		38.57	-25.62	21.91
2	-5.70	5.47	-7.74	10.10		37.72	-25.89	22.41
2.5	-5.96	5.58	-7.88	10.28		42.05	-26.22	24.66
3	-6.18	5.69	-8.12	10.43		43.68	-25.79	24.73

Table V: Summary of average durations, periods and intensities for coherent quadrant structures in the areas of main and separated flow for Vx-Vy.

were not presented. Unlike the relatively uniform distribution seen in the main flow, the separation zone displays a high degree of structural organization (Figure 40b). Here, quadrants 2 and 4 (interaction events) consistently display the longest durations, shortest period and highest intensities (Table V), whereas only one quadrant 1 and two quadrant 3 events can be identified after applying a threshold (H=0.5) (Figure 40b).

For the lateral-vertical plane, structures in quadrants 1 and 4 represent motion towards the inner bank oriented towards the water surface and bed respectively, whereas quadrant 2

and 3 structures indicate fluid motion towards the outer bank that are directed towards the water surface and river bed (Figure 41). Figure 42 presents the coherent quadrant events identified in the lateral-vertical plane in the region of main (Figure 42a) and separated (Figure 42b) flow. As can be seen in Figure 42a, the main flow signal is characterized by multiple coherent structures in all quadrants at the highest threshold level (H=3); not only does this indicate that these are particularly intense events, but also that there is a lack of preference for burst, sweep or interaction events. Nevertheless, events detected in the Vy-Vz plane reveal subtle trends in duration, period and intensity. Structures involving fluid motion away from the shear layer (quadrants 1 and 4) display longer durations than those oriented towards the shear layer (quadrants 2 and 3) at all threshold levels (Table VI). This is particularly evident in the case of events where fluid motion is oriented away from the shear layer and towards the water surface (quadrant 1), as their durations are substantially longer than those detected in all other quadrants. Incidentally, this type of fluid motion also displays the shortest period at H = 0. Quadrants 3 and 4 exhibit similar periods up to hole sizes of 2, whereas the period of quadrant 4 increases at H >= 2 (Table VI). Yet, despite the longer durations of events oriented away from the vertical shear layer (quadrants 1 and 4), they are always less intense than those identified in quadrants 2 and 3 (Table VI). Much like the case

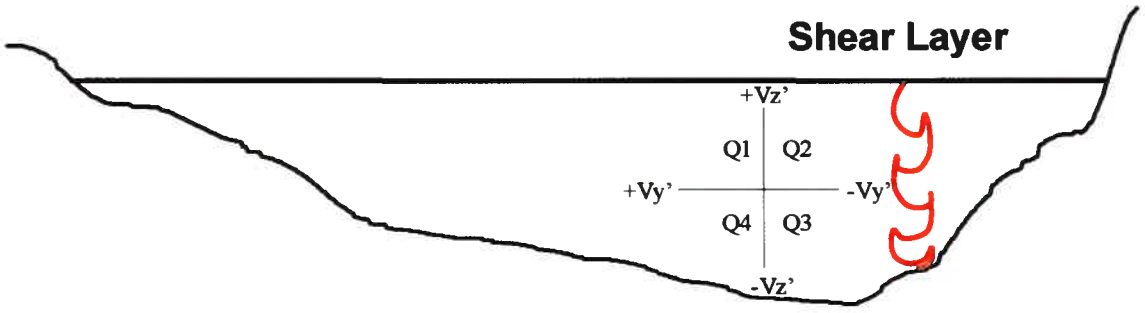

Figure 41: Quadrant location for lateral-vertical plane.

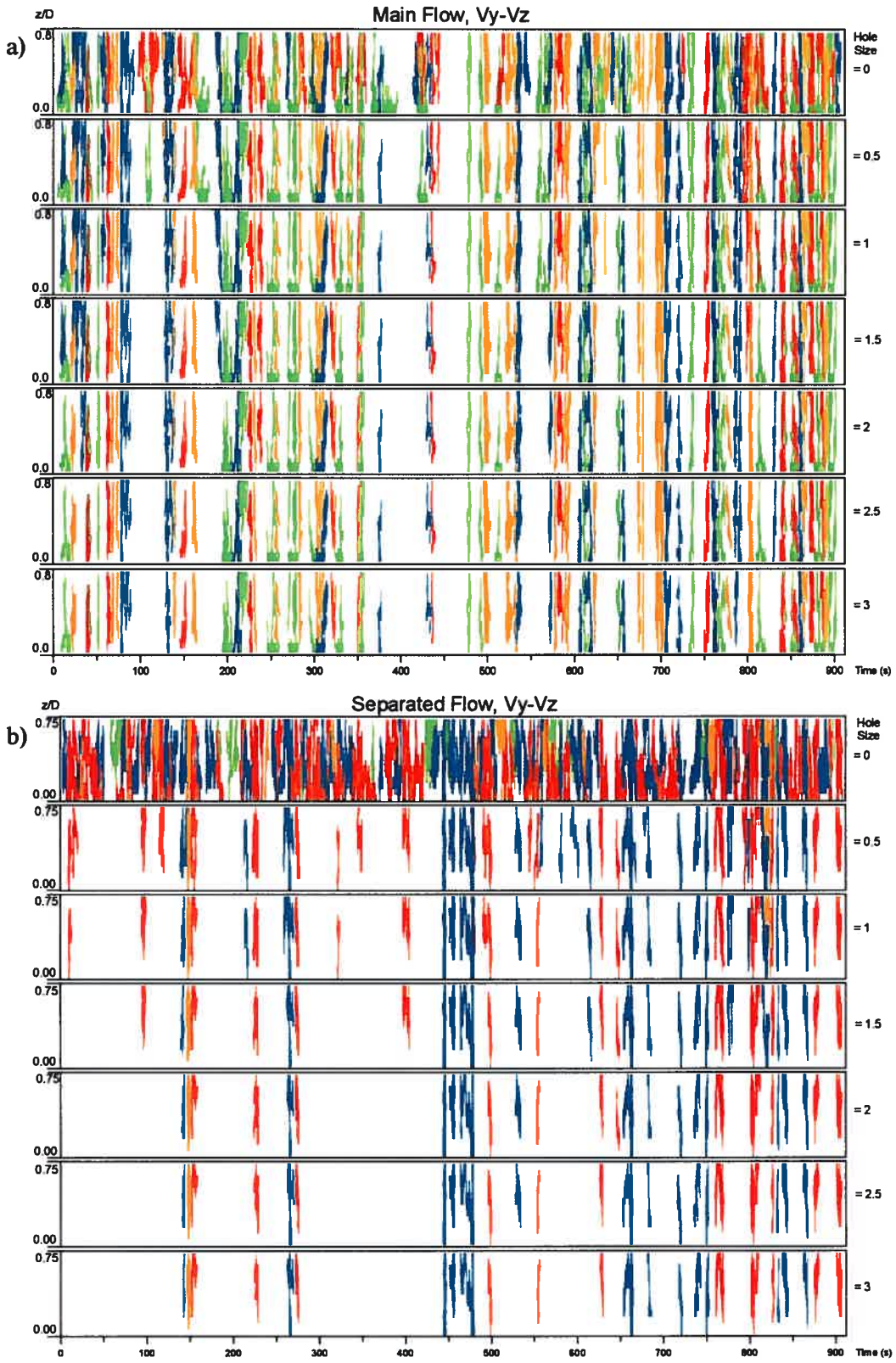

Figure 42: Coherent quadrant structures identified in the lateral-vertical plane using different hole sizes in the areas of main (a) and separated (b) flow (Q1=green, Q2=red, Q3=orange, Q4=blue).

	Duration (s)							
	Main Flow				Separated Flow			
Hole Size	1	2	3	4	1	2	3	4
0	9.4	6.0	5.7	6.4	8.5	11.0	6.0	7.9
0.5	9.2	4.7	5.2	6.1		5.9	6.3	6.6
1	8.6	4.6	5.1	5.9		5.6	6.0	6.2
1.5	8.4	4.7	5.3	5.8		5.8	4.0	6.1
2	8.4	4.8	5.1	5.8		5.6	4.0	6.0
2.5	8.1	4.7	5.1	5.8		5.5	4.0	5.9
3	8.0	4.5	5.0	6.0		5.5	4.0	5.8
	Period (s)							
0	25.9	31.2	30.2	30.2	64.7	20.1	69.7	18.5
0.5	32.3	50.3	33.5	37.7		41.2	452.8	41.2
1	36.2	56.6	36.2	37.7		53.3	452.8	47.7
1.5	41.2	60.4	39.4	39.4		64.7	905.5	53.3
2	41.2	64.7	39.4	45.3		75.5	905.5	64.7
2.5	39.4	69.7	39.4	47.7		82.3	905.5	64.7
3	41.2	69.7	39.4	56.6		82.3	905.5	69.7
	Intensity (N/m^2)							
0	-0.66	1.04	-1.03	0.68	-1.92	2.33	-4.16	3.45
0.5	-0.80	1.36	-1.24	0.86		4.40	-4.76	7.42
1	-0.88	1.55	-1.32	0.89		4.96	-4.94	8.36
1.5	-0.95	1.62	-1.42	0.93		5.43	-6.03	9.30
2	-0.96	1.69	-1.45	0.96		5.58	-6.12	10.18
2.5	-0.97	1.78	-1.47	0.97		5.78	-6.24	10.47
3	-1.02	1.81	-1.48	1.03		5.85	-6.38	11.06

Table VI: Summary of average durations, periods and intensities for coherent quadrant structures in the areas of main and separated flow for Vy-Vz.

of the downstream-lateral plane, flow in the separation zone still reveals a high degree of structural organization. Here, the signal is clearly dominated by events occurring in quadrants 2 and 4 at hole sizes greater or equal to 0.5 (Figure 42b). Of these, quadrant 4 displays slightly longer durations, shorter periods and the intensity of these events is roughly double of those identified in quadrant 2 at hole sizes > 0 (Table VI).

In general, the PC-ADP data shows that it can provide reliable mean flow measurements throughout the upper 70% of a velocity profile. However, near-bed velocities

and measurements taken in separation zones must be treated with caution due to spatial averaging issues. Spatial averaging issues become an even larger problem when comparing turbulences statistics between the two instruments. However, the PC-ADP does seem to be capable of detecting large-scale turbulent flow structures, whose characteristics are consistent with what is seen in the literature. This suggests that spatial and temporal averaging issues of the PC-ADP tend to have a significant impact on the values of turbulence statistics, while still allowing the device to adequately detect the patterns of turbulent velocity fluctuations over time.

4.3 Bend Scale Flow Properties

Having established that the PC-ADP can indeed provide reliable measurements of mean flow properties, and since it is possible to obtain a much higher sampling density than what can be achieved with an ADV over the same amount of time, this instrument was used to investigate the three-dimensional flow structure along the bend. However its abilities to accurately quantify turbulence statistics are questionable, and therefore ADV measurements are also required.

Much like turbulent velocity fluctuations, secondary currents contribute to overall bed shear stress levels, yet they are often treated as second order terms, and therefore omitted from channel design calculations. However, it is well documented that meander loops are characterized by a very distinct helical flow pattern, and secondary currents play a fundamental role in bed morphology of meander loops, and therefore on their evolution. As such, both secondary currents and turbulent velocity fluctuations have practical implications in predicting channel development, especially in instances where a reach is regulated by a decommissioned dam upstream, which maintains relatively stable discharge. However, there

is no consensus on the dominant structure of secondary circulation cells. Moreover, no *in situ* studies have been performed to characterize turbulence distributions along meander loops. Therefore, the aim of this section is to investigate the characteristics of these two features along the study bend.

4.3.1 Mean Flow Properties (PC-ADP)

The PC-ADP was used to investigate the changes in flow structure properties along the study bend on three separate field surveys (August 28, 2003, September 24, 2003 and October 13, 2003) while the respective flow stages were at 21.1%, 22.3% and 28.9% of bankfull levels. Although bank stabilization techniques were implemented prior to collecting these measurements, the impact on flow structure is minimal since the wetted portion of the cross-section was below the level where the bank slope had been reduced and where vegetation had been added.

As can be seen in Figure 43 (August 28, 2003), the bend entrance (Figure 43a) is characterized by elevated downstream flow speeds (V_{max} = 0.30 m/s) with a concentrated high velocity core (V_{max}/V_{avg} = 2.87) in the thawleg located along the outer bank. By contrast, the bend apex (Figure 43b) displays lower values of V_{max} (0.23 m/s) and V_{max}/V_{avg} (2.00), indicating that the high velocity core not only decelerates, but must also diffuses laterally as it travels through the bend to maintain continuity of discharge. In addition, secondary current patterns at the bend entrance differ greatly from those at the apex. While the former is characterized by lateral divergence away from the high velocity core, the latter contains a

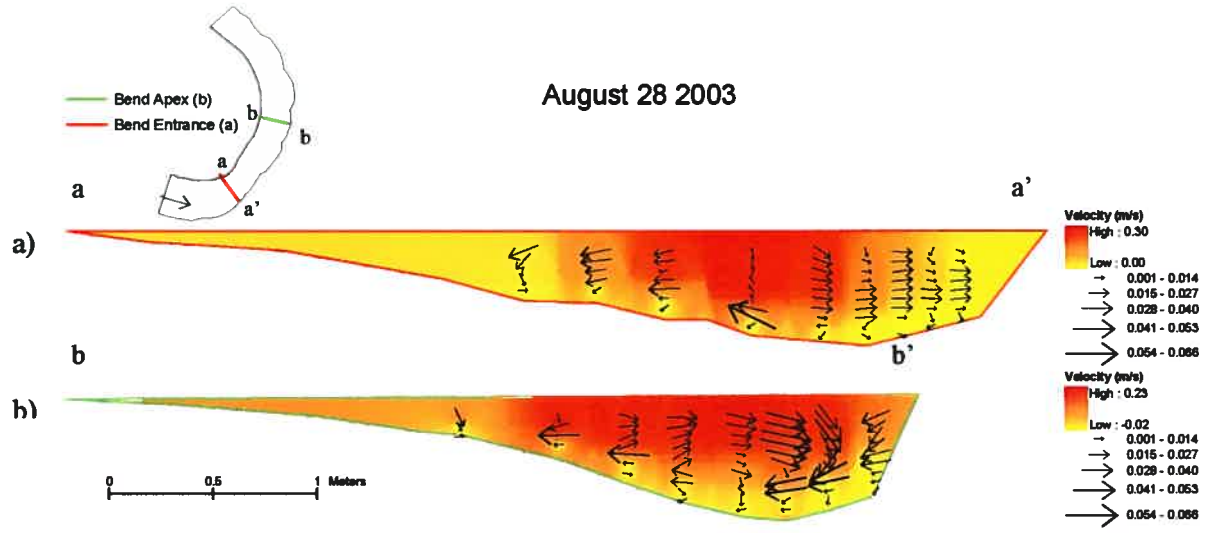

Figure 43: Three-dimensional flow structure at entrance (a) and apex (b) of the bend.

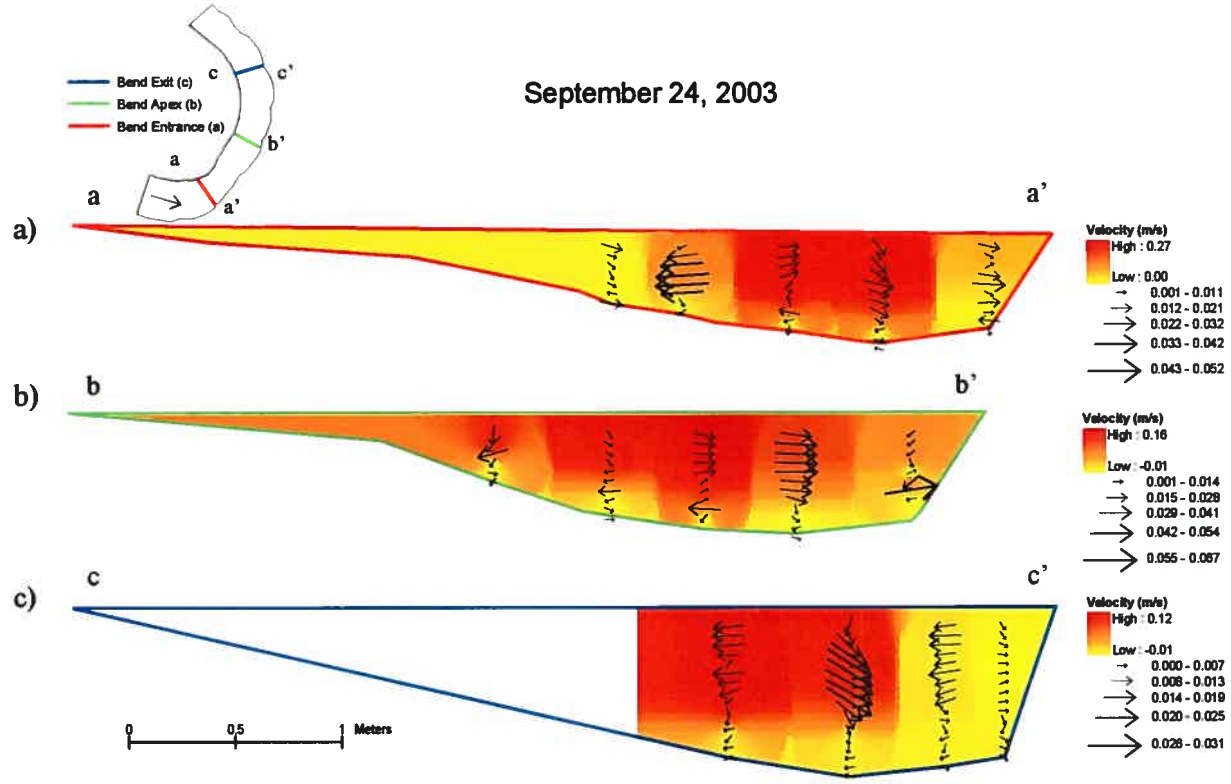

Figure 44: Three-dimensional flow structure at entrance (a), apex (b) and exit (c) of the bend.

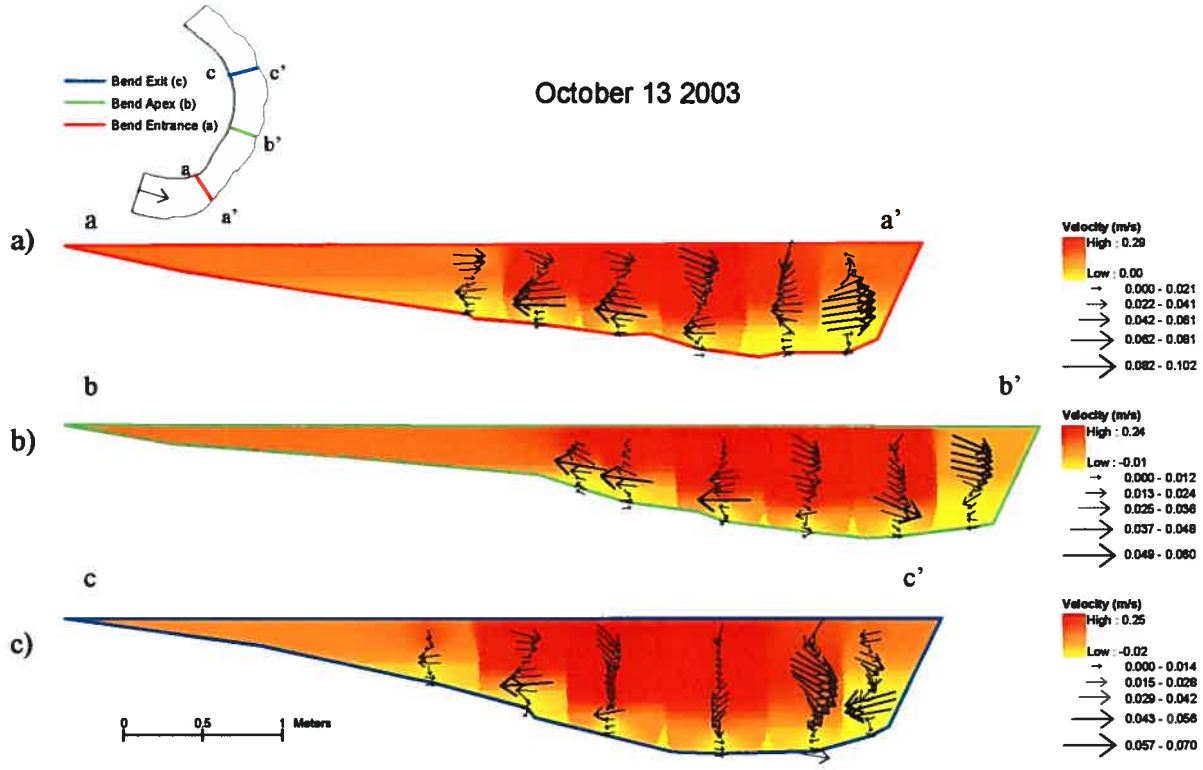

Figure 45: Three-dimensional flow structure at entrance (a), apex (b) and exit (c) of the bend.

large central circulation cell and what appears to be a second weaker counter-rotating cell next to the outer bank.

Figure 44 presents the flow measurements obtained with the PC-ADP on September 24, 2003. The bend entrance (Figure 44a) is again characterized by elevated downstream flow speeds (V_{max} = 0.27 m/s) and a concentrated high velocity core along the outer half of the channel (V_{max}/V_{avg} = 2.69). A similar trend of lower flow speeds (V_{max} = 0.16 m/s) and a lateral expansion of the high velocity core (V_{max}/V_{avg} = 1.84) towards the apex (Figure 44b) persists throughout the meander loop to the bend exit (Figure 44c) (V_{max} = 0.12 m/s,

V_{max}/V_{avg} = 1.67). Although the strength of secondary currents is reduced, the pattern remains quite similar to that seen in the August 28th dataset at the bend entrance, which is characterized by lateral flow divergence away from the channel centerline. It is somewhat odd that the bend apex does not display the well defined circulation cells that were seen in the previous dataset. Presumably, this lack of definition is related to both the lower number of measured profiles, which will impact the rotation angle required to achieve zero net lateral discharge; additionally, the apex is characterized by lower downstream velocities, resulting in weaker centrifugal forces. Nonetheless, near-surface and near-bed flow patterns do suggest the presence of a large circulation cell and a smaller, weaker counter-rotating cell next to the outer bank. Al similar two-cell structure can be seen at the bend exit, but the spatial extent of the outer bank cell appears to have increased by this point (Figure 44c).

Lastly, the flow measurements obtained using the PC-ADP on October 13, 2003 are presented in Figure 45. While this clearly reinforces the notion of decreasing flow speeds from the entrance (Figure 45a) (V_{max} = 0.29 m/s), towards the apex (Figure 45b) (V_{max} = 0.25 m/s) and exit of the bend (Figure 45c) (V_{max} = 0.25 m/s), the relatively constant values of V_{max}/V_{avg} (1.66, 1.62 and 1.74 respectively) indicate no expansion or contraction of the high velocity core. Structurally, the secondary currents here are quite different from those seen in the previous survey dates. Velocities in the lateral-vertical plane are roughly double of those contained in the other measurements at the bend entrance. Moreover, this dataset reveals two distinct circulation cells that persist throughout the bend: a main cell occupying the central region of the channel and a weaker counter-rotating cell adjacent to the outer bank. Furthermore, the second cell grows in size from the entrance to the apex and then shrinks

towards the bend exit. The emergence of these unique features can be attributed to a higher discharge level, which not only intensifies centrifugal forces, but also reduces the effects of topographic steering on the flow throughout the meander loop.

4.3.2 Turbulent Flow Properties

To investigate the flow turbulence properties, three-dimensional velocity measurements were collected using the ADV on six surveys before the stabilization measures were implemented. Of these datasets, two correspond with periods of low flow (August 3, 2001 and July 24, 2002 where flow stages are 22.2% and 23.3% of bankfull levels), two with periods of moderate flow (May 27, 2003 and July 19, 2002 where flow stages are 28.1% and 29.0% of bankfull levels) and two with periods of high flow (May 15, 2003 and June 19, 2002 where flow stages are 32.8% and 41.2% of bankfull levels).

Table VII presents the average near-surface and near-bed RMS values of the downstream (Vx), lateral (Vy) and vertical (Vz) velocity components for each field date. In terms of variations with flow depth, near-bed turbulence intensities in the downstream and cross-stream directions are on average 33% higher (with standard deviations of 7% and 16% respectively) than those observed at the water surface in all the datasets. Although the vertical component occasionally shows slightly higher near-bed values (by 6% on average), the large standard deviation (16%) suggests that turbulence intensity remains fairly consistent throughout the water column. As for trends between the three components, the highest RMS levels are consistently associated with the downstream component, followed by the lateral (90% of Vx, standard deviation = 8.5%) and the vertical (57% of Vx, standard deviation = 8.3%) velocity components. While reach averaged statistics do provide a general overview of the turbulent properties, their spatial distributions are required to shed light on the specific

Date	Flow Stage	% of Bankfull	Location	RMS (m/s) Vx	Vy	Vz	Percentage Vy/Vx	Vz/Vx
August 3, 2001	Low	22.2%	Surface	0.019	0.015	0.011	78.6%	58.1%
			Bed	0.024	0.023	0.011	94.1%	46.0%
July 24, 2002	Low	23.3%	Surface	0.022	0.020	0.014	90.0%	62.3%
			Bed	0.027	0.022	0.014	79.7%	51.6%
May 27, 2003	Medium	28.1%	Surface	0.037	0.034	0.023	91.8%	63.4%
			Bed	0.050	0.044	0.028	87.9%	56.4%
July 19, 2002	Medium	29.0%	Surface	0.025	0.022	0.016	88.3%	63.0%
			Bed	0.035	0.028	0.018	80.2%	50.0%
May 15, 2003	High	32.8%	Surface	0.049	0.046	0.033	94.5%	66.9%
			Bed	0.068	0.059	0.040	87.5%	58.3%
June 19, 2002	High	41.2%	Surface	0.056	0.052	0.037	94.1%	66.8%
			Bed	0.072	0.080	0.030	110.5%	41.0%
		Average	Surface	**0.035**	**0.032**	**0.022**	**89.5%**	**63.4%**
			Bed	**0.046**	**0.043**	**0.023**	**90.0%**	**50.6%**
		Standard Deviation	Surface	**0.015**	**0.015**	**0.011**	**5.9%**	**3.2%**
			Bed	**0.021**	**0.023**	**0.011**	**11.4%**	**6.4%**

Comparison of Near-Bed and Near-Surface RMS Values

Date	Flow stage	% of Bankfull	Vx	Vy	Vz
August 3, 2001	Low	22.2%	26.2%	51.0%	0.0%
June 19, 2002	High	41.2%	29.5%	52.0%	-20.5%
July 19, 2002	Medium	29.0%	41.7%	28.8%	12.5%
July 24, 2002	Low	23.3%	24.2%	10.0%	2.8%
May 15, 2003	High	32.8%	38.6%	28.3%	20.9%
May 27, 2003	Medium	28.1%	34.7%	29.0%	19.9%
		Average	32.5%	33.2%	5.9%
		S.D.	7.0%	15.9%	15.5%

Table VII: Average near-surface and near-bed turbulence statistics for each dataset.

dynamics of an individual bend.

Figures 46 to 48 present the downstream, lateral and vertical turbulence intensities for each of the respective surveys in the areas next to the water surface (a, b and c) and adjacent to the bed (d, e and f) for low, medium and high flow. Although their absolute values do vary, the resulting turbulence intensities of a single dataset remain fairly consistent regardless

of flow depth or velocity component being examined. When viewed collectively, it is apparent that the zones of elevated turbulence intensity for each survey are concentrated along the outer bank in one or two principal locations: near the entrance and exit of the meander loop. Moreover, the location of maximum turbulence intensity appears to be discharge dependent. As can be seen in Figure 46, where flow stages are at their lowest, near-bed and near-surface turbulence intensities display maximum values at the bend entrance. Both dates display similar turbulence intensities along the downstream flow component in this area, but the lateral and vertical components are lower in the August 3, 2001 survey, which is related to the upstream bed morphology at the time the data was collected.; the presence of a large sediment plug upstream of the bend in the August 3, 2001 survey prevented collecting velocity data in this region. The sediment plug prevented the development of a coherent circulation cell at the bend entrance, resulting in lower turbulence intensities along the lateral and vertical flow components. As the flow stage reaches moderate levels (Figure 47), a second zone of elevated turbulence intensity begins to develop towards the bend exit in conjunction with the initial zone observed along the entrance of the meander bend. Both the patterns and absolute values of turbulence intensity are virtually identical between the two survey dates, and while the RMS levels are higher than those in the low flow datasets, turbulence intensity is reduced. This indicates that there is a non-linear relationship between flow velocity and turbulence intensity. At high flow (Figure 48), near-bed turbulence intensities are greatly reduced at the bend entrance, and the exit region contains the highest values for all velocity components, irrespective of flow depth. Although the patterns of turbulence intensity are similar between the two surveys, the June 19, 2002 survey displays unusually high near-bed turbulence levels. Although the reason for this is not

clear, it is possible that there was some obstruction on the bed affecting flow that was not noticed at the time the data was collected. Nonetheless, the high flow dataset generally displays the lowest turbulence intensities of the three flow stages, further indicating that the relation between velocity and turbulence intensity is non-linear.

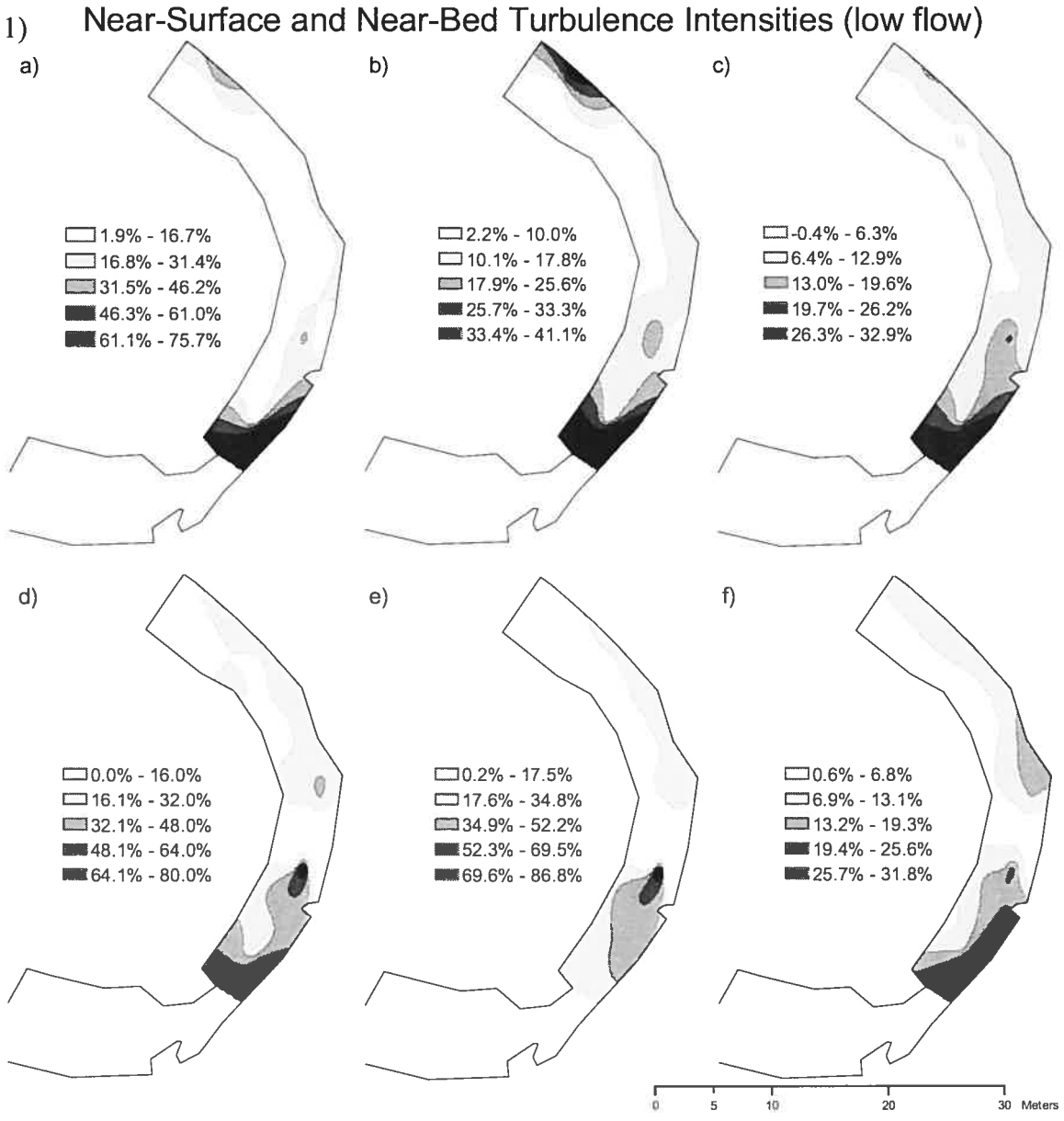

Figure 46: Low flow downstream, cross-stream and vertical turbulence intensity distributions in near-surface (a, b and c) and near-bed (d, e and f) regions for August 3, 2001 (1) and July 24, 2002 (2) respectively (interpolation cropped at upstream section due to lack of data).

2) Near-Surface and Near-Bed Turbulence Intensities (low flow)

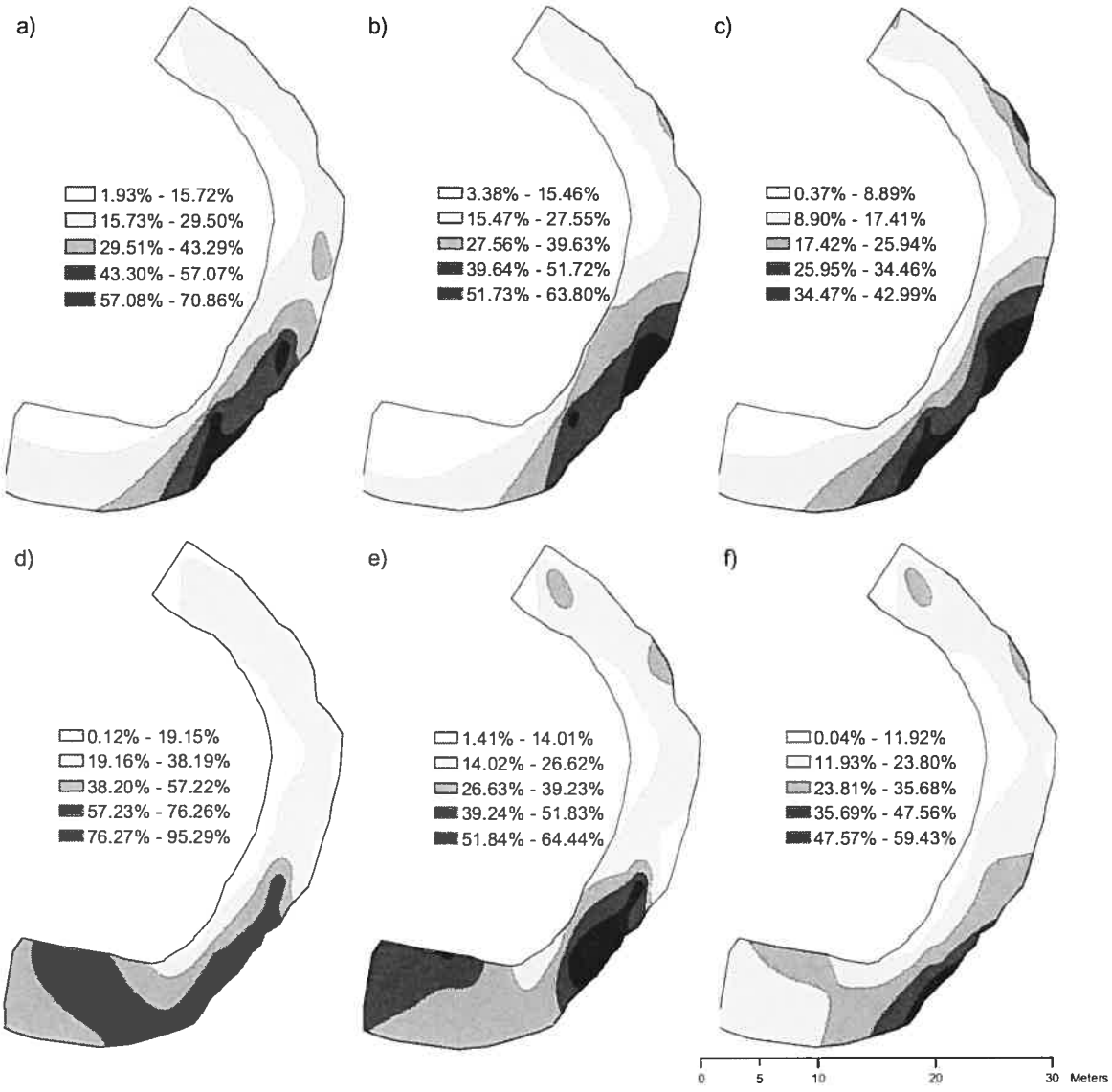

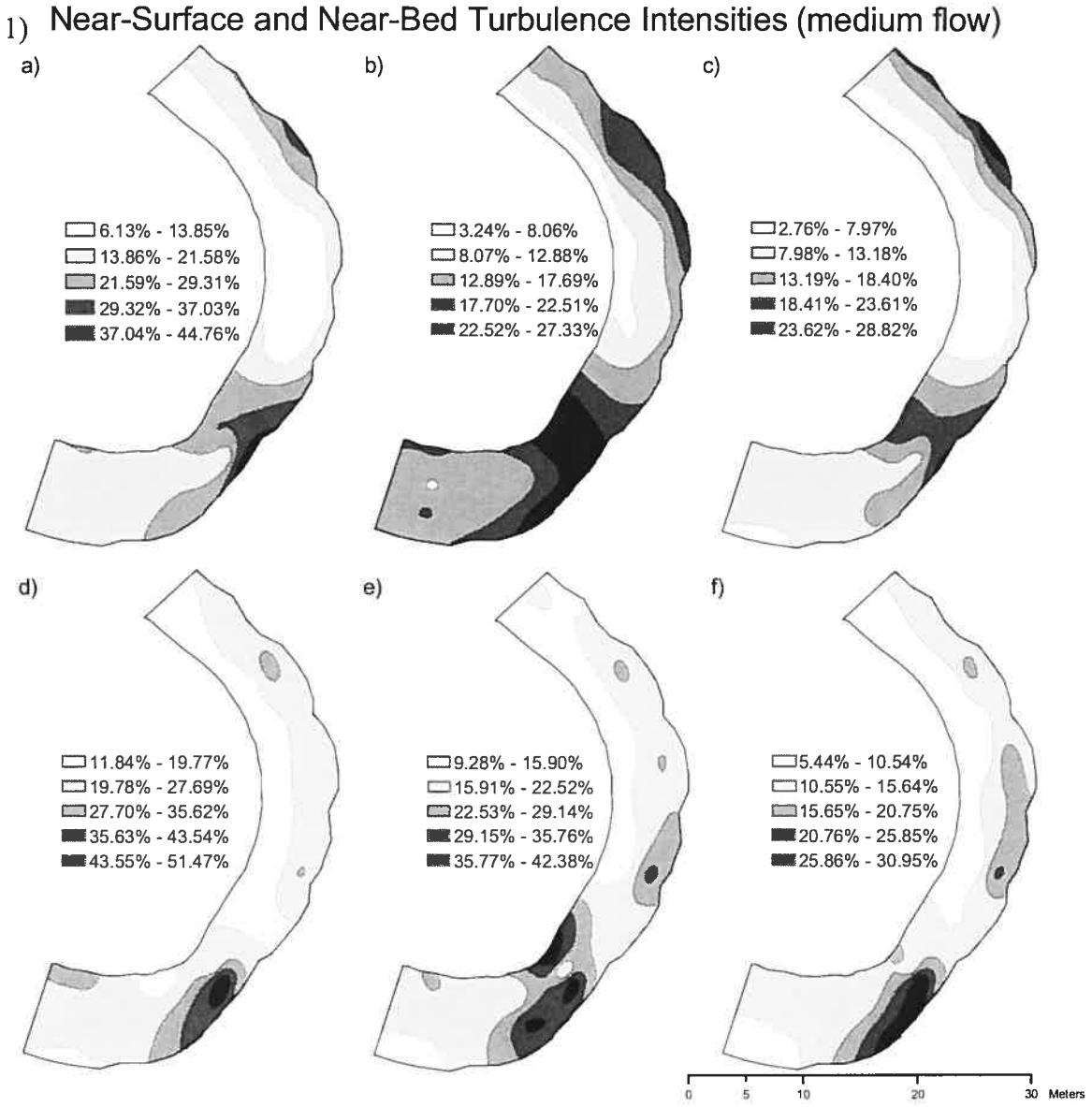

Figure 47: Medium flow downstream, cross-stream and vertical turbulence intensity distributions in near-surface (a, b and c) and near-bed (d, e and f) regions for May 27, 2003 (1) and July 19, 2002 (2) respectively.

2) Near-Surface and Near-Bed Turbulence Intensities (medium flow)

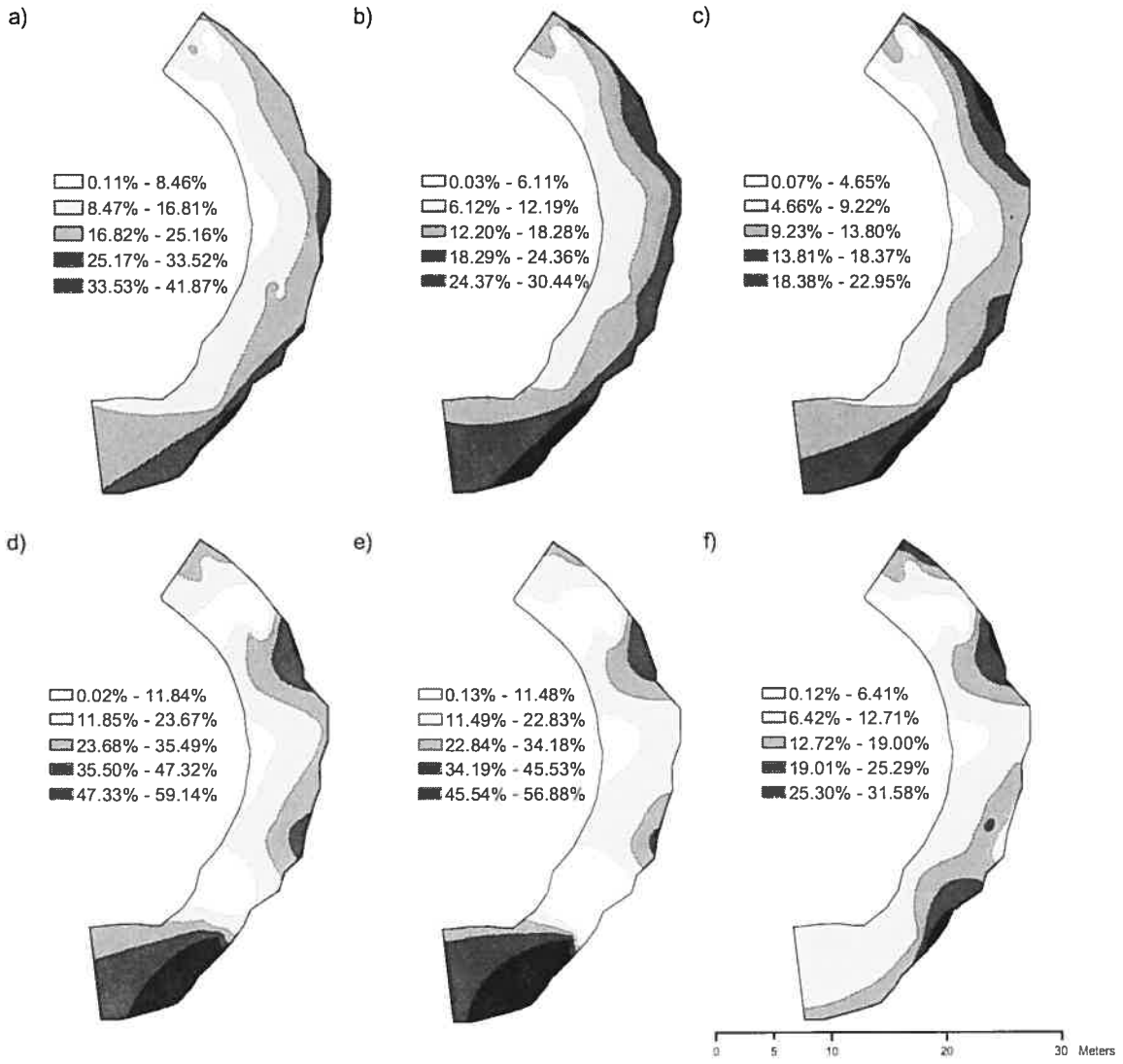

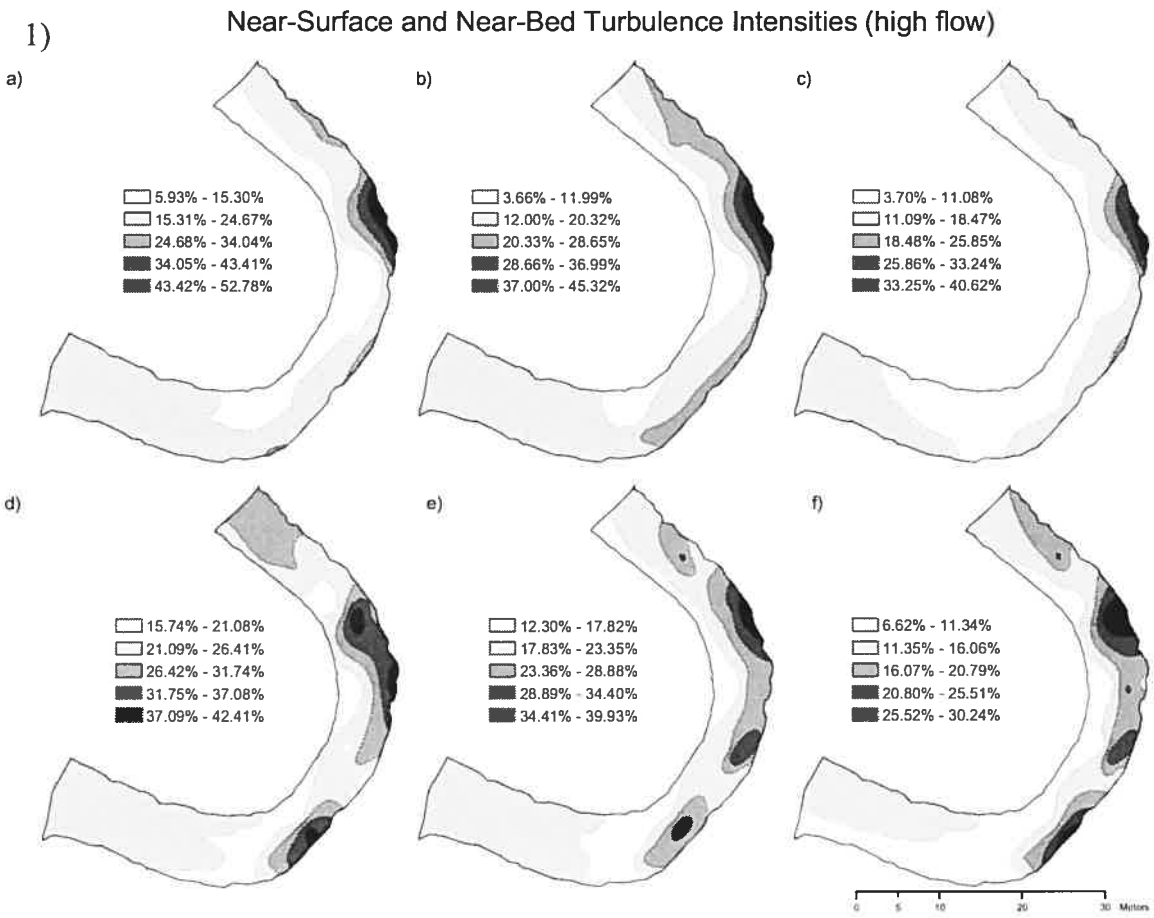

Figure 48: High flow downstream, cross-stream and vertical turbulence intensity distributions in near-surface (a, b and c) and near-bed (d, e and f) regions for May 15, 2003 (1) and June 19, 2002 (2) respectively.

2) Near-Surface and Near-Bed Turbulence Intensities (high flow)

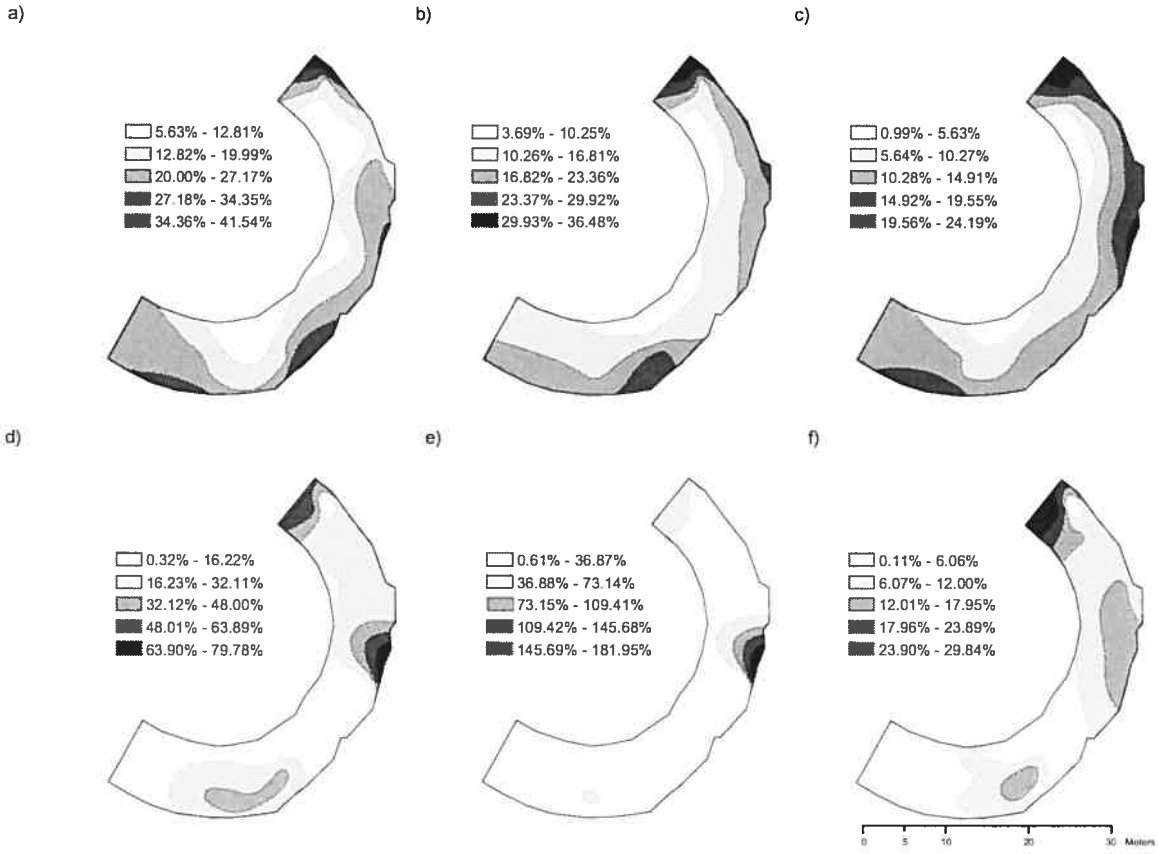

4.4 Bend Evolution

One of the fundamental aims of applied fluvial geomorphology is to predict how a channel will develop over time. While there is a variety of methods available to help in answering this question, they all involve an understanding of bed shear stress distributions. Therefore, the question that must be addressed is: how can one accurately estimate the shear forces exerted by a flow on the channel bed. Various studies have evaluated the ability of the different approaches to quantify this variable (ex: Biron *et al.*, 2004b). However, identifying a definitive technique that can be applied universally remains elusive. As such, this section will first describe the morphological changes that were observed at the study site. Then, the most suitable approach to estimate bed shear stress will be appraised by comparing predicted

values with field observations of sediment transport. These findings will then be applied to the flow data collected over three years, and the resulting bed shear stress patterns will be compared to the changes in channel topography over the same period to gauge its ability to predict channel evolution.

4.4.1 Chronology of Channel Change

Annual changes in bed and bank topography were evaluated before (July 2002 to May 2003), during (May 2003 to June 2003) and after (June 2003 to May 2004) stabilization measures were implemented. Average elevation changes of 0.2m over an area of $3m^2$ was used as the criteria for identifying the most dynamic sections of the reach.

Figure 49 presents the annual changes in bed and bank topography prior to the implementation of stabilization measures (July 2002 to May 2003). Over this period, channel volume increased by 57 m^3 to 1558 m^3 from its initial value of 1502 m^3 (Table VIII) by way of localized bank erosion at the bend entrance and exit. The effects of failure events were only slightly mitigated by areas of sediment deposition along the inner bank and the bed toward the bend exit.

Figure 50 presents the topographic changes resulting from bank protection (May 2003 to June 2003). Given that the technique adopted along this bend involves reducing the cross-stream slope of the outer bank to 30°, the channel volume increased by an additional 142 m^3 to 1700 m^3 (Table VIII). While the stabilization work obscured any evidence of bend migration, there appears to be evidence of a depositional feature at the meander apex.

Figure 51 presents the annual changes in bed and bank topography following the implementation of stabilization measures (June 2003 to May 2004), during which channel volume decreased by 98 m^3 to 1602 m^3 (Table VIII). Although meander evolution is

Areas of Significant Annual Elevation Change

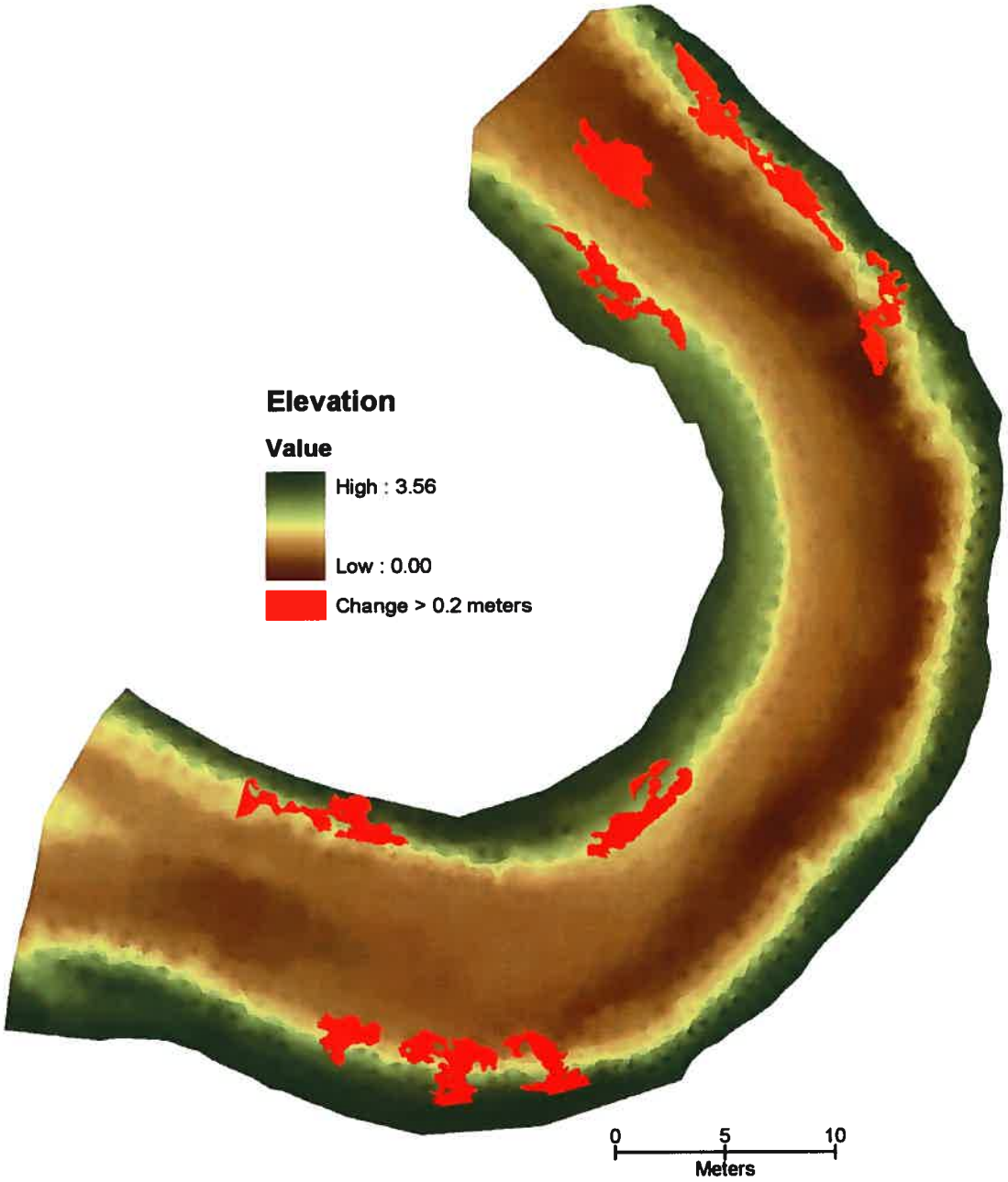

Figure 49: Locations of significant topographic change prior to implementing stabilization measures (July 4, 2002 to May 15, 2003).

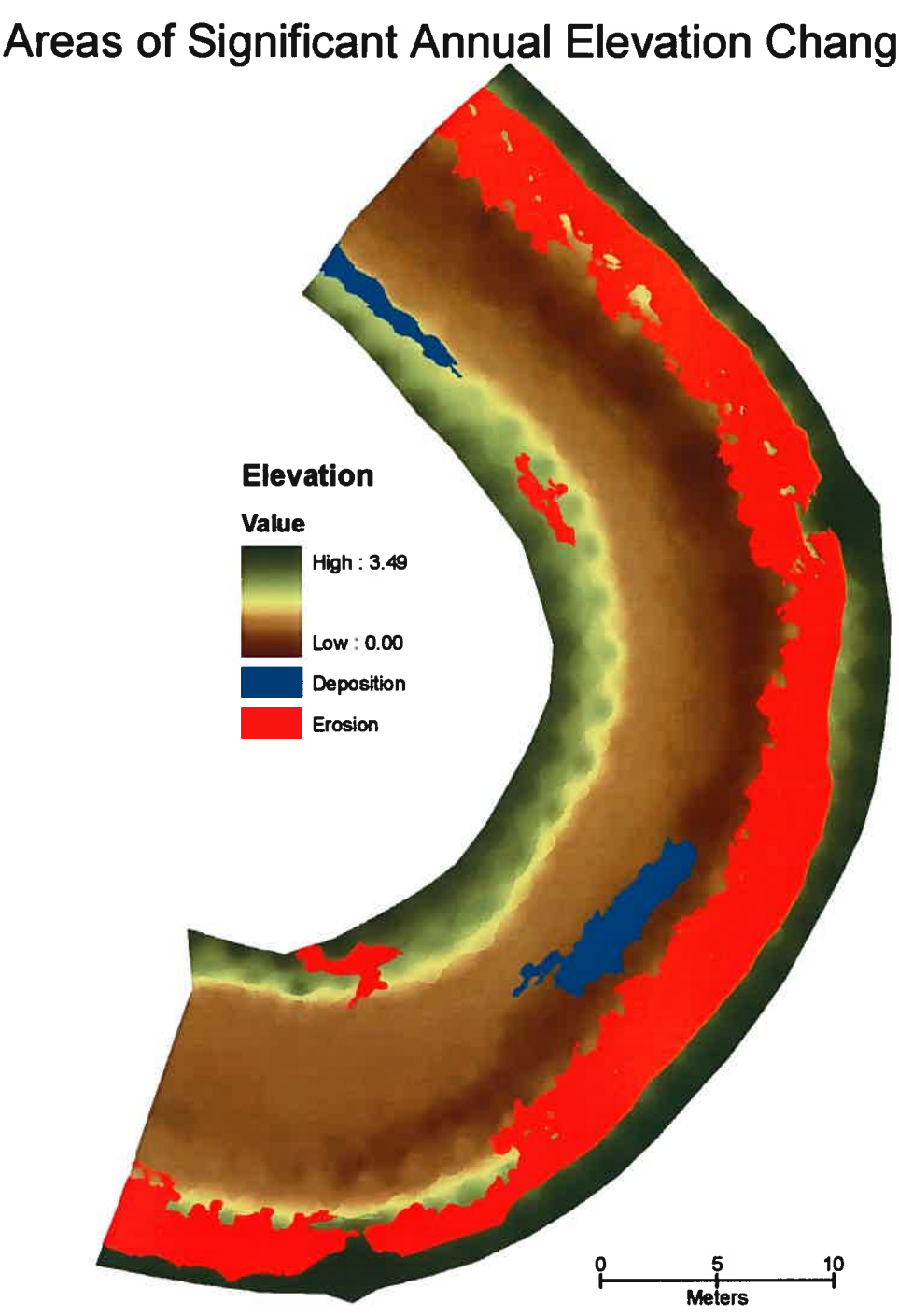

Figure 50: Locations of significant topographic change resulting from the implementation of stabilization measures (May 15, 2003 to June 25, 2003). It should be noted that the significant changes along the outer bank are a direct result of the grade reduction associated with stabilization rather than direct fluvial erosion.

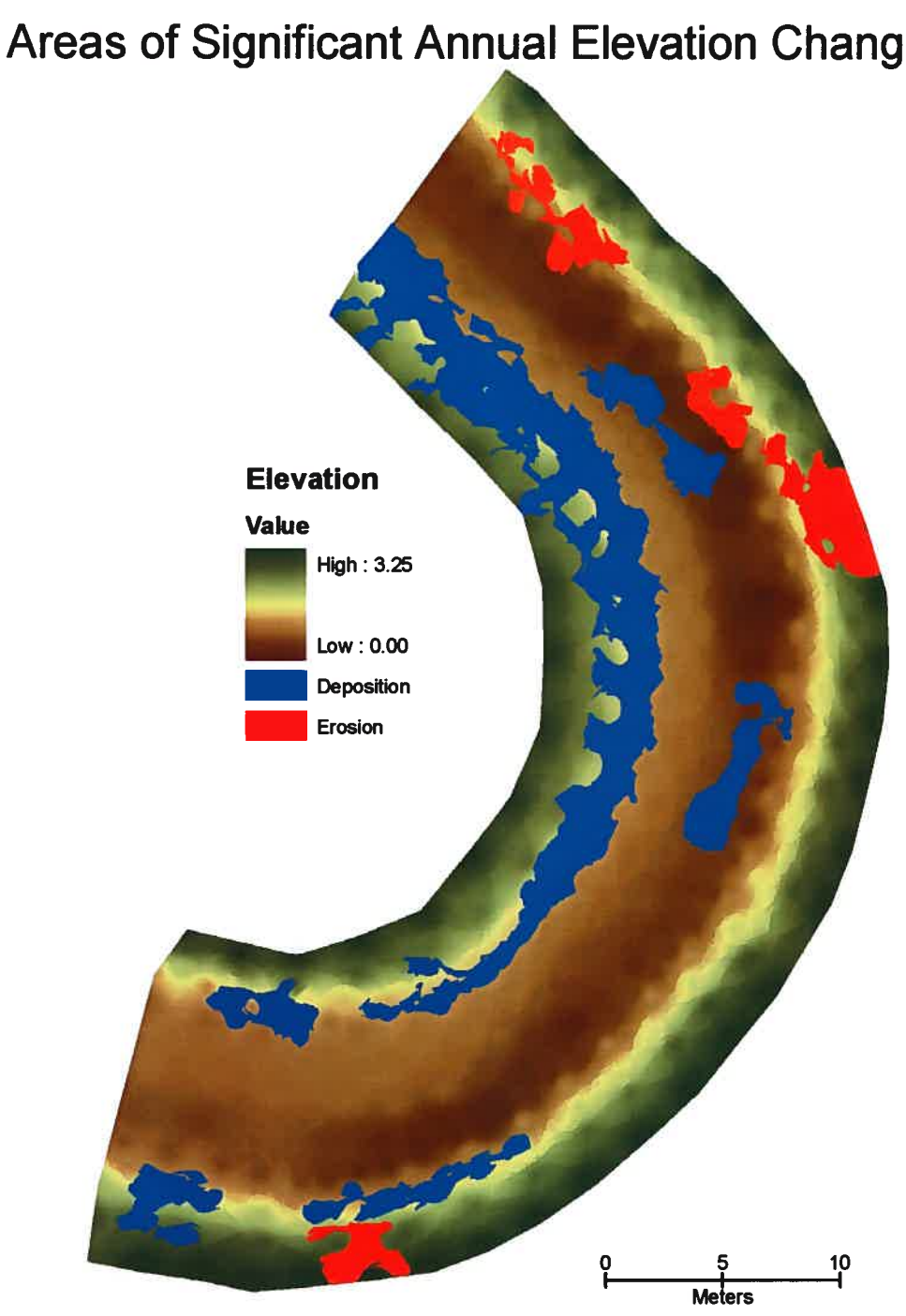

Figure 51: Locations of significant topographic change over a 1 year period following the implementation of stabilization measures (June 25, 2003 to May 10, 2004).

dominated by massive sediment deposition along the entire length of the inner bank over this period, localized failure events persist at the entrance and exit of the bend.

	2D Area (m^2)	3D Area (m^2)	Volume (m^3)
July 4 2002	831.5	1041.4	1501.5
May 15 2003	831.5	1040.8	1558.4
June 25 2003	831.5	985.0	1700.3
May 10 2004	831.5	971.0	1601.9

Table VIII: Channel areas and volumes prior to (July 4, 2002), immediately before (May 15, 2003), immediately after (June 25, 2003) and 1 year after (May 10, 2004) the implementation of stabilization measures.

4.4.2 Evaluation of Techniques to Estimate Bed Shear Stress

The following appraisal of the different techniques for estimating bed shear stress was performed using the ADV and PC-ADP measurements obtained for the preceding section on instrument evaluation. While collecting this dataset, small ripples and sporadic bedload sediment transport events were observed in both the non-separated flow, and to a lesser degree in the area of flow separation.

Figure 52a presents the shear stress values obtained using the steady flow and turbulence based techniques in the area of non-separated flow using the ADV; the Corrsin (1957) approach was omitted as it produced values identical to the traditional Reynolds stress. Results from the ADV dataset clearly demonstrate that two of the turbulence based approaches (Reynolds $u'w'$ and TKE) systematically produce higher shear stress estimates than their steady flow counterparts. Moreover, all of the steady flow approaches indicate shear stress levels that are far below the critical value (Shields = 0.656 N/m^2) required to initiate sediment transport, which runs contrary to the field observations of sporadic transport

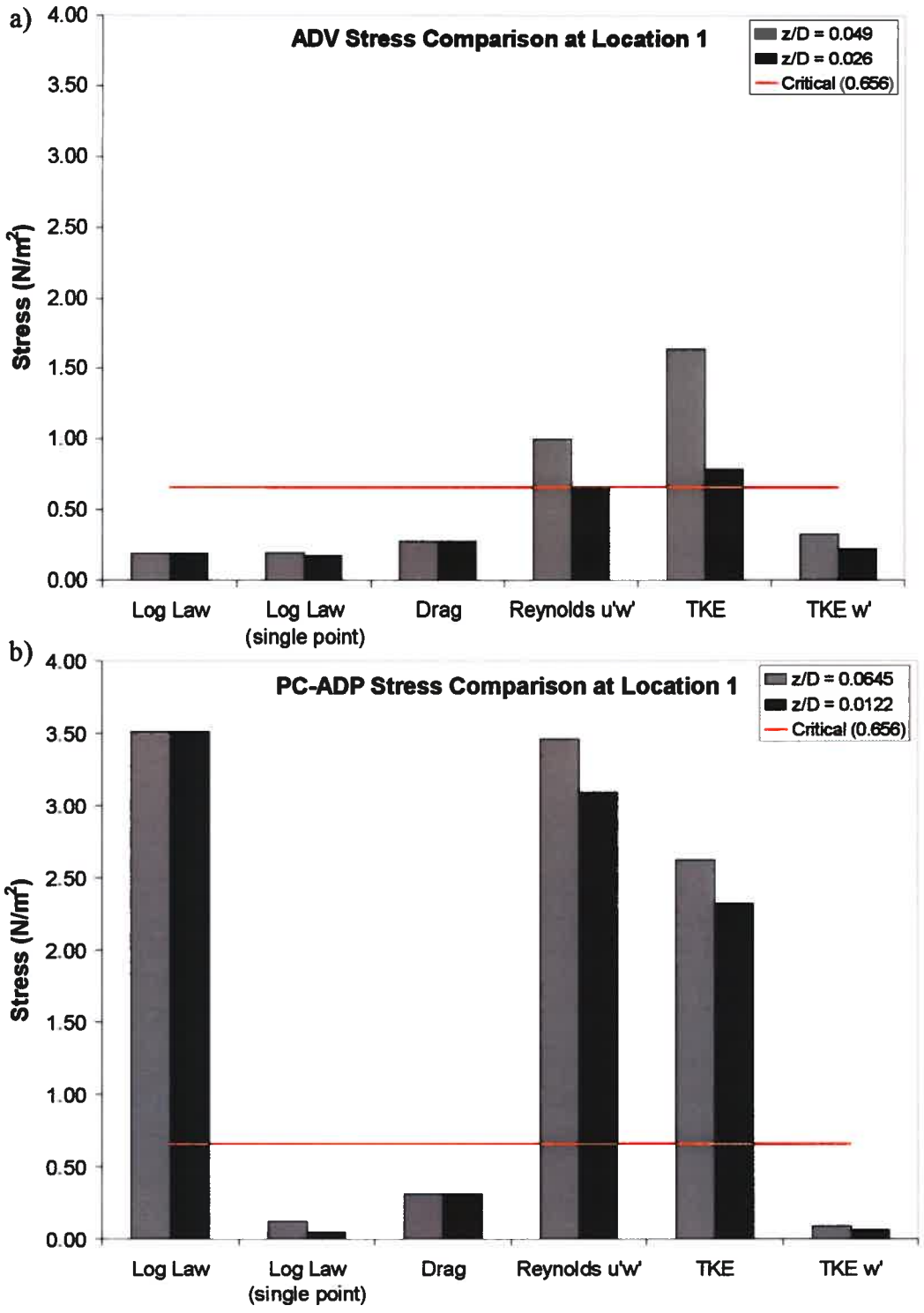

Figure 52: Comparison of shear stress estimates at location 1 with ADV (a) and PC-ADP (b) (data in the bottom two points of the velocity profile). The horizontal line is the critical stress required to initiate sediment transport (0.656 N/m2).

		z/D	Log Law	Log Law (single point)	Drag	Reynolds u'w'	Reynolds u'w' magnitude	TKE	TKE w'
Location 1	ADV	0.048	0.192	0.198	0.280	1.001	1.001	1.641	0.327
		0.026	0.192	0.172	0.280	0.651	0.651	0.790	0.227
	PC-ADP	0.065	3.512	0.120	0.314	3.461	3.461	2.618	0.087
		0.012	3.512	0.050	0.314	3.093	3.093	2.321	0.060
Location 2	ADV	0.059		0.001	0.030	-0.120	0.120	1.066	0.404
		0.038		0.002	0.030	0.701	0.701	0.606	0.348

Table IX: Summary of shear stress values (in N/m2) obtained using various techniques with the ADV and PC-ADP in the region of main (location 1) and separated (location 2) flow.

(Table IX). Similar discrepancies have been noted by Drake *et al.* (1988), who observed that although their estimations of bed shear stress using mean flow techniques were below the critical threshold, sediments were being transported in the form of patches that were discrete in both space and time. Yet, with the exception of the vertical turbulent kinetic energy method, all turbulence based approaches indicate that the flow is capable of initiating sediment transport, which suggests that both the Reynolds and the three dimensional turbulent kinetic energy methods are appropriate.

By contrast, results obtained from the PC-ADP dataset show that the bed shear stress estimates differ by a few orders of magnitude both between and within the turbulence and steady flow techniques (Figure 52b). The estimated bed shear stress values obtained through the single point log-law and drag coefficient approaches are far below the critical value of 0.66 N/m^2 required to initiate sediment motion. Alternatively, the Reynolds, three-dimensional turbulent kinetic energy and classical log-law methods yield values in the order of 3.2 N/m^2 (Table IX); this indicates that the flow is capable of transporting sediments with an a b axis as large as 4.5 mm, which is roughly twice the size of the largest bed particles. Field observations clearly indicated that sediment transport rates were far lower than what

such stress estimates would otherwise indicate. This point serves to further highlight the significant impacts that spatial averaging of the near bed flow field has on turbulence statistics, and its implications for adequately characterizing the logarithmic portion of the velocity profile. As for the vertical turbulent kinetic energy approach, the estimate of bed shear stress is far too low; hence the viability of this technique in the near bank region of a river bend is equally questionable. Based on these findings, and those comparing the turbulence statistics in the instrument evaluation section, the PC-ADP was omitted from the subsequent analysis.

Figure 53 presents the shear stress estimates using the ADV in the region of flow separation. Given the non-logarithmic nature of the velocity profile in this region, it was impossible to obtain an accurate value of shear velocity; as such, the multi-point log-law method was not included in the analysis. However, results from the single point logarithmic approach is presented for demonstration purposes. As was the case in the region of the main flow, the non-turbulence and vertical turbulent kinetic energy based approaches give estimates that are too low to produce the sporadic transport events observed at the site. While the Reynolds and three-dimensional turbulent kinetic energy results again appear reasonable, they display very different trends with depth; the Reynolds stress in the downstream-vertical plane increases dramatically with bed proximity whereas the converse is true for the estimates obtained using Huthnance *et al.* (2002) technique and the turbulent kinetic energy approach. Yet, unlike the vertical TKE method, the three-dimensional turbulent kinetic energy procedure displays lower stress levels in the region of flow separation compared to the main channel. Given that shear stress is defined as a force acting parallel to a surface, and that the near-bed downstream and lateral velocities in this region are virtually zero, it

appears as though the three-dimensional TKE is the better of the two approaches. Moreover, stress levels estimated using the near bed measurement (z/D=0.038) with this technique appear to be more consistent with the near equilibrium sediment mobility conditions observed at the site.

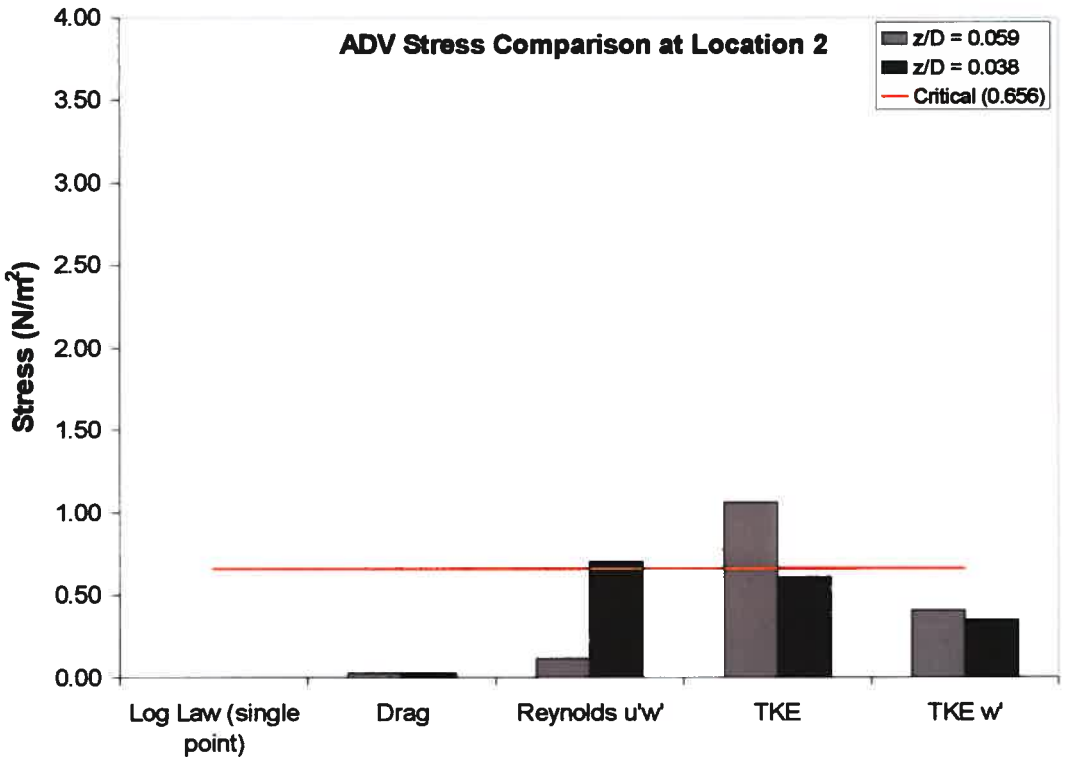

Figure 53: Comparison of shear stress estimates at location 2 with ADV data in the bottom two points of the velocity profile. The horizontal line is the critical stress required to initiate sediment transport (0.656 N/m2).

4.4.3. Bed Shear Stress Distributions in River Bends (ADV)

The three-dimensional turbulent kinetic energy approach (Equation 12) was used to estimate bed shear stress for the two low-flow (August 3, 2001 and July 24, 2002), two moderate-flow (May 27, 2003 and July 19, 2002) and two high-flow (May 15, 2003 and June 19, 2002) surveys.

Figure 54(1) and 54(2) present the bed topography of the meander bend, velocity and shear stress distributions at low-flow. As can be seen in Figure 54(1)a and 54(2)a, the bend is characterized by multiple pools that begin to develop midway between entrance and apex, and persist all the way to the bend exit. The skew between the surface (blue) and bed (red) flow vectors seen in Figure 54(1)b and 54(2)b indicate the presence of a helical flow pattern throughout the bend, but the strongest motion is found in the entrance-apex and apex-exit regions. The highest bed shear stresses (1.81 N/m^2) are found near the channel centerline at the apex (Figure 54(1)c), whereas the highest near bank value (0.85 N/m^2) is located midway between the entrance and apex of the meander loop. This coincides with the location of maximum bed shear stress observed on July 24, 2002 (0.74 N/m^2) (Figure 54(2)c).

At moderate flow (Figure 55), the multiple pools are still present, although they are less prominent than those observed at low flow. Conversely, the distributions of secondary current intensity are similar to those seen in the previous survey dates, but the helical motion appears to have intensified (Figure 55(1)b and 55(2)b). While the highest bed shear stresses are again situated midway between the bend entrance and exit (1.61 N/m^2 and 1.49 N/m^2 respectively) (Figure 55(1)c and 55(2)c), they each display secondary near-bank zones of elevated bed shear stress at the apex (0.79 N/m^2 and 0.68 N/m^2) and exit (0.53 N/m^2 and 0.76 N/m^2) of the bend.

At high flow (Figure 56), the channel bed displays a relatively continuous single pool that extends from midway between the entrance and apex of the bend that persists to the exit of the meander loop (Figure 56(1)a and 56(2)a). Moreover, minimum bed elevation values are higher at high flow than what is seen at the other stages. This suggests that a higher flow stages serves to create a more uniform bed by scouring the sediments from the pseudo-riffles

1) August 3 2001 Bed Topography, Velocity and Shear Stress Distributions (low flow)

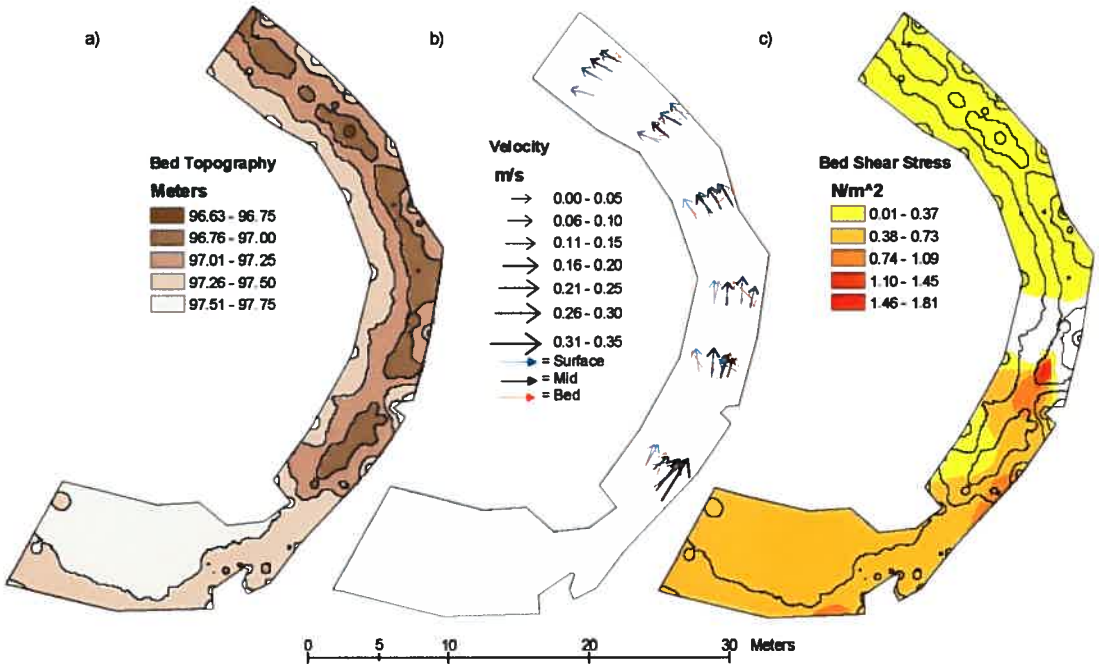

2) July 24 2002 Bed Topography, Velocity and Shear Stress Distributions (low flow)

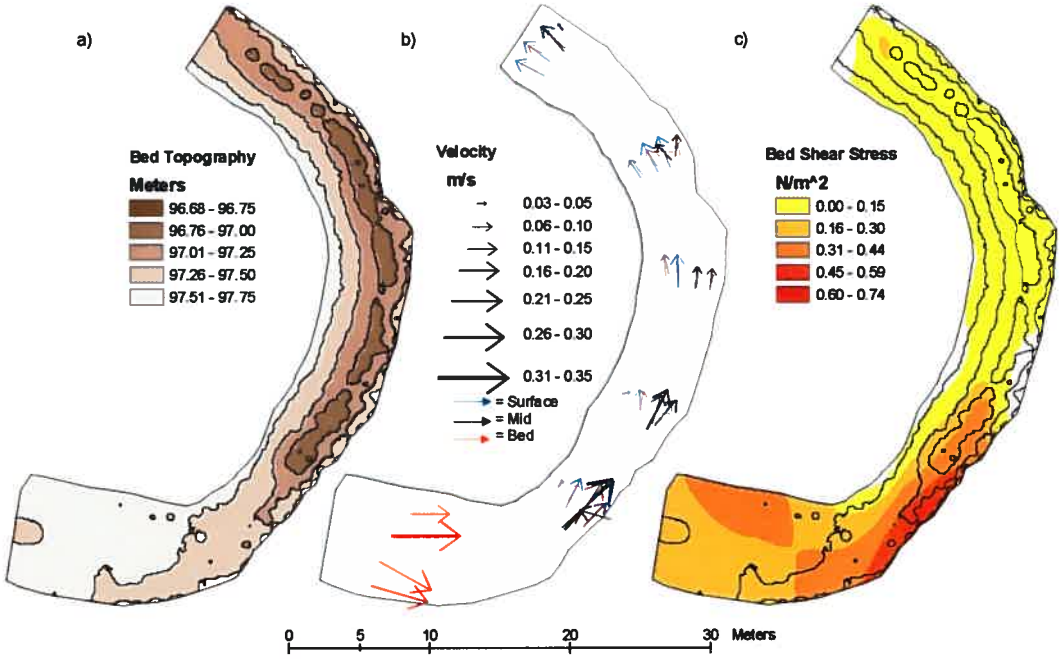

Figure 54: Topography (a), velocity (b) and bed shear stress (c) distributions at low flow (August 3, 2001 (1) and July 24, 2002 (2)).

1) July 19 2002 Bed Topography, Velocity and Shear Stress Distributions (medium flow)

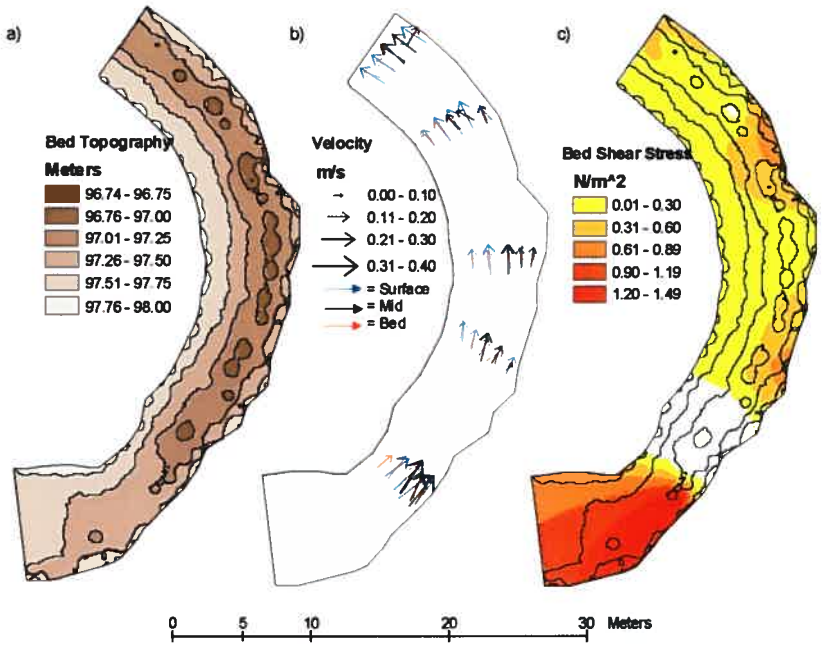

2) May 27 2003 Bed Topography, Velocity and Shear Stress Distributions (medium flow)

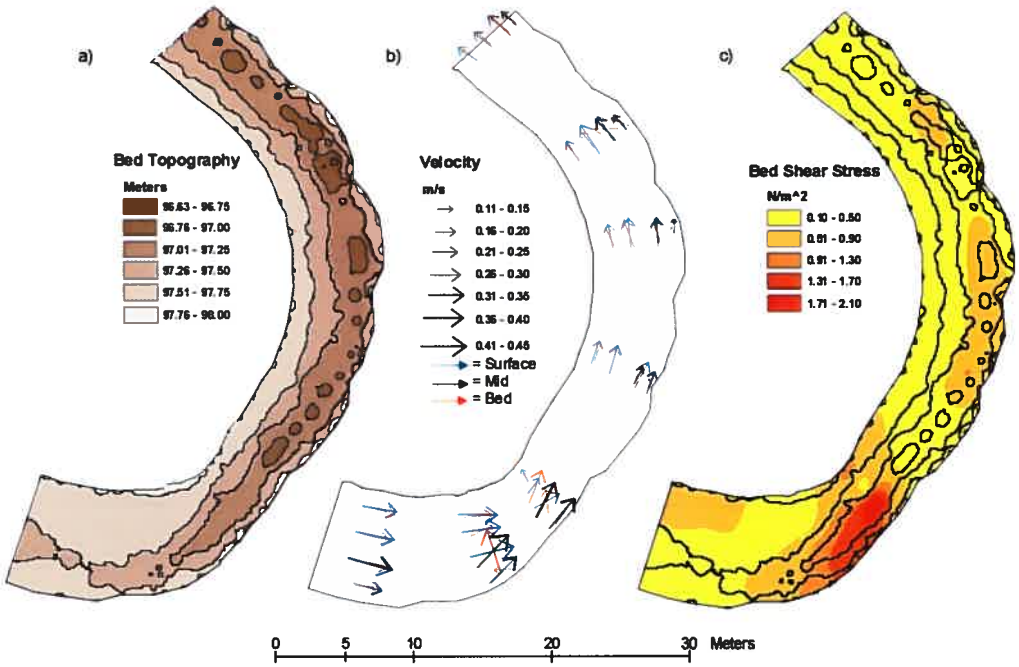

Figure 55: Topography (a), velocity (b) and bed shear stress (c) distributions at medium flow (July 19, 2002 (1) and May 27, 2002 (2)).

1) May 15 2003 Bed Topography, Velocity and Shear Stress Distributions (high flow)

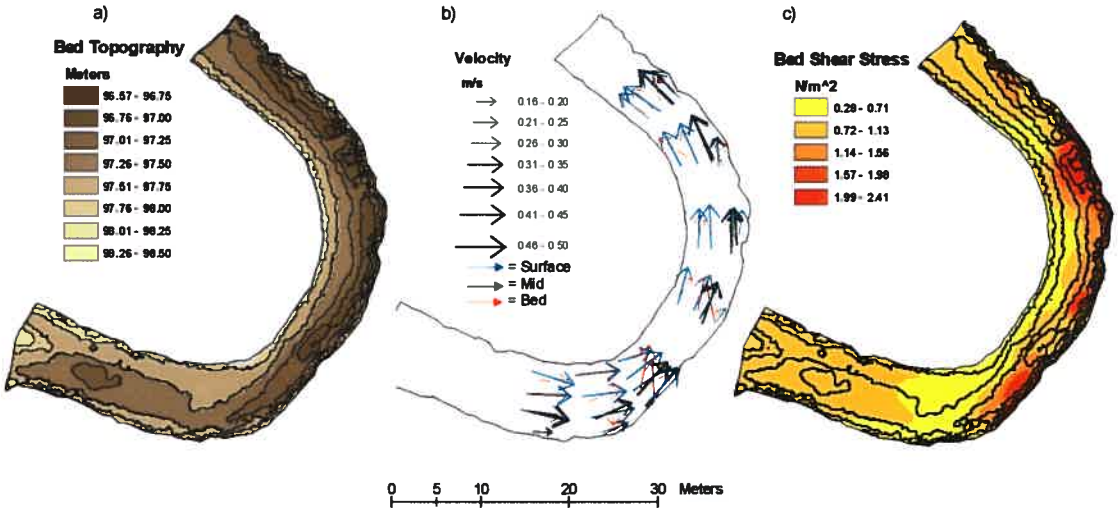

2) June 19 2002 Bed Topography, Velocity and Shear Stress Distributions (high flow)

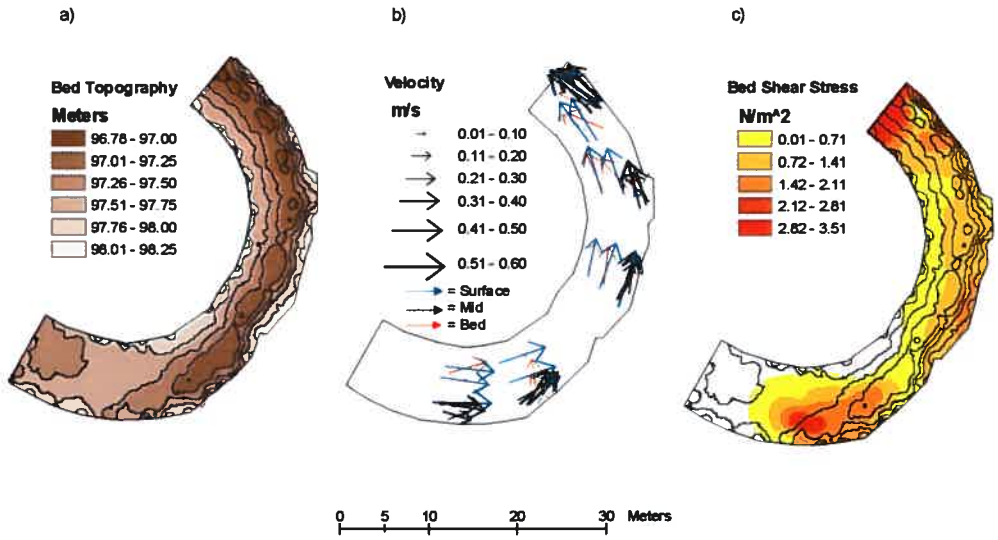

Figure 56: Topography (a), velocity (b) and bed shear stress (c) distributions at high flow (May 15, 2003 (1) and June 19, 2002 (2)).

and subsequently depositing them in the depressions downstream of the crests. Previous research on bed development in large amplitude meander bends support this hypothesis (Whiting and Dietrich, 1993b). Here, the authors conclude that the spontaneous development of multiple pools result from a weak centrifugal force that is not capable of supressing a sinuous thawleg. Although the study bend along the Petite Barbue River is not a large

amplitude meander, it is entirely possible that flow velocities, which also affect centrifugal force, are only high enough on the May 15, 2003 and June 19, 2002 surveys to suppress sinuous flow, thereby scouring the areas between the multiple pools at high flow.

As indicated by the continued skew between the near-surface (blue) and near-bed (red) flow vectors (Figure 56(1)b and 56(2)b), the flow continues to display strong secondary currents. Whereas the rotation of the circulation cell remains consistent throughout the bend at low and intermediate flows, and the June 19, 2002 survey (Figure 56(2)b), there is a reversal in the rotation of the cell from the apex to the exit of the bend in the May 15, 2003 measurements (Figure 56(1)b). The reason of this reversal is not clear. The bed shear stress patterns at high flow stages (Figure 56(1)c and 56(2)c) are markedly different from those seen at lower flow stages. While there are still zones of elevated shear stress at the entrance (1.89 N/m^2 and 1.78 N/m^2) and apex (1.54 N/m^2 and 1.70 N/m^2), the highest values are actually located at the exit of the bend (2.20 N/m^2 and 2.71 N/m^2). Clearly bed characteristics, secondary current strength and bed shear stress patterns are all strongly linked with flow stage.

5.1 Instrument Evaluation

As with any technology, a new sampling device must undergo thorough testing before they can be incorporated into the arsenal of tools available for fluvial studies. Ideally this is performed by comparing its data against that of another proven instrument under a variety of conditions. This is the case for the PC-ADP, which was evaluated against an ADV for mean flow properties and turbulence statistics in the main portion of flow and a vertically oriented separation zone. Although the larger spatial and temporal averaging of the PC-ADP velocity measurements to diverge from those of the ADV, especially in the near-bed region, the qualitative agreement between the two devices suggest that the PC-ADP is indeed a valuable tool for fluvial geomorphologists.

In terms of mean flow properties, both devices produce similar downstream velocities in the main and separated flows (correlation coefficients of 0.905 and 0.916 respectively). Recalling that a slope of 1 would indicate that the results of the two devices are in perfect agreement with each other, the slope in the main portion of the channel is 1.43 and 0.66 in the separation zone (Table II). While these values initially give the impression that the PC-ADP is over-predicting and under-predicting flow speed in the two respective areas, they are misleading. An underlying assumption behind using a slope of 1 as a method of evaluating the performance of the PC-ADP against the ADV is that the y-intercept should be equal to 0, since there would otherwise be a constant offset in flow speeds between the two samples. Although the separation zone has a y-intercept that is almost equal to zero (0.045), this is not the case for the main flow measurement (y-intercept = -0.151). Recalling from Figure 33 that the agreements between the two devices is initially high at the water surface but it begins to

weaken towards the bed, theses slopes and intercepts are the direct result of spatial averaging effect in a highly complex flow field. In both cases, the PC-ADP's sampling volume likely extends across the vertical shear layer in the near-bed region. As such, the velocity measurements incorporate the characteristics of both the main and separated flows. Therefore, measurements from the main portion of the channel are lower than those obtained with the ADV because it includes part of the slower separated flow into its sample, thereby explaining its slope being greater than 1 and a negative y-intercept. Similarly, the measurements from the separation zone are higher than expected due to the partial inclusion of the faster flow in the main portion of the channel into the sample, causing the slope to be less than 1. A near zero y-intercept should also be expected in the separation zone since the flow is almost stagnant in the bottom 20% of the profile.

As for the lateral component of flow, both the main and separation zones display small, negative y-intercepts (-0.0416 and -0.0313) and slopes less than 1 (0.7211 and 0.7401) (Table II). While negative intercepts are likely the result of slight sensor misalignment, a slope of less than 1 indicates that the PC-ADP under predicts lateral current strength at both locations. These findings should be examined in light of the near-bank flow structure in river bends. To form a circulation cell, cross-stream water velocities must decrease and downwelling will intensify as the current approaches the outer bank (Chang, 2002). Hence unlike the ADV measurements, the PC-ADP's sampling volume is probably extending into the region where vertical flow becomes the dominant secondary current, thereby explaining its lower cross-stream velocities. This hypothesis is consistent with the results in Figure 33a, which shows that the divergence in measurements between the two devices increases with and increase in the PC-ADP sampling volume towards the bed. Not surprisingly, the

correlation of the two instruments is much lower in the separation zone compared to the main portion of the channel (r = 0.664 versus r = 0.975). There are two possible explanations for this difference. The fist is that the PC-ACP is including a weaker counter-rotating cell next to the bank that lies just beyond the ADV sampling volume. Alternatively, the sampling volume of the PC-ADP may actually be extending into the outer bank in the bottom half of the profile.

Unlike the downstream and lateral components, the correlation coefficient for the vertical component is lower in the main flow (r = 0.597) and negative in the separated flow (r = -0.678). Similarly, the intercepts and slopes obtained from the regression analysis for the areas of main and separated flow (y-int = -0.009, slope = 0.546 and y-int = -0.012 and -0.214, respectively) confirm that the agreement between the two devices is worst for the vertical component of flow. However, his is related to the limited range of velocities rather than to a true discrepancy between the two devices since the regression is being performed over a tightly clustered set of points. As such, it is impossible to draw any conclusions from the regression analysis. However, Figure 33 a and b show that the qualitative agreement between the two devices is quite high. This confirmed that it is appropriate to use the PC-ADP in uniform flows, but that some caution is required in interpreting PC-ADP data in complex flow fields and near the channel boundaries.

In contrast to the mean flow velocities, turbulence statistics reveal large discrepancies between the ADV and the PC-ADP. This is perhaps not surprising considering that turbulence properties display a high degree of spatial variability in rivers with complex flow fields (Blanckaert and Graf, 2001). Furthermore, the sampling frequency between the two devices is markedly different (2 Hz and 25 Hz for the PC-ADP and ADV respectively),

which may create additional difficulties when comparing turbulence results. To investigate the impact of sampling frequency, the ADV signal was reduced from 25 Hz to ~2 Hz using two methods, after which the RMS was re-calculated and compared to its initial value. The first approach was to decimate the signal by taking the average velocity for each half-second interval in the signal, but this technique is not ideal as it greatly reduces the number of samples used in the calculation of RMS levels. Therefore, a second method involving running a low-pass filter taking the average of the 12 neighbouring samples for each 25 Hz measurement was adopted to maintain the same number of samples for the RMS calculation. In either case, the resulting values differed from those obtained using the un-modified signal of the ADV (Table X), which should be expected since either method reduces the variance of the signal. As such, while the PC-ADP can be used in turbulence studies involving low-frequency velocity fluctuations operating on a spatial scale that exceeds the size of its sampling volume, such as large-scale coherent flow structures, it is inappropriate for those focusing on high-frequency variations acting over small spatial scales.

	Unmodified ADV Signal	Method 1	Method 2
RMS Vx (cm/s)	3.395	2.838	2.881
RMS Vy (cm/s)	3.242	2.601	2.587
RMS Vz (cm/s)	2.002	1.430	1.408

Table X: Effects of two methods of temporal averaging on the calculation of turbulence statistics from ADV data.

5.2 Turbulence dynamics Across a Vertical Shear Layer

5.2.1 Large Scale Coherent Flow Structures

Time series analysis of the PC-ADP data has detected high and low speed structures in the regions of main and separated flow. The properties of these events vary between the

two locations due to the very different flow conditions observed on either side of the vertical shear layer.

The velocity signal from the main portion of the channel reveals that high-speed wedges are characterized by shorter durations and periods than low-speed events, which is consistent with the findings of previous studies in a straight gravel-bed river under low thresholds values (S.D.=0.5) (Buffin-Bélanger *et al.*, 2000b). Yet, whereas Buffin-Bélanger *et al.* (2000b) determined that shorter durations and periods begin to be associated with low speed structures when using standard deviations of 1.5, the present analysis shows that only the relative periods of the structures undergo such a reversal at higher threshold values. While there is no obvious explanation for these differences, it may be related to the different conditions under which the data was collected. Unlike the data of Buffin-Bélanger *et al.* (2000b), which were collected upstream of a large pebble cluster in a gravel bedded river, the measurements used in the present analysis were taken slightly downstream of where a pool begins to develop at the entrance of a sand bedded meander loop. Although it would have been desirable to compare the turbulence intensities of the two environments using the PC-ADP, it was not possible due to questions surrounding the accuracy of RMS values obtained with this instrument. However, ADV measurements indicate turbulence intensities of 19% and 25% in the zones of main and separated flow, which is higher than those reported by Buffin-Bélanger and Roy (1998) for a gravel-bed river. This is somewhat surprising, yet the unique bed geometry at the entrance of this particular bend serves to enhance turbulence production in two ways. First, the riffle section immediately upstream of where these measurements were taken is very shallow flow due to the presence of a sediment tongue, followed by a relatively deep pool with a steep entrance face. As such, continuity dictates

that the flow undergoes massive deceleration as it enters the bend (Chang, 2002), which is known to generate turbulence production (Song and Chiew, 2001). Secondly, the slope of the channel bed appears especially steep at the bend entrance, which is probably maintained by the development of strong secondary currents in this region. Therefore the flow may become separated as it enters the pool in a similar manner to what is seen over dune crests (Bennett and Best, 1995) or backwards facing step of Nelson *et al.* (1995), leading to further enhancement of turbulence production. This particular type of bed configuration may also explain why the structures identified in this study are characterized by longer durations and periods than those seen in Buffin-Bélanger *et al.* (2000b) should the flow become separated as it enters the pool. Time series analyses of flow separation over the lee side of dune crests have noted that their shear layers display a distinct flapping motion (Lapointe, 1992). In effect, this serves to produce extended periods of time where instantaneous velocities deviate from the mean value in a coherent manner, resulting in structures with longer durations and periods. The same logic can be applied to explain the longer duration and periods seen in the separation zone with respect to the main flow signal, where it appears as though the vertical shear layer occasionally extends into the sampling volume.

Unlike Buffin-Bélanger *et al.* (2000b) study where two-dimensional velocity measurements were used, coherent structures can also be identified in the cross-stream and vertical planes. The planform geometry of a meander loop generates additional forces that produce relatively strong secondary currents compared to what is seen in straight reaches. As water travels around a bend, its path is deflected towards the outer bank by centrifugal action (Chang, 2002), resulting in a super elevation of the water surface, which creates a fluid pressure gradient directed towards the inner bank. Due to the interaction of these two forces,

meander loops develop a helical flow pattern. Since centrifugal force (F_C) is related to the square of flow speed as defined by the equation

$$F_C = Vx^2/r_c \tag{21}$$

where Vx is the downstream velocity component, and r_c is the radius of curvature along the channel centerline (Chang, 2002), the presence of high-speed and low speed-wedges will cause temporal variations in the force balance, which should result in associated coherent structures in the lateral and vertical planes. This implies that high-speed structures near the outer bank should result in a net outward fluid motion in the lateral plane, thereby causing a temporary super-elevation in the water surface that result in a net fluid motion towards the bed along the vertical axis, whereas the converse would be expected for low-speed structures. By extension, this means that there should be some similarity in event period and duration between the three axes. In order to confirm this hypothesis, the most coherent high-speed and low-speed structures were isolated in the main and separated flow signals by identifying those events with a relatively long duration that persisted at higher thresholds. Subsequently, they were time-matched with the records of their lateral and vertical components. As can be seen in Figure 57a, bedward oriented structures coincide with high-speed events (black windows) and surface directed structures with low-speed events (yellow windows) not only in terms of period and event duration, but also in the times at which they occur. However, laterally oriented events only match up with their respective high-speed and low-speed structures in terms of duration. The reason for the longer relative periods among outwardly oriented structures despite the shorter period of high speed wedges is likely related to the nature of the force balance in the near-bed region of the channel. Although high-speed structures will also temporarily increase centrifugal force acting on the fluid column in the

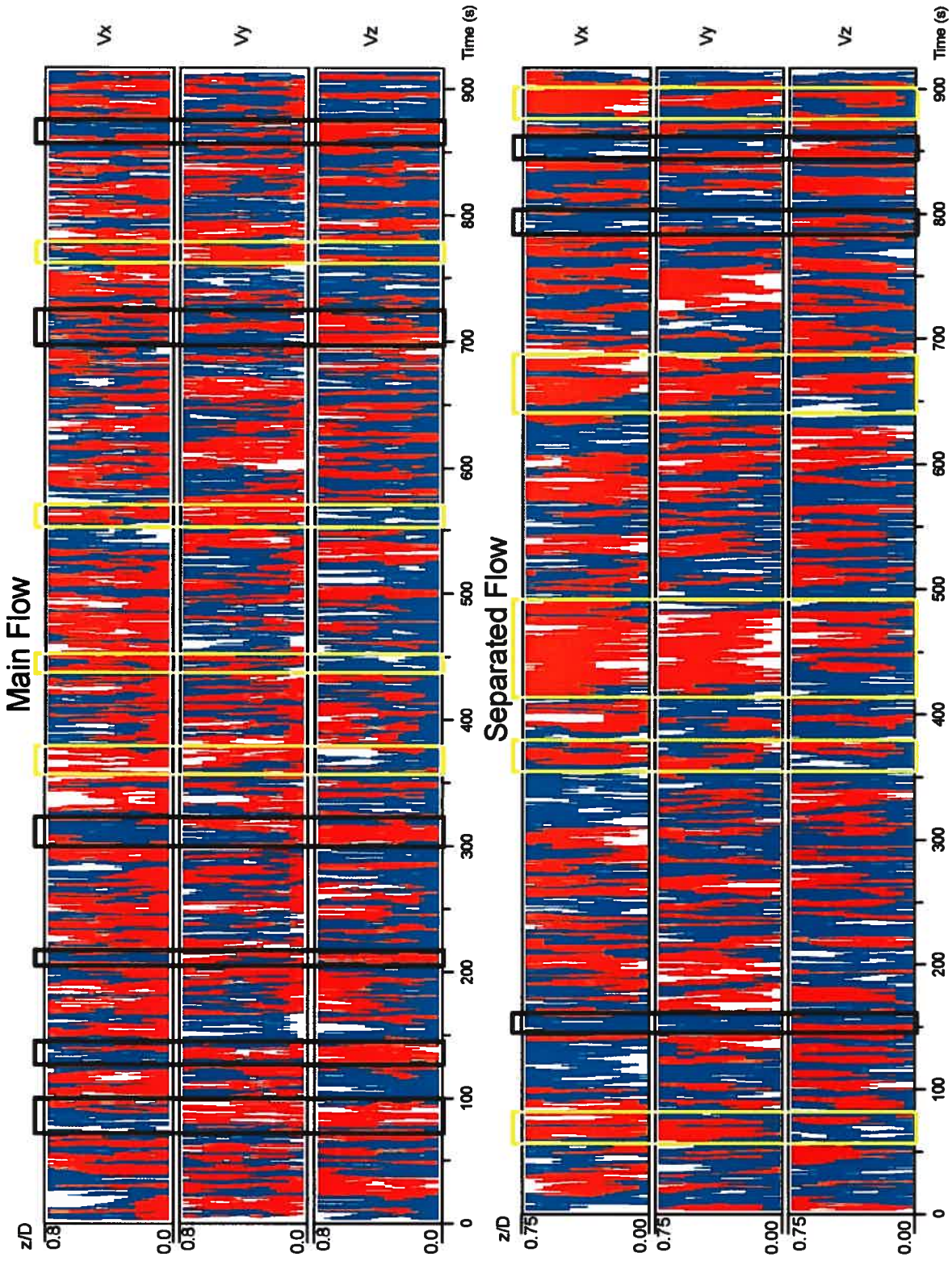

Figure 57: Pairing of downstream flow structures (Fast = Blue, Black outline, Slow = Red, Yellow outline) with events in the lateral (Blue = Outer Bank, Red = Inner Bank) and vertical (Blue = Surface, Red = Bed) planes in the areas of main (a) and separated (b) flow.

bottom portion of the channel, it is not sufficiently strong to overpower the inwardly directed pressure gradient force, hence the rarity of outwardly directed coherent structures. In terms of the separated flow measurement, coherent events detected in the lateral plane match the trends seen in the downstream velocity component in terms of duration, period and time of occurrence (Figure 57b). The apparent lack of association between structures in the downstream and vertical axes likely relate to the dynamics of the shear layer, although determining an exact reason for this phenomenon has proven elusive.

5.2.2 Burst-Sweep Properties

As was the case for coherent flow structures along the downstream, lateral and vertical planes, time series analysis of the PC-ADP data reveal the presence of large-scale quadrant events in the two signals. Although they typically display shorter durations, periods and appear less organized than what was previously seen, a distinct pattern in their quadrant distributions begins to emerge upon applying progressively larger thresholds. Moreover, the trends seen in the main flow signal are very different from those in the separation zone, which again is likely due to the presence of a vertical shear layer.

The downstream-vertical plane of the main flow measurement is dominated by brief bursting events (quadrant 2) and slightly longer and stronger sweeps (quadrant 4), which are the more frequent of the two (Figure 38a). Conversely, only a few weak interaction events are detected in the data initially (quadrants 1 and 3), and are virtually absent from the record after applying a threshold to the signal. Although very few studies have attempted to detect large-scale burst-sweep events (e.g. Buffin-Bélanger *et al.*, 2000b), the results of which were inconclusive, these trends generally agree with what has been learned from the analysis of

velocity point data in terms of event duration, intensity and quadrant distribution (Grass, 1971; Luchik and Tiederman, 1987; Robinson, 1991; Lapointe, 1992). Unlike these studies, sweeping structures are more common than bursts. It is likely that this discrepancy results from either the difference in size of these two events or the frequency and size of the sampling volume of the instrument. Previous investigations have suggested that slow speed fluid events that constitute bursts are typically shorter in duration than sweeps (Nelson *et al.*, 1995) implying that they act over a smaller planform area. Therefore, their lower frequency may result from them not meeting the criteria of occupying 75% of the flow depth used in this analysis. Alternatively, the spatial and temporal averaging effects of the PC-ADP may be high enough so as to mask some of the briefer, smaller burst events.

Contrary to this clear tendency towards quadrant 2 and 4 events, there is no obvious preference towards any particular quadrant in the separation zone (Figure 38b). Again, this may be related to the shear layer having a flapping motion, resulting in the signal record containing periods of main channel and separation zone flow properties. Indeed, previous work on vertical shear layers has demonstrated that all four quadrants can dominate at different locations around these zones (Biron *et al.*, 1996). It is interesting to note that quadrants 1 and 3 are the most common under low thresholds in the separation zone. The flow orientation in this zone should be used as a reference in determining which quadrant is representative of bursts, sweeps or interaction events. Since the near-bed flow is oriented upstream in the separation zone, quadrants 1 and 3 actually represent burst and sweep events respectively, hence their higher frequency with respect to quadrants 2 and 4 is in agreement with what would be expected.

Unlike the case of the downstream-vertical plane, the downstream lateral plane of the main flow signal displays no preference for any particular combination of quadrants (Figure 40a). This should also be expected when one considers that the Reynolds stress, and hence the quadrant distribution, represents a momentum flux (Best, 1993). A necessary precursor to having an organized form of momentum exchange is the presence of a significant velocity gradient such as that contained in a logarithmic velocity profile. Since one would expect only minimal variations in downstream flow speeds over small distances away from the channel centerline, and hence just a very weak velocity gradient, the main flow signal lacks any driving force to produce organized momentum exchange, thereby explaining the lack of a dominant pair of quadrants.

In the separation zone, however, there is a clear domination of quadrants 2 and 4 in the downstream-lateral plane (Figure 40b). This may be explained by the velocity gradient observed while traveling laterally from the bank towards the channel centerline that characterize river bends (Chang, 2002). This produces a strong force acting to promote momentum exchange between the area of main and separated flow. In addition, if one uses the bank rather than the shear layer to define the naming of quadrants, these events (quadrants 2 and 4) represent bursting and sweeping motions respectively. Clearly there is a great deal of difficulty associated with what constitutes bursting and sweeping events in any plane other than the downstream-vertical, but it appears as if the proper reference surface (i.e shear layer versus bank face) is determined by the sharpest velocity gradient. Yet the presence of a vertical shear layer next to the bank is analogous to the separation zone formed on the lee side of a dune crest, where the bed is always used as the reference point (Bennett and Best, 1995). Therefore the bank face should be the surface used in naming the quadrants

as it will allow one to draw comparisons with previous studies of flow separation over bedforms.

Much like the downstream-lateral plane, the lateral vertical plane displays only a weak tendency towards quadrant preference in the main flow measurement (Figure 42a). Initially, the frequency of all quadrant events appears to be equal, and it is only at higher threshold values that the periods of quadrant 1 and 3 events are roughly half of those found in quadrants 2 and 4. Considering that the flow near the bed, where these structures are generated, is directed towards the inner bank, the classical quadrant framework would predict the highest frequencies to occur in quadrants 2 and 4, which correspond to bursting and sweeping motions respectively. Yet the findings of this study appear logical when viewed from a momentum flux perspective. Recall that lateral current strength decreases from its maximum values in the near-surface and near-bed regions to their minimum values at the middle of the water column where centrifugal and pressure-gradient forces are equal; the vertical component of flow also decreases from the banks to the channel centerline. Hence, the point of minimum energy in the lateral-vertical plane in meander loops is situated in the middle of the helical flow cell since this is where secondary current strength is the weakest. Therefore, these structures are transferring momentum along the strongest energy gradient (quadrants 1 and 3). The same argument applies to the separation zone, where quadrant 2 and 4 structures clearly dominate the signal (Figure 42b). In this case, it is the bank face rather than the bed that acts as the surface over which these structures are generated. Therefore, momentum is being exchanged between the point of high energy near the water surface adjacent to the bank and low energy at mid flow depth towards the channel centerline (quadrants 2 and 4). The higher degree of quadrant preference seen here probably indicates

that the energy gradient is much stronger in the separated flow than in the main portion of the channel.

5.3 Bend Scale Flow Properties

5.3.1 Mean Flow Properties (PC-ADP)

Analysis of the mean flow measurements obtained with the PC-ADP reveals that the three-dimensional flow structure at the bend varies with flow stage. Although the high velocity core and secondary current properties remain quite constant between the two lower stage level datasets (August 28, 2003 and September 24, 2003), the significant differences seen in the higher stages dataset (October 13, 2003) indicate that flow structure is stage dependent.

During the low discharge level of August 28, 2003, the high velocity core begins to expand and decelerate as it travels around the meander loop, which is the direct result of changes in cross-section geometry between the measured transects (Figure 43). Between the entrance and apex of the bend, the channel cross-sectional area is reduced by 21%. While this alone would cause maximum flow speeds to increase, there is only a mild decrease in its wetted perimeter (10%). As such, the wetted perimeter to area ratio actually increases by 14% between the entrance and apex of the meander loop. The effect of this relative increase in frictional surface area is to reduce the values of V_{max}, which must be offset by an expansion of the high velocity core to maintain continuity of discharge. In terms of secondary currents, there is a lag between the bend entrance and the development of a coherent circulation cell, which is directly related to the flow stage. In order to develop a coherent circulation cell in a meander loop, the effects of centrifugal action must be felt

across the entire width of the channel. However, the strength of this force is relatively weak at low flow stages, so there is a delay between the bend entrance and the development of significant super-elevation of the water surface. The implication of this is that there is a similar lag between when centrifugal force begins to take effect and form the top half of the cell and the point at which it can be countered by the inwardly oriented pressure gradient force along the bottom half of the channel to complete the circulation. Moreover, measurements from the bend apex appear to suggest the presence of a smaller, weaker counter-rotating cell next to the outer bank, which is probably related to the roughness of the bank itself. The lower downstream flow speed found here will reduce centrifugal forces (Equation 21) so that the inwardly oriented pressure gradient dominates the force balance. As such, the flow travels towards the inner bank until it reaches the outer edge of the main cell where the two forces are roughly balanced and downwelling occurs.

Given the similarity in flow stages with the August 28, 2003 dataset, it is reassuring to see that the flow structure at the entrance and apex remains the same in the September 24, 2003 measurements (Figure 44). Moreover, this dataset contains measurements from the bend exit. Here, the flow structure is quite similar to what is seen at the apex, although the weaker counter-rotating cell appears to have increased in size. This apparent growth of the outer bank cell is again related to the slow flow speeds found in this region, which would cause the pressure gradients to dominate the force balance until it reaches the point of downwelling in the main cell.

Based on the analysis of the October 13, 2003 dataset, it is apparent that even a moderate increase in discharge levels (from 22% to 29%) can have a marked impact on the flow structure of meander loops (Figure 45). While the trend of reduced flow speeds

between the bend entrance and exit is still present, there is no expansion of the high velocity core and the pattern of secondary currents is quite distinct from the previous two datasets, both of which are related to the elevated water velocities. Compared to the previous two sets of measurements, centrifugal action is stronger. Therefore it is capable of suppressing lateral expansion of the high velocity core from the outer towards the inner bank and creates more pronounced secondary currents. This is clearly demonstrated at the bend entrance, which is characterized by two circulation cells rather than lateral divergence from the channel centerline. It is interesting to note that in addition to the classical main and weaker counter-rotating cell, measurements from the bend apex seem to suggest the presence of a third cell immediately adjacent to the outer bank rotating in the same manner as the main cell. At the bend exit, the third cell has completely vanished and the counter-rotating cell has undergone significant decay. Recalling that centrifugal force is inversely related to radius of curvature (Equation 21), the counter-rotating cell is suppressed at the bend entrance and exit since these are the points where the local radii of curvature is at a minimum. Additionally, there is a more pronounced point bar that redirect the high velocity core towards the bank and, acting in conjunction with a slight bank protrusion, constricts the flow at this transect. These two effects would also strengthen secondary currents in a meander loop. These variations in flow structure have important implications for bend development. In their flume study, Blankaert and Graf (2001) concluded that the presence of a counter-rotating cell can actually reduce channel migration rates at it acts like a buffer between the high velocity core and the bank toe. As such, these measurements indicate that bank failure rates will be the highest at the bend entrance and exit, which is in agreement with the shear stress distributions (Figure 54 to 56). Clearly, discharge levels, and hence structure and strength of secondary currents

throughout the bend, play an important role in meander loop evolution. More measurements at higher discharge levels, however, are required to generalize these findings.

5.3.2 Turbulent Flow Properties (ADV)

Analysis of the velocity measurements obtained with the ADV has revealed distinct patterns in the bends turbulent flow properties. Firstly, all three flow axis show a distinct trend of increasing RMS values from the bed to the water surface (Table VII), and with the exception of the May 15 2003 measurements, the same is true for turbulence intensities. Secondly, all of the datasets show a clear pattern of decreasing RMS levels in the lateral and vertical velocity components compared to those observed in the downstream component. Finally, analysis of the low, medium and high flow datasets reveal that the location of maximum turbulence intensity is indeed variable and appears to be stage dependent.

Near-bed turbulence intensities in the downstream and cross-stream directions are higher than those observed at the surface in all six datasets (Figure 46 to 48), which agrees with the findings of previous research on the shape of turbulence profiles (Song and Chiew, 2001). However, this trend is far less pronounced along the vertical axis, which is probably related to the differences in flow structure of river bends compared to those in a straight, rectangular flume tank. Unlike the latter where secondary currents display no coherent structure, the helical flow patterns in meanders create a relatively high degree of shear along the lateral component in the upper half of the velocity profile. As a result, this will produce coherent motions analogous to bursting and sweeping events seen along the downstream axis, which represent a source of near-surface turbulence production in the vertical flow component that is not seen in straight reaches. As for trends between the three components,

the highest RMS levels are consistently associated with the downstream component, followed by the lateral, then the vertical directions. Similar results have been noted in flume studies of river bends (Blanckaert and Graf, 2001).

Figure 46 to 48 also illustrate that the locations of maximum turbulence intensity are highly dependent on flow stage. The sites of highest near bed and near surface intensities for all three components are initially located at the bend entrance, but they clearly begin to shift towards the exit region with increasing discharge levels. These findings conform with textbook examples of how shear stress patterns change with flow stage (Chang, 2002), where the site of maximum bank erosion in river bends will migrate downstream at higher discharges. Given the link between shear stress levels and turbulence intensity, this variable should display a similar trend. Although the reason for this shift is not entirely clear, it is probably related to the diminishing role that topographic steering plays in determining flow structure with elevated discharge levels (Whiting and Dietrich, 1991). As such, this retards the point at which the high velocity core becomes deflected towards the outer bank, resulting in the highest bank failure rates to occur beyond the bend apex (Dietrich and Smith, 1984). Yet there still appears to be a point of elevated shear stress at the bend entrance during periods of medium and high flow, which probably results from the flow becoming separated as it enters the pool for the near-bed measurements, and from the high velocity core beginning to make contact with the outer bank for samples taken close to the water surface. These patterns have important implications on the evolution of a meander loop.

5.4 Bend Evolution

5.4.1 Evaluation of Techniques to Estimate Bed Shear Stress

Unlike previous appraisals of the different techniques to estimate bed shear stress, the analysis performed here is unique in that: 1) it is performed along a reach with relatively strong secondary currents, 2) it compares the situation on both sides of a vertical shear layer that acts as a boundary between two distinct types of flows, and, 3) it is performed using two different sampling devices.

The first step of this analysis is to compare the abilities of the ADV and PC-ADP to accurately estimate bed shear stress using various techniques. Although it was not possible to take direct measurements of bed shear stress for the comparison, sporadic bedload sediment transport events were observed at the time this data was collected in both the non-separated flow, and to a lesser degree in the area of flow separation. Therefore the critical shear stress required to initiate particle motion provided a reasonable proxy for the forces acting on the bed.

In general, the ADV yields more realistic estimations of bed shear stress regardless of the technique being used. Of the unsteady flow techniques, the PC-ADP greatly overestimates the forces acting on the bed using the Reynolds $u'w'$ and the three-dimensional TKE approaches, but underestimates when TKE w' is applied. While the ADV also underestimates bed shear stress using the TKE w' approach, it provides more reasonable values than the PC-ADP. However, the ADV provides very reliable estimates of the forces acting on the bed using the other two unsteady approaches (Reynolds $u'w'$ and TKE). The divergence in results between the two devices is expected since the PC-ADP signal displays

much higher RMS values in the downstream component of flow and lower values along the vertical component versus the ADV for the near-bed region (Figure 34 a). It is somewhat surprising, however, that the log-law estimates obtained with the PC-ADP are so different from the critical value given the similarity in mean flow properties between the two devices. These findings do make sense when one considers how the PC-ADP's sampling volume grows in planform area with increasing distance from the device. The log-law approach of estimating bed shear stress requires calculating the velocity gradient from the bottom portion of the profile, which coincides with the region where spatial averaging is the most severe with the PC-ADP.

Based on the main flow ADV measurements, it is obvious that the most accurate estimates are obtained using either the Reynolds or three-dimensional turbulent kinetic energy techniques. These findings are consistent with the field observations of Drake *et al.* (1988) who noted that transport events occurred in patches that were random in time and space even though their estimate of bed shear stress using a non-turbulence technique was well below the critical threshold. It has been recognized that turbulent structures play a fundamental role in sediment transport (Clifford and French, 1993), and this is especially true for the case of near-equilibrium conditions where instantaneous downstream velocities above their mean value will cause the sediments to become mobile (Nelson *et al.*, 1995). These findings are also in agreement with the laboratory study of Biron *et al.* (2004b), who found that the Reynolds shear stress is the best method for simple boundary layers, whereas the three-dimensional turbulent kinetic energy approach yields the best estimate of bed shear stress in complex flow fields. Moreover, it is not surprising that the three-dimensional TKE method produces the best estimations in river bends since their flows are characterized by

strong secondary currents (Knighton, 1998). By definition, shear stress is a force that is oriented parallel to a surface (Chang, 2002), and studies performed in straight flume tanks have clearly demonstrated that sediment transport events are directly correlated with downstream turbulence intensities (Nelson *et al.*, 1995). This explains why only the Reynolds and three-dimensional turbulent kinetic energy approaches produce accurate values.

While either of these approaches is suitable in the main portion of the channel, the Reynolds method clearly fails in the separation zone, as can be seen in the negative stress values it produces (Table IX). This highlights one of the fundamental problems associated with this technique: it is highly sensitive to flow orientation, structure and its degree of organization, which can lead to negative stress estimations. For this reason, as Biron *et al.* (2004b) concluded, the three-dimensional turbulent kinetic energy approach is the ideal method of estimating bed shear stress in complex flow fields, as it is insensitive to flow orientation and it is the only method that incorporates all three velocity components into its approximation.

5.4.2 Chronology of Channel Change

By comparing the annual changes in the river's bed and bank topography prior to, during and following the implementation of bank stabilization measures, it has been possible to identify two distinct trends in the evolution of the bend. Firstly, the bend entrance and exit regions continue to experience significant bank failure events in spite of having been stabilized. Secondly, the river reacted to the stabilization measures through a massive sediment deposition event along the inner bank of the channel.

Prior to stabilizing the banks, the most dynamic sections of the river were found at the entrance and exit of the bend along both the inner and outer banks (Figure 49), resulting in a relatively large increase in total channel volume between July, 2002 and May, 2003 (57 m^3). This was followed by the immediate changes to the channel associated with implementing this particular type of stabilization scheme. As would be expected, reducing the slope of the outer bank resulted in a massive increase in channel volume (142 m^3) (Figure 58), but it also prevented the identification of failure events along the outer bank. However, the locations of dynamic regions along the inner bank remained the same (Figure 50), suggesting that the bend will continue to develop in a predictable manner. The sites of bank erosion over the one year period following stabilization coincides with the initial points of failure, and the channel has reacted to this work through massive sediment deposition along the inner bank (Figure 51). These localized zones of bank failure match up with the bed shear stress distributions (Figure 54 to 56), where the maximum values were found at the bend entrance at low-flow stages and at the bend exit at high flow stages.

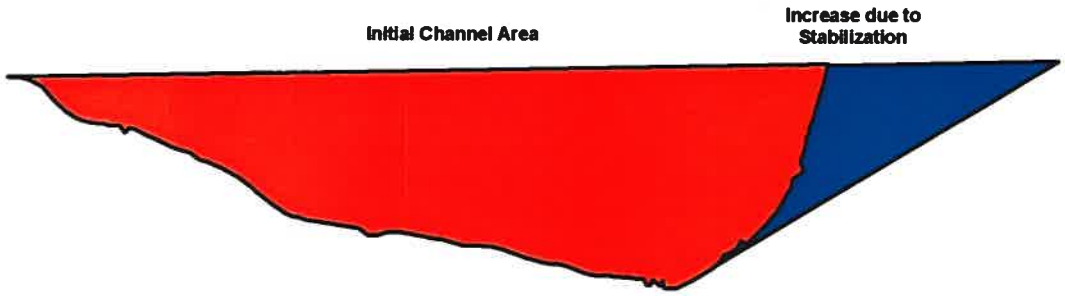

Figure 58: Effect of bank stabilization on cross-sectional area.

The site of maximum bank erosion rates should be concentrated to one zone, which migrates downstream with increasing discharge levels (Chang, 2002). Considering that large scale bank failure events are commonly associated with high flow stages, it is surprising that

the initial point of bank failure is found so early in the bend, followed by a second site towards the bend exit. Although previous work on the spontaneous development of multiple pools in meander loops has suggested that bank failure events need not be limited to a single zone (Whiting and Dietrich, 1993b), these studies were performed along a large amplitude river bend. Previous studies have shown that straight reaches display a sinuous flow pattern (Rhoads and Welford, 1991). As such, Whiting and Dietrich (1993b) concluded the development of multiple pools in large amplitude meander loops were the result of weak centrifugal forces, which could not fully suppress the sinuous flow pattern. However, the meander loop in this study displays a relatively small radius of curvature, and therefore the multiple points of bank failure seen in this study are unlikely to have resulted from a sinuous thawleg. A more plausible explanation for the trends seen in this study is related to this being a regulated river. The effect of the upstream dam is to maintain relatively low flow stages throughout the majority of the year, interspersed with only a few flooding situations following the spring snow-melt and major precipitation events (Figure 18). As a result, these two distinct types of flow conditions serve to create a unique distribution of failure events throughout the bend. During low discharge levels, the flow structure is being controlled by topographic steering over the point bar (Whiting and Dietrich, 1991), which re-directs it towards the outer bank early on at the bend entrance. Upon making contact with the bank, the thawleg is deflected back towards the channel centerline throughout the bend apex, and once again makes contact towards the exit region. This causes knick points to develop along the outer bank, which lowers the radius of curvature at the bend entrance and exit relative to the apex of the meander loop, the effects of which are enhanced by large failure events during

bankfull conditions. Hence it can be said that the pattern of channel migration is determined by low-discharge flow properties, but evolution itself actually occurs during high flow stages.

A second point of interest to emerge from this analysis is how quickly and dramatically the river reacted to stabilization measures. To explain this phenomenon, one must work under the premise that the fluid forces of undisturbed rivers are in a state of quasi-equilibrium with the channel sediments. The stabilization scheme involved reducing the slope of the bank face from near-vertical to 30 degrees, the effect of which is a massive increase in the channels cross-sectional area (Figure 58). To maintain discharge, mean flow speeds must be reduced, which creates a non-equilibrium situation. These lower velocities greatly reduce the river transport capacity, resulting in sediment deposition along the inner bank. By doing so, cross-sectional area is reduced and flow speeds return to their pre-stabilized values. Therefore, the river is re-establishing its quasi-equilibrium conditions, as is seen in the initial increase in channel volume of 142 m^3 following stabilization and the subsequent decrease of 98 m^3 over the following year. This raises some valid concerns about the effectiveness of this particular form of bank stabilization, along with the fact that there is still evidence of failure events at the entrance and exit of the bend. However, this analysis is limited to the initial period of channel adjustment, and assuming that the stabilization measures are strong enough to prevent the re-development of near-vertical bank faces, channel migration rates should be greatly reduced.

6. Conclusion

As man made structures continue to encroach on the natural environment, the need for sound restoration techniques and management strategies that promote sustainable development will continue to grow. Since rivers have the potential to cause immense damage on existing infrastructure through flooding and channel migration, the subject of river engineering has been gaining more attention from fluvial geomorphologists in recent years. Yet there is no universal law to predict how meander loops will evolve since their development is site specific. As such, there is an ongoing need for researchers to take direct flow measurements to improve our understanding of how bend planform geometry changes over time.

One of the most recently introduced devices to collect instantaneous water velocity measurements is the PC-ADP, which was evaluated against the ADV in this study. This comparison demonstrated that while the two devices do not yield identical turbulence statistics due to the spatial and temporal averaging effects of the PC-ADP, the latter can produce reliable mean flow measurements if the spatial variation in velocities is small across the sampling volume. Moreover, previous work has shown that it is just as capable of detecting burst and sweep events as the ADV (Vallée, 2003), and therefore can be used to identify large-scale coherent flow structures. As such, it was successfully used to show that all three velocity components contain distinct high and low speed structures that are coherent over the majority of the water column in the areas of both main and separated flow within a meander loop. Future research involving an array of ADVs is required to determine if the long time scales of the events are structurally coherent or if they are simply a by-product of spatial and temporal averaging.

Flow patterns in river bends are characterized a high velocity core located along the outer bank and the development of secondary circulation cells. Velocity measurements confirm that the meander loop used in this study does indeed display this type of flow pattern, however, the locations of circulation cell development and maximum turbulence intensity are discharge dependent. The high velocity core begins to slow down and expand as it travels through the meander loop, and while it displays secondary circulation cells at all flow stages, the development of a coherent cell occurs further downstream from the bend entrance at low discharges. It would be worth investigating the structure of the outer bank cell further with more precise instruments since its dimensions will affect bank erosion rates. The same discharge dependency exists for the site of maximum turbulence intensity, which tends to migrate downstream and decrease in strength with increasing flow stage. However, it would be desirable to obtain a bankfull dataset to see if this trend persists at higher discharge levels.

With the increasing availability of three-dimensional velocimeters, shear stress measurements should be made using the TKE method in these complex flow fields. However, flume studies should be performed to resolve the following issues: 1) at what point (non-dimensional) in the water column should samples be taken to make accurate single-point estimates of bed shear stress in complex flow fields; 2) re-evaluate the coefficient for three-dimensional TKE based on height above the bed (non-dimensional) using direct measurements in conjunction with visualization studies of sediment transport events. Using the aforementioned approach, there is a clear match between the shear stress distributions and the bank failure events observed over the course of this study at the bend entrance and exit. As for the effects of stabilization on the channel itself, longer-term studies are required to

determine how the initial readjustment through massive deposition along the inner bank will develop after a few years in place. Failure events appear to persist along the entrance and exit regions after the first year of implementation. Due to the length of this study, the success of this "soft-engineering" approach to stabilizing river banks could not be clearly gauged. None the less, it is clear from the failure events observed following the stabilization that the bank treatment used on the Petite Barbue River could be improved. Since the survival rates of the bank vegetation appeared to be low, the first step would be to used more mature plantings and subsequently send a field crew to the site to monitor their establishment. Secondly, structures should be added below the water line as this would decrease near-bank flow speeds, and hence scour of the bank toe to further reduce failure events.

As a final point, it would be interesting to see the effect of localized bank stabilization measures on the channel downstream of the protected reach. Since stabilization involves reducing the bank slope, it creates a constriction at the interface between the protected and non-protected sections of the river, which may accelerate bank erosion rates downstream of the study reach. However, this potential issue could have been avoided at the Petite Barbue since the bend used in this study is immediately followed by a second meander loop. Therefore, the constriction could be eliminated by extending the stabilization measures so there would be a smooth transition between the protected section and the inner bank face of the second loop.

Abernethy, B. and Rutherfurd, I.D. (1998). Where along a river's length will vegetation most effectively stabilize stream banks? *Geomorphology*, 23, 55-75.

Allen, P.M., Arnold, J. and Jakubowski, E. (1999). Prediction of stream channel erosion potential. *Environmental and Engineering Geoscience.* 5(3), 339-351.

Andrle, R. (1994). Flow structure and development of circular meander pools. *Geomorphology.* 9, 261-270.

Bennett and Best, J.L. (1995). Mean flow and turbulence structure over fixed, two-dimensional dunes: implications for sediment transport and bedform stability. *Sedimentology.* 42, 491-513.

Best, J.L. (1993). On the interactions between turbulent flow structure, sediment transport and bedform development: some considerations from recent experimental research. In: *Turbulence: Perspectives on flow and sediment transport.* (eds: Clifford, N., French, J.R. and Hardisty, J.) 197-213. New York: Wiley and Sons Ltd.

Biedenhern, D.S., Elliott, C.M. and Watson, C.C. (1997). *The WES Stream Investigation and Streambank Stabilization Handbook.*

Biron, P.M., DeSerres, B., Best, J.L. and Roy, A.G. (1993). Shear layer turbulence at an unequal depth channel confluence. In: *Turbulence: Perspectives on flow and sediment transport.* (eds: Clifford, N., French, J.R. and Hardisty, J.) 197-213. New York: Wiley and Sons Ltd.

Biron, P.M., Lane, S.N., Roy, A.G., Bradbrook, K.F. and Richards, K.S. (1998). Sensitivity of bed shear stress estimated from vertical velocity profiles: the problem of sampling resolution. *Earth Surface Processes and Landforms*. 23, 133-139.

Biron, P.M., Robson, C., Lapointe, M.F. and Gaskin, S.J. (2004a). Deflector designs for fish habitat restoration. *Environmental Management*. 33(1), 25-35.

Biron, P.M., Robson, C., Lapointe, M.F. and Gaskin, S.J. (2004b). Comparing different methods of bed shear stress estimates in simple and complex flow fields. *Earth Surface Processes and Landforms*, 29, 1403-1415.

Blanckaert, K. and Graf, W.H. (2001). Mean flow and turbulence in open-channel bend. *Journal of Hydraulic Engineering ASCE.* 127(10), 835-847.

Bogard, D.G. and Tiederman, W.G. (1986). Burst detection with single point velocity measurements. *Journal of Fluid Mechanics*. 162, 389-413.

Boyer, C., Roy, A.G. and Best, J.L. (in review). Dynamics of a river channel confluence with discordant beds: fluid turbulence, sediment transport and bed morphology. *Geophysical Review Letters.*

Bridge, J.S. and Best, J.L. (1988). Flow, sediment transport and bedform dynamics over the transition from dunes to upper stage plane beds: implications for the formation of planar laminae. *Sedimentology.* 35, 753-763.

Buffin-Bélanger, T. and Roy, A.G (1998). Effects of a pebble cluster on the turbulent structure of a depth limited flow in a gravel-bed river. *Geomorphology.* 25, 249-267.

Buffin-Bélanger, T., Roy, A.G. and Kirkbride, A.D. (2000a). Vers l'intégration des structures turbulentes de l'écoulement dans la dynamique d'un cours d'eau à lit des graviers. *Géographie Physique et Quaternaire.* 54(1), 105-117.

Buffin-Bélanger, T., Roy, A.G. and Kirkbride, A.D. (2000b). On large-scale flow structures in a gravel-bed river. *Geomorphology.* 32, 417-435.

Chang, H. (2002). *Fluvial Processes in River Engineering.* Florida: Krieger Publishing Company.

Clifford, N.J. and French, J.R. (1993). Monitoring and modeling turbulent flows: historical and contemporary perspectives. *Turbulence: Perspectives on Flow and Sediment Transport.* New York: John Wiley & Sons Ltd.

Corrsin, S. (1957). Some current problems in turbulent shear flows. *Symposium on Naval Hydrodynamics: Proceedings.* 373-402.

Couper, P., Stott, T. and Maddock, I. (2002). Insights into river bank erosion processes derived from analysis of negative erosion-pin recordings: observations from three recent UK studies. *Earth Surface Processes and Landforms.* 27, 59-79.

Daniels, M.D. and Rhoads, B.L. (2003). Influence of large woody debris obstruction on three-dimensional flow structure in a meander bend. *Geomorphology.* 51 159-173.

Daniels, M.D. and Rhoads, B.L. (2004). Effect of large woody debris configuration on three-dimensional flow structure in two low-energy meander bends at varying stages. *Water Resources Research*, 40.

Darby, S.E. and Thorne, C.R. (1996). Stability analysis for steep, eroding, cohesive riverbanks. *Journal of Hydraulic Engineering ASCE.* 122, 443-454

Darby, S.E. and Delbono, I. (2002). A model of equilibrium bed topography for meander bends with erodible banks. *Earth Surface Processes and Landforms.* 27, 1057-1085.

Darby, S.E., Alabyan, A.M. and Van de Wiel, M.J. (2002). Numerical simulation of bank erosion and channel migration in meandering rivers. *Water Resources Research*, 38(9), 1163

Demuren, A.O. (1991). Calculation of turbulence-driven secondary motion in ducts with arbitrary cross-section. *AIAA Journal,* 29(4), 531-537.

De Serres, B., Roy, A.G., Biron, P.M. and Best, J. (1999). Three-dimensional structure of flow at a confluence of river channels with discordant beds. *Geomorphology.* 26, 313-335.

Dietrich, W.E., Smith, J.D., and Dunne, T. (1983). Boundary shear stress, sediment transport and bed morphology in a sand-bedded river meander during high and low flow. *River meandering: proceedings of the conference rivers, 1983.* New York: American Society of Civil Engineers.

Dietrich, W.E. and Smith, J.D., 1984. Bed load transport in a river meander. *Water Resources Research.* 20(10), 1355-1380.

Dietrich, W.E., and Whiting, P.J. (1989). Boundary shear stress and sediment transport in river meanders of sand and gravel. *River Meandering, Water Resour. Monogr. Ser. 12.* Washington D.C.: AGU.

Drake, T.G., Shreve, R.L., Dietrich, W.E., Whiting, P.J. and Leopold, L.B. (1988). Bedload transport of fine gravel observed by motion-picture photography. *Journal of Fluid Mechanics.* 192, 193-217.

Duan, J.G., Wang, S.S.Y. and Jia, Y., 2001. The applications of the enhanced CCHE2D model to study the alluvial channel migration processes. *Journal of Hydraulic Research.* 39(5), 469-480

Falco, R.E. (1977). Coherent motions in the outer region of turbulent boundary layers. *The Physics of Fluid.* 20(10) 124-132.

Ferguson, R.I., Parsons, D.R., Lane, S.N. and Hardy, R.J., (2003). Flow in meander bends with recirculation at the inner bank. *Water Resources Research.* 39(11), 1322-1335.

Frothingham, K.M. and Rhoads, B.L. (2003). Three-dimensional flow structure and channel change in an asymmetrical compound meander loop, Embarras River, Illinois. *Earth Surface Processes and Landforms*, 28, 625-644.

Gilvear, D., Winterbottom, S., and Sichingabula, H.. (2000). Character of channel planform change and meander development: Luangwa River, Zambia. *Earth Surface Processes and Landforms*, 25 (4), 421-436.

Goring, D.G. and Nikora, V.I. (2002). Despiking acoustic Doppler velocimeter data. *Journal of Hydraulic Engineering ASCE.* 128(1), 117-126.

Grass, A.J. (1971). Structural features of turbulent flow over smooth and rough boundaries. *Journal of Fluid Mechanics*. 50(2), 233-255.

Hodskinson, A. and Ferguson, R.I. (1998). Numerical modelling of separated flow in river bends: model testing and experimental investigation of geometric controls on the extent of flow separation at the concave bank. *Hydrological Processes*. 12, 1323-1338.

Huthnance, J.M., Humphery, J.D., Knight, P.J., Chatwin, P.G., Thomsen, L. and White, M. (2002). Near-bed turbulence measurements, stress estimates and sediment mobility at the continental shelf edge. *Progress in Oceanography*. 52, 171-194.

Jackson, R.G. (1976). Sedimentological and fluid-dynamic implications of the turbulent bursting phenomenon in geophysical flows. *Journal of Fluid Mechanics*. 77(3) 531-560.

Jia, Y. and Wang, S.S.Y. (1999). Numerical model for channel flow and morphological change studies. *Journal of Hydraulic Engineering ASCE*. 125(9), 924-933.

Kabir, M.R. and Torfs, H. (1992). Comparison of different methods to calculate bed shear stress. *Water Science and Technology*. 25(8), 131-140.

Kim, H.T., Kline, S.J. and Reynolds, W.C. (1971). The production of turbulence near a smooth wall in a turbulent boundary layer. *Journal of Fluid Mechanics*. 50(1), 133-160.

Kim, S.-C., Friedrichs, C.T., Maa, J.P.-Y., and Wright, L.D. (2000). Estimating bottom stress in tidal boundary layer from acoustic Doppler velocimeter data. *Journal of Hydraulic Engineering ASCE*. 126(6), 399-406.

Kirkbride, A.D. and Ferguson, R. (1995). Turbulent flow structure in a gravel bed river: markov chain analysis of the fluctuating velocity profile. *Earth Surface Processes and Landforms*. 20(8), 721-733.

Kline, S.J., Reynolds, W.C., Schraub, F.A. and Runstadler, P.E. (1967). The Structure of turbulent boundary layers. *Journal of Fluid Mechanics*. 30(4), 741-773.

Knighton, D. (1998). *Fluvial Forms and Processes*. New York: Oxford University Press, Inc.

Lancaster, S.T. and Bras, R.L., 2002. A simple model of river meandering and its comparison to natural channels. *Hydrological Processes*. 16, 1-26

Lane, S.N., Biron, P.M., Bradbrook, K.F., Butler, J.B., Chandler, J.H., Crowell, M.D., McLelland, S.J., Richards, K.S., and Roy, A.G. (1998). Three-dimensional measurement of river channel flow processes using Acoustic Doppler Velocimetry. *Earth Surface Processes and Landforms,* 23 (13), 1247-1267.

Lane, S.N., Bradbrook, K.F., Richards, K.S., Biron, P.M., and Roy, A.G. (1999). 'Time-averaged flow structure in the central region of a stream confluence': A discussion. *Earth Surface Processes and Landforms,* 24, 361-367.

Lapointe, M. (1992). Burst-like sediment suspension events in a sand bed river. *Earth Surface Processes and Landforms*. 17, 253-270

Lee, J.M., Nahajski, A. and Miller, S. (1997). Riverbank stabilization program. *Journal of Water Resources Planning and Management ASCE.* 123(5), 292.294.

Lee S-J., and Kim, H-B. (1999). Laboratory measurements of velocity and turbulence field behind porous fences. *Journal of Wind Engineering ASCE.* 80, 311-326.

Leeder, M.R. and Bridge, P.H. (1975). Flow separation in meander bends. *Nature.* 253, 338-339.

Luchik, T.S. and Tiederman, W.G. (1987). Timescale and structure of ejections and bursts in turbulent channel flows. *Journal of Fluid Mechanics*. 174, 529-552.

Matthes, G.H. (1947). Macroturbulance in natural stream flows. *Transactions of the American Geophysical Union*. 28, 255-262.

Maurizi, A., Di Sabatino, S., Trombetti, F., and Tampieri, F. (1997). A method of analysis for turbulent flows using a streamline coordinate system. *Boundary-layer Meteorology.* 82, 379-397.

McLelland, S.J. and Nicholas, A.P. (2000). A new method for evaluating errors in high-frequency ADV measurements. *Hydrological Processes.* 14, 351-366.

Mosselman, E., Shishikura, T., and Klaassen, G.J. (2000). Effect of bank stabilization on bend scour in anabranches of braided rivers. *Physics and Chemistry of the Earth Part B Hydrology Oceans and Atmosphere.* 25(7), 699-704.

Nagata, N., Hosoda, T. and Muramoto, Y. (2000). Numerical analysis of river channel processes with bank erosion. *Journal of Hydraulic Engineering ASCE.* 126(4), 243-252.

Nelson, J.M., Shreve, R.L., McLean, S.R. and Drake, T.G. (1995). Role of near-bed turbulence in bed load transport and bed form mechanics. *Water Resources Research.* 31(8), 2071-2086.

Nicholas, A.P. (2001). Computational fluid dynamics modelling of boundary roughness in gravel-bed rivers: an investigation of the effects of random variability in bed elevation. *Earth Surface Processes and Landforms*. 26, 345-362.

Olsen, N.R.B. (2003). Three-dimensional CFD modelling of self-forming meandering channel. *Journal of Hydraulic Engineering ASCE.* 129(5), 366-372.

Petit, F. (1990). Evaluation of grain shear stresses required to initiate movement of particles in natural rivers. *Earth Surface Processes and Landforms,* 15 (2), 135-148.

Piegay, H., Cuaz, M., Javelle, E., and Mandier, P.. (1997). Bank erosion management based on geomorphological, ecological and economic criteria on the Galaure River, France. *Regulated Rivers: Research and Management,* 13 (5), 433-448.

Prandtl, L. (1935). The mechanics of viscous fluids. In: *Aerodynamic Theory: A General Review of Progress* (ed: W.F. Durand) 34-205. Berlin: Springer.

Rhoads, B.L. and Welford, M.R. (1991). Initiation of river meandering. *Progress in Physical Geography.* 15(2), 127-156.

Rhoads, B.L. and Kenworthy, S.T. (1998). Time-averaged flow structure in the central region of a stream confluence. *Earth Surface Processes and Landforms*, 23, 171-191.

Rhoads, B.L. and Kenworthy, S.T. (1999). Short communication: on secondary circulation, helical motion and Rozovskii-based analysis of time-averaged two-dimensional velocity fields at confluences. *Earth Surface Processes and Landforms*, 24, 369-375.

Richardson, W.R. and Thorne, C.R. (1998). Secondary currents around braid bar in Brahmaputra River, India. *Journal of Hydraulic Engineering ASCE.* 124(3), 325-328.

Rinaldi, M. and Johnson, P.A. (1997). Characterization of stream meanders for stream restoration. *Journal of Hydraulic Engineering ASCE.* 123(6), 567-570.

Robinson, S.K. (1991). Coherent motions in the turbulent boundary layer. *Journal of Fluid Mechanics.* 23, 601-639.

Rodriguez, J.F., Garcia, C.M. and Garcia, M.H. (in review) Mean flow and turbulence characteristics in pool-riffle structures.

Roy, A.G., Biron, P. and De Serres, B. (1996). On the necessity of applying a rotation to instantaneous velocity measurements in river flows. *Earth Surface Processes and Landforms.* 21, 817-827.

Roy, A.G. and Buffin-Bélanger, T. (2001). Advances in the study of turbulent flow structures in gravel-bed rivers. *Gravel Bed Rivers V.* New Zealand: New Zealand Hydrological Society.

Roy, A.G., Buffin-Bélanger, T., Lamarre, H. and Kirkbride, A.D. (2004). Size, shape and dynamics of large-scale turbulent flow structures in a gravel-bed river. *Journal of Fluid Mechanics*, 500, 1-27.

Shiono, K. and Muto, Y. (1998). Complex flow mechanisms in compound meandering channels with overbank flow. *Journal of Fluid Mechanics.* 376, 221-261.

Shiono, K., Muto, Y., Knight, D.W., and Hyde, A.F.L. (1999). Energy losses due to secondary flow and turbulence in meandering channels with overbank flows. *Journal of Hydraulic Research.* 37(5), 641-664.

Simon, A. and Collison, A.J.C. (2001). Pore-water pressure effects on the detachment of cohesive streambeds: seepage forces and matric suction. *Earth Surface Processes and Landforms*, 26, 1421-1442.

Simon, A., Thomas, R.E., Curini, A. and Shields, F.D.Jr. (2002). Case study: channel stability of the Missouri River, eastern Montana. *Journal of Hydraulic Engineering ASCE,* 128(10), 880-890.

Song, T. and Graf, W.H. (1994). Nonuniform open-channel flow over a rough bed. *Journal of Hydroscience and Hydraulic Engineering.* 12(1) 1-25.

Song, T. and Chiew, Y.M. (2001). Turbulence measurement in nonuniform open-channel flow using acoustic Doppler velocimeter (ADV). *Journal of Engineering Mechanics ASME.* 127(3), 219-232.

Soulsby, R.L. (1983). The bottom boundary-layer in shelf seas. In: Johns, B. (Ed.) *Physical Oceanography of Coastal and Shelf Areas,* Elsevier, Amsterdam, 189-266.

Stapleton, K.R. and Huntley, D.A. (1995). Seabed stress determination using the inertial dissipation method and the turbulent kinetic energy method. *Earth Surface Processes and Landforms*, 20, 807-815.

Sukhodolov, A. Thiele, M. and Bungartz, H. (1998). Turbulence structure in a river reach with sand bed. *Water Resources Research.* 34(5), 1317-1334.

Thompson, D.M. (2004). The influence of pool length on local turbulence production and energy slope: a flume experiment. *Earth Surface Processes and Landforms*, 29, 1341-1358.

Thorne, S.D. and Furbish, D.J. (1995). Influences of coarse bank roughness on flow within a sharply curved river bend. *Geomorphology.* 12(3), 241-257.

Vallée, B. (2003). Structures macroturbulentes et pulsations à grande échelle de l'écoulement sur un lit sablonneux en présence de rides. Unpublished MSc. Thesis, Université de Montréal.

Whiting, P.J., and Dietrich, W.E. (1991). Convective accelerations and boundary shear stress over a channel bar. *Water Resources Research.* 27(5), 783-796.

Whiting, P.J., and Dietrich, W.E. (1993a). Experimental studies of bed topography and flow patterns in large-amplitude meanders 1. observations. *Water Resources Research*. 29(11), 3605-3614.

Whiting, P.J., and Dietrich, W.E. (1993b). Experimental studies of bed topography and flow patterns in large-amplitude meanders 2. mechanisms. *Water Resources Research*. 29(11), 3615-3622.

Williams, J.J., Thorne, P.D. and Heathershaw, A.D. (1989). Measurements of turbulence in the benthic boundary layer over a gravel bed. *Sedimentology*. 36, 959-971.

Wu, W., Rodi, W. and Wenka, T. (2000). 3D numerical modelling of flow and sediment transport in open channels. *Journal of Hydraulic Engineering ASCE*. 126(1), 4-15.

Yalin, M.S. (1992). *River Mechanics*. Oxford: Pergamon.

Zhou, Y. and Antonia, R.A. (1994). Critical points in a turbulent near wake. *Journal of Fluid Mechanics*. 275, 59-81.